



National Library
of Canada

Bibliothèque nationale
du Canada

Canadian Theses Service

Service des thèses canadiennes

Ottawa, Canada
K1A 0N4

NOTICE

The quality of this microform is heavily dependent upon the quality of the original thesis submitted for microfilming. Every effort has been made to ensure the highest quality of reproduction possible.

If pages are missing, contact the university which granted the degree.

Some pages may have indistinct print especially if the original pages were typed with a poor typewriter ribbon or if the university sent us an inferior photocopy.

Reproduction in full or in part of this microform is governed by the Canadian Copyright Act, R.S.C. 1970, c. C-30, and subsequent amendments.

AVIS

La qualité de cette microforme dépend grandement de la qualité de la thèse soumise au microfilmage. Nous avons tout fait pour assurer une qualité supérieure de reproduction.

S'il manque des pages, veuillez communiquer avec l'université qui a conféré le grade.

La qualité d'impression de certaines pages peut laisser à désirer, surtout si les pages originales ont été dactylographiées à l'aide d'un ruban usé ou si l'université nous a fait parvenir une photocopie de qualité inférieure.

La reproduction, même partielle, de cette microforme est soumise à la Loi canadienne sur le droit d'auteur, SRC 1970, c. C-30, et ses amendements subséquents.

UNIVERSITY OF ALBERTA

NUMERICAL STUDIES OF SEISMIC WAVE PROPAGATION
IN POROUS MEDIA

by

Craig J. Hickey



A THESIS
SUBMITTED TO THE FACULTY OF GRADUATE STUDIES AND
RESEARCH IN PARTIAL FULFILMENT OF THE REQUIREMENTS
FOR THE DEGREE
OF
MASTER OF SCIENCE.

IN

GEOPHYSICS

DEPARTMENT OF PHYSICS

EDMONTON, ALBERTA

SPRING, 1990



National Library
of Canada

Bibliothèque nationale
du Canada

Canadian Theses Service

Service des thèses canadiennes

Ottawa, Canada
K1A 0N4

NOTICE

The quality of this microform is heavily dependent upon the quality of the original thesis submitted for microfilming. Every effort has been made to ensure the highest quality of reproduction possible.

If pages are missing, contact the university which granted the degree.

Some pages may have indistinct print especially if the original pages were typed with a poor typewriter ribbon or if the university sent us an inferior photocopy.

Reproduction in full or in part of this microform is governed by the Canadian Copyright Act, R.S.C. 1970, c. C-30, and subsequent amendments.

AVIS

La qualité de cette microforme dépend grandement de la qualité de la thèse soumise au microfilmage. Nous avons tout fait pour assurer une qualité supérieure de reproduction.

S'il manque des pages, veuillez communiquer avec l'université qui a conféré le grade.

La qualité d'impression de certaines pages peut laisser à désirer, surtout si les pages originales ont été dactylographiées à l'aide d'un ruban usé ou si l'université nous a fait parvenir une photocopie de qualité inférieure.

La reproduction, même partielle, de cette microforme est soumise à la Loi canadienne sur le droit d'auteur, SRC 1970, c. C-30, et ses amendements subséquents.

ISBN 0-315-60293-7

UNIVERSITY OF ALBERTA

RELEASE FORM

NAME OF AUTHOR: Craig J. Hickey

TITLE OF THESIS: Numerical Studies of Seismic Wave Propagation
in Porous Media.

DEGREE: Master of Science

YEAR THIS DEGREE GRANTED: SPRING 1990

Permission is hereby granted to THE UNIVERSITY OF ALBERTA LIBRARY to reproduce single copies of this thesis and to lend or sell such copies for private, scholarly or scientific research purposes only.

The author reserves other publication rights, and neither the thesis nor extensive extracts from it may be printed or otherwise reproduced without the author's written permission.

(Signed).....Craig J. Hickey.....

Permanent Address:

.....Lorne, RR#1 Park Creek.....

.....New Brunswick, Canada.....

.....EOB 120.....

Date: April 19..... 19 90.....

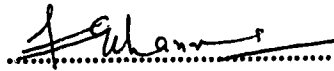
THE UNIVERSITY OF ALBERTA

FACULTY OF GRADUATE STUDIES AND RESEARCH

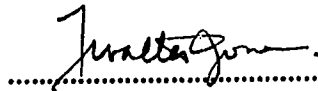
The undersigned certify that they have read, and recommend to the Faculty of Graduate Studies and Research for acceptance, a thesis entitled **Numerical Studies of Seismic Wave Propagation in Porous Media** submitted by **Craig J. Hickey** in partial fulfilment of the requirements for the degree of **Master of Science in Geophysics**.



Dr. T. J. T. Spanos (Supervisor)
Department of Physics



Dr. F. C. Khanna
Department of Physics



Dr. F. W. Jones
Department of Physics



Dr. R. Bentsen
Department of Mining, Met. & Pet. Engin.

Date: March 1 1990

*To the fond memory of my grandfather
John Doucet*

ABSTRACT

De la Cruz and Spanos (1989a) presented a complete set of equations which describe the propagation of low frequency waves through fluid filled porous media. In this theory the porous matrix is assumed to be elastic and thus wave attenuation is almost entirely due to fluid viscosity. The temperature changes associated with mechanical compressions and the respective mechanical expansions due to the temperature change, bring thermo-mechanical coupling into the analysis. Since the temperature variations within the fluid and solid are different, heat conduction between the phases occur throughout the volume of the porous medium.

An analysis of the equations yields predictions for two S waves and four P waves of which the two S waves are unaffected by thermo-mechanical coupling. The effect on the P waves is found to be small for water or air in a silica sand. However, when the fluid is given the properties of an Athabasca bitumen the effect of thermo-mechanical coupling on the attenuation of the first P wave is found to be extremely large.

The theory was used to model the asthenosphere and core-mantle boundary as zones containing partial melt. The theory confirmed that the presence of a partial melt can account for the negative velocity gradients and low Q^* values observed. Thermo-mechanical coupling appears to be an important process within the core-mantle boundary. However, more experimental work is needed in determining physical properties of the component materials constituting these zones before any quantitative estimates of velocity and attenuation are made.

ACKNOWLEDGEMENTS

To my supervisor, Dr. Tim Spanos, I express my sincere gratitude for the assistance and constructive discussions regarding the research contained in this thesis. His assistance and support extended far beyond the bounds of an academic supervisor.

I would like to thank fellow graduated student John Eastwood for his discussions and ideas pertaining to this thesis and the many other not so relevant topics.

Sincere thanks to Joan Hube and Dr. Norman Udey for their help in solving many of the computer problems encountered and to Dr. Vincenté de la Cruz for the assistance regarding the theoretical formulation discussed in this thesis.

The financial support provided by Alberta Oil Sands Technology and Research Authority and the Canadian Society of Exploration Geophysicists is greatly appreciated.

Last but not least, I am forever grateful to Rose for the many hours of word processing. To her, I owe so much for the continuous support and reassurance which enabled me to complete this thesis.

TABLE OF CONTENTS

<u>Chapter</u>	<u>Page</u>
LIST OF TABLES	ix
LIST OF FIGURES	x
1. INTRODUCTION	1
2. THEORY	6
2.1 MICROSCOPIC OR PORE-SCALE EQUATIONS	6
2.2 VOLUME AVERAGING	10
2.3 MACROSCOPIC EQUATIONS	13
2.4 COMPARISON WITH BIOT'S THEORY	19
2.5 ROTATIONAL WAVES	23
2.6 DILATATIONAL WAVES	25
3. NUMERICAL SOLUTION	29
3.1 METHOD OF SOLUTION	29
3.2 EMPIRICAL PARAMETERS	31
3.2.1 Permeability (K)	32
3.2.2 Induced mass coefficient (ρ_{12})	41
3.2.3 Solid (δ_s) and fluid (δ_f) compliance factor	47
3.2.4 Intercomponent conduction coefficient (γ)	53
3.3 LIMITING CASES	60
3.3.1 Solid limit	60
3.3.2 Fluid limit	65
3.3.3 Numerical Calculation of Limits	70

4.	CASE STUDIES	75
4.1	AIR FILLED SILICA SAND	76
4.2	WATER FILLED SILICA SAND	82
4.3	BITUMEN FILLED SILICA SAND	87
4.4	STRUCTURES OF THE DEEP EARTH	94
4.4.1	Asthenosphere	101
4.4.2	Core-Mantle Boundary	108
5.	CONCLUSION	119
	REFERENCES	124

LIST OF TABLES

<u>Table</u>	<u>Description</u>	<u>Page</u>
1	Relationship in notation between the Biot and de la Cruz - Spanos theory	20
2	Comparison of coefficients for the Biot (1956a) theory and the de la Cruz - Spanos theory (1989a)	22
3	Physical properties properties of water and silica sand and the associated empirical parameters	35
4	Physical parameters for air and the associated empirical parameters	77
5	Physical parameters for bitumen and the associated empirical parameters	90
6	The parameters describing the Preliminary Reference Earth Model (PREM). The variable x is the normalized radius: $x=r/a$ where $a=6371$ km. The parameters listed are valid at a reference period of 1 s. The effective isotropic velocities between 24.4 and 220 km can be approximated by $V_p=4.1875 + 3.9382x$ and $V_s=2.1519 + 2.3481x$ (Dziewonski and Anderson, 1981).	99
7	Physical properties properties of the asthenosphere and the associated empirical parameters	104
8	Physical properties properties of the core-mantle transition zone, D", and the associated empirical parameters. The solid is assumed to be perovskite and the fluid is the molten iron alloy of the outer core	112

LIST OF FIGURES

<u>Figure</u>	<u>Page</u>
1 Dependence of average on averaging volume	11
2 Procedure and array assignment for the numerical calculation of the dispersion relation for dilatational waves	30
3 1st P-wave; Attenuation vs. $\log(K)$ vs. f	36
4 1st P-wave; Phase angle vs. $\log(K)$ vs. f	36
5 1st P-wave; Relative magnitude vs. $\log(K)$ vs. f	37
6 1st S-wave; Attenuation vs. $\log(K)$ vs. f	37
7 1st P-wave; Phase velocity vs. $\log(K)$ vs. f	39
8 1st S-wave; Phase velocity vs. $\log(K)$ vs. f	39
9 2nd P-wave; Attenuation vs. $\log(K)$ vs. f	40
10 2nd P-wave; Phase velocity vs. $\log(K)$ vs. f	40
11 1st P-wave; Phase velocity vs. $\log(f)$ vs. ρ_{12}	43
12 1st S-wave; Phase velocity vs. $\log(f)$ vs. ρ_{12}	43
13 2nd P-wave; Phase velocity vs. $\log(f)$ vs. ρ_{12}	44
14 2nd S-wave; Phase velocity vs. $\log(f)$ vs. ρ_{12}	44
15 1st P-wave; Attenuation vs. $\log(f)$ vs. ρ_{12}	45
16 1st S-wave; Attenuation vs. $\log(f)$ vs. ρ_{12}	45
17 2nd P-wave; Attenuation vs. $\log(f)$ vs. ρ_{12}	46
18 2nd S-wave; Attenuation vs. $\log(f)$ vs. ρ_{12}	46
19 1st P-wave @ 100 hz; Attenuation vs. δ_s vs. δ_f	50

20	2nd P-wave @ 100 hz; Attenuation vs. δ_s vs. δ_f	50
21	Projection of the constraints on the δ_s and δ_f plane. The line originating at the origin with positive slope is the line representing δ_s and δ_f values which concur with the Biot theory {cf equation (50)}.	51
22	1st P-wave @ 5000 hz; Attenuation vs. δ_s vs. δ_f	52
23	2nd P-wave @ 5000 hz; Attenuation vs. δ_s vs. δ_f	52
24	1st P-wave; Phase velocity vs. δ_s vs. f	54
25	1st P-wave; Attenuation vs. δ_s vs. f	54
26	2nd P-wave; Phase velocity vs. δ_s vs. f	55
27	2nd P-wave; Attenuation vs. δ_s vs. f	55
28	1st P-wave; Attenuation vs. $\log(\gamma)$ vs. f	59
29	1st P-wave; Phase velocity vs. $\log(\gamma)$ vs. f	59
30	1st P-wave; Phase velocity vs. η vs. $\log(K)$, illustrating the convergence of the numerical solution in the solid and fluid limits	72
31	2nd P-wave; Phase velocity vs. η vs. $\log(K)$, illustrating the convergence of the numerical solution in the solid and fluid limits	72
32	1st S-wave; Phase velocity vs. η vs. $\log(K)$, illustrating the convergence of the numerical solution in the solid and fluid limits	73
33	2nd S-wave; Phase velocity vs. η vs. $\log(K)$, illustrating the convergence of the numerical solution in the solid and fluid limits	73
34	1st P-wave; Phase velocity vs. f for an air filled silica sand with 30% porosity. Thermal solution includes thermo-mechanical coupling	79

35	1st P-wave; Attenuation vs. f for an air filled silica sand with 30% porosity. Thermal solution includes thermo-mechanical coupling	79
36	2nd P-wave; Phase velocity vs. f for an air filled silica sand with 30% porosity. Thermal solution includes thermo-mechanical coupling	80
37	2nd P-wave; Attenuation vs. f for an air filled silica sand with 30% porosity. Thermal solution includes thermo-mechanical coupling	80
38	1st S-wave; Phase velocity vs. f for an air filled silica sand with 30% porosity	81
39	1st S-wave; Attenuation vs. f for an air filled silica sand with 30% porosity	81
40	1st P-wave; Phase velocity vs. f for a water filled silica sand with 30% porosity. Thermal solution includes thermo-mechanical coupling	84
41	1st P-wave; Attenuation vs. f for a water filled silica sand with 30% porosity. Thermal solution includes thermo-mechanical coupling	84
42	2nd P-wave; Phase velocity vs. f for a water filled silica sand with 30% porosity. Thermal solution includes thermo-mechanical coupling	85
43	2nd P-wave; Attenuation vs. f for a water filled silica sand with 30% porosity. Thermal solution includes thermo-mechanical coupling	85
44	1st S-wave; Phase velocity vs. f for a water filled silica sand with 30% porosity	86
45	1st S-wave; Attenuation vs. f for a water filled silica sand with 30% porosity	86
46	1st P-wave; Phase velocity vs. f for a bitumen filled silica sand with 30% porosity. Thermal solution includes thermo-mechanical coupling	91

47	1st P-wave; Attenuation vs. f for a bitumen filled silica sand with 30% porosity. Thermal solution includes thermo-mechanical coupling	91
48	1st S-wave; Phase velocity vs. f for a bitumen filled silica sand with 30% porosity	93
49	1st S-wave; Attenuation vs. f for a bitumen filled silica sand with 30% porosity	93
50	P and S velocity distributions within the Earth (Bullen, 1963)	96
51	1st P wave; Phase velocity vs. % partial melt for a model of the asthenosphere at a frequency of 1 hz. Thermal solution includes thermo-mechanical coupling	105
52	1st P wave; Attenuation vs. % partial melt for a model of the asthenosphere at a frequency of 1 hz. Thermal solution includes thermo-mechanical coupling	105
53	1st S wave; Phase velocity vs. % partial melt for a model of the asthenosphere at a frequency of 1 hz.	106
54	1st S wave; Attenuation vs. % partial melt for a model of the asthenosphere at a frequency of 1 hz.	106
55	1st P wave; Phase velocity vs. f for a model of the asthenosphere with 5% partial melt. Thermal solution includes thermo-mechanical coupling	107
56	1st P wave; Attenuation vs. f for a model of the asthenosphere with 5% partial melt. Thermal solution includes thermo-mechanical coupling	107
57	1st S wave; Phase velocity vs. f for a model of the asthenosphere with 5% partial melt	109
58	1st S wave; Attenuation vs. f for a model of the asthenosphere with 5% partial melt	109
59	1st P wave; Phase velocity vs. % partial melt for a model of the core-mantle transition zone at a frequency of 1 hz. Thermal solution includes thermo-mechanical coupling	113

60	1st P wave; Attenuation vs. % partial melt for a model of the core-mantle transition zone at a frequency of 1 hz. Thermal solution includes thermo-mechanical coupling	113
61	1st S wave; Phase velocity vs. % partial melt for a model of the core-mantle transition zone at a frequency of 1 hz.	115
62	1st S wave; Attenuation vs. % partial melt for a model of the core-mantle transition zone at a frequency of 1 hz.	115
63	1st P wave; Phase velocity vs. f for a model of the core-mantle transition zone with 5% partial melt. Thermal solution includes thermo-mechanical coupling	116
64	1st P wave; Attenuation vs. f for a model of the core-mantle transition zone with 5% partial melt. Thermal solution includes thermo-mechanical coupling	116
65	1st S wave; Phase velocity vs. f for a model of the core-mantle transition zone with 5% partial melt.	117
66	1st S wave; Attenuation vs. f for a model of the core-mantle transition zone with 5% partial melt.	117

1. INTRODUCTION

The attenuation and dispersion of seismic waves propagating in a porous solid filled with a compressible viscous fluid can be used to obtain fundamental details about the constituent materials and their interaction. This information is of fundamental importance to the oil industry for both exploration techniques and monitoring of in-situ production processes. It also contributes significantly to the interpretation and understanding of anomalous deep Earth features, such as the low velocity zone, which are observed on global seismic records.

The first models for seismic wave propagation in porous media were proposed by Gassman (1951a,b) and Biot (1956a,b). The Biot theory has long been regarded as the basis for solving wave propagation problems in porous media and predicts the existence of two compressional waves and one rotational wave. The theory is based upon a model consisting of two superposed and interacting continua, one representing the solid component, the other the fluid component. It is assumed that the porous medium is macroscopically homogeneous and isotropic and that the macroscopic fluid motions can be adequately described by Darcy's equation. Thermo-elastic effects are ignored in Biot's formulation. The macroscopic equations are constructed through macroscopic energy arguments in conjunction with phenomenological arguments of the effect of the fluid motions. The theory has six macroscopic parameters, the medium permeability K , induced mass coefficient ρ_{12} , A and N which correspond to Lamé's constants and two additional macroscopic

elastic parameters Q and R . For high frequency waves an additional parameter $F(\omega)$ allows for the description of a frequency dependent permeability.

These macroscopic parameters are not defined uniquely in terms of pore-scale mechanisms. This has resulted in many misinterpretations of these parameters in the Biot theory. For example, the standard interpretations given to the frame bulk modulus and frame shear modulus as parameters which can be measured directly by compressing and shearing of the porous matrix is incorrect, since it totally ignores the fundamental role of porosity (Spanos *et al.*, 1990). The standard interpretation used is valid only in the limit as porosity approaches zero. It has also prompted experimenters to determine these parameters by correlating the theory such that it produces a best fit with experiments (Johnson and Plona, 1982; Winkler and Plona, 1982; Winkler, 1983, 1985, 1986). This sort of curve fitting appears to have led to a rather questionable correlation between theory and experiments.

Other researchers (Toksoz *et al.*, 1979; Johnston *et al.*, 1979) have concluded that when many of the specific pore scale details, not allowed for in Biot's theory, are altered one observes changes in velocity and attenuation data. This sort of dependence on pore-scale detail is believed to be due to the rather high frequencies used in these experiments. (Eastwood *et al.*, 1990). These high frequencies were sufficiently close to the pore-scale that the basic assumptions used to create a scale independent macroscopic continuum description has been violated. However, particular changes in pore scale detail could induce changes in the macroscopic parameters. Hence, the absence of a physical understanding of these parameters

could be the source of the discrepancy.

In order to completely understand the Biot theory and its limits of application one must obtain a description of Biot's macroscopic empirical parameters in terms of physical mechanisms. Once this is attained, it will facilitate development of proper experimental procedures to measure the necessary parameters.

Geertsma and Smit (1961) analyze Biot's low frequency theory for the velocity and attenuation of the waves of both the first and second kind. They conclude that the wave of the second kind dies out with increasing distance from the source and that only the wave of the first kind need be considered in seismic studies. Berryman(1981) determined expressions for Biot's empirical parameters as a function of frame and fluid moduli for a fully consolidated frame.

Burridge and Keller (1981) derived the equations governing the macroscopic mechanical behavior of a porous medium starting with the appropriate equations and boundary conditions at the pore-scale. The macroscopic equations are constructed from the pore-scale equations using the two-space method of homogenization and are valid only when the size of the pores is small compared to the macroscale. When the assumption used in their analysis, ie. the dimensionless viscosity of the fluid is small, coincide with those of Biot (1956a,b) their equations appear to be identical in form. From comparison of their equations with those of Biot's they obtain expressions for Biot's coefficients (see Burridge & Keller, 1981 eq 43a-43h). Some are merely averages of component materials, such as the mass density of the bulk material; however, others are far from obvious. The complex expressions associated with the mathematical rigor of this work lack the physical transparency needed to fully comprehend Biot's

macroscopic parameters in terms of pore scale mechanisms.

De la Cruz and Spanos (1985) developed a complete set of macroscopic equations for seismic wave propagation in porous media using volume averaging. The theory is constructed from the pore scale equations and boundary conditions using volume averaging to provide the initial framework. They incorporate order of magnitude considerations and plausible physical arguments to yield a theory which is somewhat more physically transparent. The theory predicts two compressional and two rotational waves. The wave attenuation is affected by the fluid viscosity, firstly owing to the Darcy resistance and secondly to viscous dissipation within the fluid. When the main underlying assumptions equating the de la Cruz - Spanos theory and the Biot (1956a) theory are imposed one obtains an interpretation of Biot's phenomenological parameters in terms of pore scale quantities and two empirical parameters (cf. 2.4).

This theory was generalized subsequently to include the effects of inertial coupling between phases and thermo-mechanical coupling (de la Cruz and Spanos, 1989a). The macroscopic equations contain the basic component material parameters and a set of macroscopic parameters which describe average properties of the medium. (permeability K , porosity η , inter-component conduction coefficient γ , induced mass coefficient ρ_{12} and two parameters δ_s and δ_f determined from the combined effect of dilations and the change in relative proportions of the phases).

An alternate method of analyzing attenuation of seismic waves is obtained by assuming rocks behave as linear viscoelastic solids (Gordon and Davies, 1968; Walsh, 1968). In order for this type of analysis to be valid one must assume that the effect on the elastic

waves by macroscopic motions of the fluid are minor, which necessitates a low porosity and permeability (Spencer, 1979). In viscoelastic solids the shear and bulk moduli are complex and frequency dependent. The actual forms of the moduli for two-phase systems are determined by simple models consisting of discrete spring and dash pot elements linked in parallel (Kelvin-Voigt model) or in series (Maxwell model). This type of analysis incorporates attenuation; however, it does not appear to contain the needed dependence on the component material properties. Therefore, it would be difficult to associate changes in wave character to changes of the component materials.

The objective of this work is to solve the system of equations, derived by de la Cruz and Spanos (1989a), which describes seismic wave propagation in porous media. A numerical approach is used and the algorithm will be verified in the solid and fluid limiting cases. Numerical calculations will be used to illustrate the importance and physical limits of the various macroscopic empirical parameters. The phase velocity and attenuation of seismic waves will be calculated for several models: air filled silica sand, water filled silica sand, bitumen filled silica sand, asthenosphere (LVZ) and the core-mantle transition zone (D'') in order to illustrate the importance of different component materials on the various waves. Furthermore, the importance of thermo-mechanical coupling for the various physical situations will be examined.

2. THEORY

The model considered for wave propagation by de la Cruz and Spanos (1985, 1989a) consists of an elastic matrix containing pores of random sizes, shapes and orientations which are filled with a compressible viscous fluid. A gross description of the physical system, at a scale much larger than the largest pore size, is obtained by averaging over solid motions, solid temperatures, fluid motions, fluid temperatures and the coupling at the fluid-solid interfaces. The approach is based upon the mathematical techniques of volume averaging (Whitaker, 1966, 1969) aided by physical arguments and order of magnitude considerations. Using volume averaging will place an upper limit on the frequency of disturbance which can be described by the developed system of equations. In the development, the constraint of linearity in both displacements and velocities plays a prominent role. This means that any motion is regarded as a small deviation from the static and uniform unperturbed configuration.

2.1 MICROSCOPIC OR PORE-SCALE EQUATIONS

Firstly, each component at the pore-scale is characterized by well established equations, which are referred to here as microscopic equations (Landau and Lifshitz, 1975a, b). The fluid parameters and variables are denoted by using a subscript or superscript f and those of the solid by the subscript or superscript s .

Inside the compressible viscous fluid the equation of motion is

given by the Navier - Stokes equation:

$$\frac{\partial (\rho_f v_i^f)}{\partial t} + \partial_k (p_f \delta_{ik} + \rho_f v_i^f v_k^f - \sigma_{ik}^f) = 0 \quad (1)$$

where

$$\sigma_{ik}^f = \mu_f \left(\frac{\partial v_i^f}{\partial x_k} + \frac{\partial v_k^f}{\partial x_i} - \frac{2}{3} \frac{\partial v_l^f}{\partial x_l} \delta_{ik} \right) \quad (2)$$

is the viscosity stress tensor with the effects of bulk viscosity being neglected. The parameters ρ_f , p_f , μ_f and v_i^f represents the mass density, pressure, viscosity and velocity respectively. The subscripts i , k , l , take values x , y , z and a sum over repeated indices (except f and s) is implied in all equations. δ_{ik} is the Kronecker delta function. The equation of continuity for the fluid is given as

$$\frac{\partial \rho_f}{\partial t} + \nabla \cdot (\rho_f \mathbf{v}^f) = 0 \quad (3)$$

To include thermo-mechanical coupling we need the energy equation (linearized in \mathbf{v}) for the fluid and is given as

$$\rho_f T_f \left(\frac{\partial S}{\partial t} + \mathbf{v}^f \cdot \nabla S \right) = \nabla \cdot (\kappa_f \nabla T) \quad (4)$$

where $T_f(\vec{x}, t)$ is the actual temperature, and where $(T_f - T_0)$ is treated as a first order quantity. T_0 is the ambient temperature, S is the entropy per unit mass and κ_f is the thermal conductivity of the fluid. Substituting the thermodynamic relation

$$T_f dS = c_p^f dT_f - \frac{T_f}{\rho_f} \alpha_f dp_f, \quad (5)$$

where c_p^f is the specific heat of the fluid at constant pressure and α_f is the thermal expansion of the fluid, yields

$$\rho_f c_p^f \frac{\partial T_f}{\partial t} - T_f \alpha_f \frac{\partial p_f}{\partial t} + \mathbf{v}_f \cdot [\rho_f c_p^f \nabla T_f - T_f \alpha_f \nabla p_f] - \nabla \cdot (\kappa_f \nabla T_f) = 0 \quad (6)$$

Restricting the analysis to cases where the unperturbed configurations correspond to zero velocity, uniform temperature T_0 , uniform pressure p_0 and porosity η_0 , (6) becomes

$$\rho_f c_p^f \frac{\partial T_f}{\partial t} - T_f \alpha_f \frac{\partial p_f}{\partial t} - \nabla \cdot (\kappa_f \nabla T_f) = 0 \quad (7)$$

where the coefficients of the derivatives can be taken to be the unperturbed values.

Inside the elastic solid the equation of motion is given by

$$\rho_s \frac{\partial^2 u_i^s}{\partial t^2} = \frac{\partial \sigma_{ik}^s}{\partial x_k} \quad (8)$$

where

$$\sigma_{ik}^s = -K_s \alpha_s (T_s - T_0) \delta_{ik} + K_s u_{ll}^s \delta_{ik} + 2\mu_s \left(u_{ik}^s - \frac{1}{3} u_{ll}^s \delta_{ik} \right) - p_0 \delta_{ik} \quad (9)$$

is the stress tensor. The parameters ρ_s , u_{ik}^s , K_s , μ_s and α_s are the mass density, displacement vector, bulk modulus, shear modulus and

thermal expansion coefficient. T_0 and p_0 are the unperturbed temperature and unperturbed pressure of the static configuration. Also

$$u_{ik}^s = \frac{1}{2} (u_{i,k}^s + u_{k,i}^s) + \text{2nd order in } \mathbf{u}^s \quad (10)$$

where the commas denote partial differentiation with respect to space.

The linearized equation of heat transfer in the solid is

$$\rho_s c_v^s \frac{\partial T_s}{\partial t} + \alpha_s K_s T_s \frac{\partial(\nabla \cdot \mathbf{u}^s)}{\partial t} - \kappa_s \nabla^2 T_s = 0 \quad (11)$$

where c_v^s is the specific heat at constant volume and κ_s is the thermal conductivity of the solid.

The interactions between the components are controlled by the pore-scale interfaces, at which the following boundary conditions are assumed. The mechanical boundary conditions are no-slip

$$\mathbf{v}^f = \frac{\partial \mathbf{u}_s}{\partial t} \quad (12)$$

and continuity of stress

$$-p \mathbf{n}_i + \sigma_{ik}^f \mathbf{n}_k = \sigma_{ik}^s \mathbf{n}_k \quad (13)$$

where \mathbf{n}_i is the normal vector.

The thermal boundary condition is

$$\kappa_f \nabla T_f = \kappa_s \nabla T_s \quad (14)$$

The next step is to reformulate the problem at a larger or macroscopic scale.

2.2 VOLUME AVERAGING

The principle objective in reformulating the problem at a larger scale is to filter out the over abundance of physical detail at the pore-scale in such a manner that no specific reference to pore-scale motions remains. To do this de la Cruz and Spanos (1985, 1989a) applied an averaging procedure, called volume averaging, pioneered by Hubbard (1956), Whitaker (1966, 1969) and Slattery (1969).

In the volume averaging procedure one constructs regions V in the porous medium of identical shapes, volumes, orientations and ascribes an average value for physical quantities within the volume V to a point \mathbf{x} which uniquely defines V . For example, de la Cruz and Spanos (1983) assume V to be spheres and each V is specified uniquely by the centre of the sphere \mathbf{x} . Also by choosing spheres the problem of orientation is avoided. If we assume $G_f(\mathbf{x})$ to be a physical quantity of the fluid and that $G_f(\mathbf{x})$ equals zero everywhere outside the fluid the volume average of G_f over any region V is defined as

$$\langle G_f \rangle = \frac{1}{V} \int_V G_f(\mathbf{x}) dV \quad (15)$$

where $\langle G_f \rangle$ is a function of the center of the volume elements.

If one assumes the center of the volume element is within the solid

and plot $\langle G_f \rangle$ as a function of the radius of the volume V one might obtain a curve similar to figure 1 (Whitaker, 1969).

Since the center of the volume V was assumed to be in the solid then $\langle G_f \rangle$ is zero at the origin. As one starts increasing the volume size, portions of the fluid are contained within the volume, and $\langle G_f \rangle$ increases from zero through fluctuations due to random distribution of fluid at the pore-scale. For values of V larger than V^* the pore-scale variations are smoothed out, and therefore a restriction that $V > V^*$ is imposed.

As one moves the volume element to different locations in the porous medium, $\langle G_f \rangle$ becomes a continuous function of \mathbf{x} . However, for values of V larger than V^* the function $\langle G_f \rangle$ is independent of V . A precise value for V^* cannot be determined, but one can assume that it must be orders of magnitude larger than the pore-scale. However, if the structures are much larger than the volume element, V^* , the appropriate macroscopic boundary conditions (de la Cruz and Spanos, 1989b) must be used.

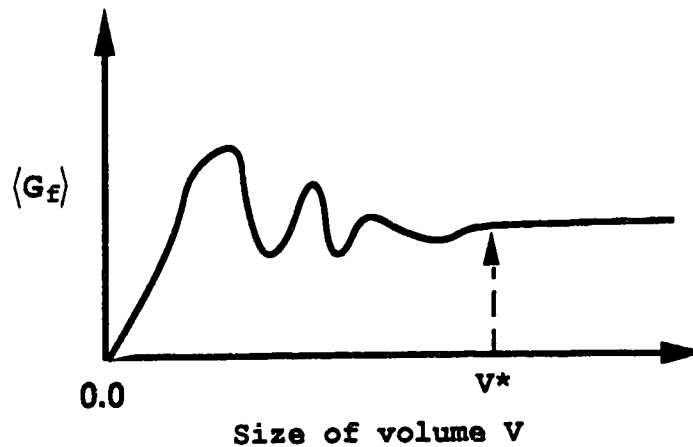


Figure 1 Dependence of average on averaging volume.

A related quantity \overline{G}_f is defined as

$$\overline{G}_f = \frac{1}{V_f} \int_V G_f(\mathbf{x}) dV \quad (16)$$

where V_f is the volume of fluid is the volume V . This is related to $\langle G_f \rangle$ as follows

$$\overline{G}_f = \frac{1}{\eta} \langle G_f \rangle \quad (17)$$

where η is the porosity of the medium.

In the development of the average equations one will be dealing with gradients and time derivatives of such quantities. Slattery (1969) and Whitaker (1969) developed the following relationships between the averages of derivatives and the derivatives of averages

$$\int_V \partial_i G_f dV = \partial_i \int_V G_f dV + \int_{A_{fs}} G_f n_i dA \quad (18)$$

and

$$\int_V \partial_t G_f dV = \partial_t \int_V G_f dV - \int_{A_{fs}} G_f \mathbf{v} \cdot \mathbf{n} dA \quad (19)$$

Here A_{fs} refers to the area of the fluid-solid interfaces, \mathbf{n} is the unit

normal on those interfaces directed towards the solid, and \mathbf{v} is the velocity of the fluid-solid interface element. If the porous medium can be characterized by its average quantities then it is said to behave as a macroscopically homogeneous and isotropic media.

If one is to describe some process in the porous medium, say the propagation of a wave, then a lower bound on the scale at which deformations are described must be imposed. As the frequency of disturbance is increased the amount of pore-scale detail in the macroscopic description must also be increased. However, for a "homogeneous" medium, provided one deals with wavelengths much larger than the pore-scale, the equations are scale independent.

2.3 MACROSCOPIC EQUATIONS

The volume average procedure used in reformulation of the microscopic equations is illustrated by taking the volume average of the continuity equation for the fluid (3):

$$\frac{1}{V} \int_V \left[\frac{\partial \rho_f}{\partial t} + \nabla \cdot (\rho_f \mathbf{v}^f) \right] dV = 0 \quad (20)$$

Applying identities (18) and (19) yields

$$\begin{aligned} \frac{\partial}{\partial t} \left[\frac{1}{V} \int_V \rho_f dV \right] - \frac{1}{V} \int_{A_{fs}} \rho_f \vec{v}^f \cdot \vec{n} dA + \frac{\partial}{\partial x_i} \left[\frac{1}{V} \int_V \rho_f v_i^f dV \right] \\ + \frac{1}{V} \int_{A_{fs}} \rho_f v_i^f n_i dA = 0 \end{aligned} \quad (21)$$

The integrals over the fluid - solid surface cancel and rewriting (21) using (15) and (16) we obtain

$$\frac{\partial (\eta \bar{\rho}_f)}{\partial t} + \nabla \cdot \eta \bar{\rho}_f \bar{\mathbf{v}}^f = 0 \quad (22)$$

Now assuming that the perturbation is a small deviation from the unperturbed configuration and using the following notation

$$\rho_f = \rho_f^0 + \rho_f' \quad (23)$$

$$\eta = \eta_0 + \eta' \quad (24)$$

where ρ_f^0 and η_0 are the unperturbed values, (22) is rewritten as

$$\frac{\partial}{\partial t} [\eta_0 \rho_f^0 + \eta_0 \bar{\rho}_f' + \eta' \rho_f^0] + \nabla \cdot \bar{\mathbf{v}}^f [\eta_0 \rho_f^0 + \eta_0 \bar{\rho}_f' + \eta' \rho_f^0] = 0 \quad (25)$$

Assuming the unperturbed fluid velocity is zero makes $\bar{\mathbf{v}}^f$ the perturbation in fluid velocity. Hence the unperturbed continuity, equation retaining only first order quantities, (25) simplifies to

$$\frac{\partial}{\partial t} [\eta_0 \bar{\rho}_f' + \eta' \rho_f^0] + \nabla \cdot [\bar{\mathbf{v}}^f \eta_0 \rho_f^0] = 0. \quad (26)$$

Dividing (26) by $\eta_0 \rho_f^0$

$$\frac{\partial}{\partial t} \left[\frac{\eta'}{\eta_0} + \frac{\rho'_f}{\rho_f^0} \right] + \nabla \cdot \bar{\mathbf{v}}^f = 0 \quad (27)$$

yields the macroscopic continuity equation for the fluid, an expression obtained by de la Cruz and Spanos (1985).

Following a similar procedure de la Cruz and Spanos (1989a) developed the following system of macroscopic equations (see de la Cruz and Spanos, 1989a) for details.

The equations of motion are

$$\begin{aligned} \rho_f \frac{\partial \bar{\mathbf{v}}^f}{\partial t} = & -\nabla \bar{p}_f + \mu_f \left[\nabla^2 \bar{\mathbf{v}}^f + \frac{1}{3} \nabla (\nabla \cdot \bar{\mathbf{v}}^f) \right] - \frac{\mu_f \eta_0}{K} (\bar{\mathbf{v}}^f - \bar{\mathbf{v}}^s) \\ & + \frac{\rho_{12}}{\eta_0} \frac{\partial}{\partial t} (\bar{\mathbf{v}}^f - \bar{\mathbf{v}}^s) \end{aligned} \quad (28)$$

and

$$\begin{aligned} \rho_s \frac{\partial^2 \bar{\mathbf{u}}_s}{\partial t^2} = & K_s \nabla (\nabla \cdot \bar{\mathbf{u}}_s) - \frac{K_s}{1 - \eta_0} \nabla \eta + \mu_s \left[\nabla^2 \bar{\mathbf{u}}_s + \frac{1}{3} \nabla (\nabla \cdot \bar{\mathbf{u}}_s) \right] + \\ & \frac{\mu_f \eta_0^2}{K (1 - \eta_0)} (\bar{\mathbf{v}}^f - \bar{\mathbf{v}}^s) - \frac{\rho_{12}}{1 - \eta_0} \frac{\partial}{\partial t} (\bar{\mathbf{v}}^f - \bar{\mathbf{v}}^s) - K_s \alpha_s \nabla \bar{T}_s \end{aligned} \quad (29)$$

where K is the permeability of the porous matrix and ρ_{12} is the induced mass coefficient. These parameters must be determined experimentally and are scalar quantities for a macroscopically isotropic and homogeneous medium.

The heat equations for the coupled continua are

$$\rho_f c_p^f \frac{\partial \bar{T}_f}{\partial t} - T_0 \alpha_f \frac{\partial \bar{p}_f}{\partial t} - \kappa_f \nabla^2 \bar{T}_f + \frac{\gamma}{\eta_0} (\bar{T}_f - \bar{T}_s) = 0 \quad (30)$$

and

$$\rho_s c_v^s \frac{\partial \bar{T}_s}{\partial t} - T_0 K_s \alpha_s \left[\frac{1}{1 - \eta_0} \frac{\partial \eta}{\partial t} - \frac{\partial \nabla \cdot \bar{\mathbf{u}}_s}{\partial t} \right] - \kappa_s \nabla^2 \bar{T}_s - \frac{\gamma}{1 - \eta_0} (\bar{T}_f - \bar{T}_s) = 0 \quad (31)$$

where γ is inter- component conduction coefficient .

The pressure equations are derived as follows

$$\frac{1}{K_f} \frac{\partial \bar{p}_f}{\partial t} = -\nabla \cdot \bar{\mathbf{v}}^f - \frac{1}{\eta_0} \frac{\partial \eta}{\partial t} + \alpha_f \frac{\partial \bar{T}_f}{\partial t} \quad (32)$$

and

$$\frac{1}{K_s} (\bar{p}_s - p_0) = -\nabla \cdot \bar{\mathbf{u}}_s + \frac{\eta - \eta_0}{1 - \eta_0} + \alpha_s (\bar{T}_s - T_0) \quad (33)$$

Rewriting (27) one obtains the equation of continuity for the fluid as

$$\frac{1}{\rho_f^0} \frac{\partial \bar{p}_f}{\partial t} + \frac{1}{\eta_0} \frac{\partial \eta}{\partial t} + \nabla \cdot \bar{\mathbf{v}}^f = 0 \quad (34)$$

and a similar analysis for the solid component yields

$$\frac{(\bar{p}_s - \rho_s^0)}{\rho_s^0} - \frac{\eta - \eta_0}{1 - \eta_0} + \nabla \cdot \bar{\mathbf{u}}_s = 0 \quad (35)$$

In the previous eight macroscopic equations there are the following

nine variables; \bar{T}_f , \bar{T}_s , \bar{u}_s , \bar{v}^f , \bar{p}_s , \bar{p}_f , $\bar{\rho}_s$, $\bar{\rho}_f$ and η . Therefore we need an additional equation for completeness. de la Cruz and Spanos (1989a) adopted the following relation

$$\frac{\partial \eta}{\partial t} = \delta_s \nabla \cdot \bar{v}_s - \delta_f \nabla \cdot \bar{v}_f \quad (36)$$

where δ_s and δ_f are dimensionless empirical parameters. It describes the interaction between the dilatation of the individual phases and the change in relative proportions of the phases. The time or frequency dependence of the right hand side of (36) is contained in the $\nabla \cdot \bar{v}_s$ and $\nabla \cdot \bar{v}_f$ terms.

The previous set of equations can now be reduced by subsequent substitutions. Substituting (32) and (36) into the fluid equation of motion (28) yields

$$\begin{aligned} \rho_f \frac{\partial^2 \bar{u}^f}{\partial t^2} = & -\nabla \left[-K_f \nabla \cdot \bar{u}^f - \frac{K_f}{\eta_0} (\delta_s \nabla \cdot \bar{u}^s - \delta_f \nabla \cdot \bar{u}^f) + K_f \alpha_f (\bar{T}_f - T_0) \right] + \\ & \mu_f \left[\nabla^2 \frac{\partial \bar{u}^f}{\partial t} + \frac{1}{3} \nabla \left(\nabla \cdot \frac{\partial \bar{u}^f}{\partial t} \right) \right] - \frac{\mu_f \eta_0}{K} \frac{\partial}{\partial t} (\bar{u}^f - \bar{u}^s) + \frac{\rho_{12}}{\eta_0} \frac{\partial^2}{\partial t^2} (\bar{u}^f - \bar{u}^s) \end{aligned} \quad (37)$$

The solid equation of motion (29) is reformulated as follows using (36)

$$\begin{aligned} \rho_s \frac{\partial^2 \bar{u}_s}{\partial t^2} = & K_s \nabla (\nabla \cdot \bar{u}_s) - \frac{K_s}{1 - \eta_0} \nabla [\delta_s \nabla \cdot \bar{u}_s - \delta_f \nabla \cdot \bar{u}_f] + \\ & \mu_s \left[\nabla^2 \bar{u}_s + \frac{1}{3} \nabla (\nabla \cdot \bar{u}_s) \right] + \frac{\mu_f \eta_0^2}{K (1 - \eta_0)} \frac{\partial}{\partial t} (\bar{u}^f - \bar{u}^s) - \\ & \frac{\rho_{12}}{1 - \eta_0} \frac{\partial^2}{\partial t^2} (\bar{u}^f - \bar{u}^s) - K_s \alpha_s \nabla \bar{T}_s \end{aligned} \quad (38)$$

The fluid heat equation (30) is recast in the following form by substituting (32)

$$\begin{aligned} (\rho_f c_p^f - T_0 \alpha_f^2 K_f) \frac{\partial \bar{T}_f}{\partial t} - T_0 \alpha_f K_f \frac{\partial}{\partial t} \left[-\nabla \cdot \bar{\mathbf{u}}^f - \frac{1}{\eta_0} (\delta_s \nabla \cdot \bar{\mathbf{u}}^s - \delta_f \nabla \cdot \bar{\mathbf{u}}^f) \right] \\ - \kappa_f \nabla^2 \bar{T}_f + \frac{\gamma}{\eta_0} (\bar{T}_f - \bar{T}_s) = 0 \end{aligned} \quad (39)$$

It should be noted that the coefficient of the first term is the definition of the heat capacity at constant volume (Zemansky, 1957)

$$c_v^f = c_p^f - \frac{T_0 \alpha_f^2 K_f}{\rho_f} \quad (40)$$

Since c_v^f can never be a negative quantity, physical parameter sets must comply with the following constraint

$$c_p^f > \frac{T_0 \alpha_f^2 K_f}{\rho_f} \quad (41)$$

Using (36) the solid heat equation (31) is rewritten as follows

$$\begin{aligned} \rho_s c_v^s \frac{\partial \bar{T}_s}{\partial t} - T_0 K_s \alpha_s \left[\frac{1}{1 - \eta_0} \frac{\partial}{\partial t} (\delta_s \nabla \cdot \bar{\mathbf{u}}^s - \delta_f \nabla \cdot \bar{\mathbf{u}}^f) - \frac{\partial \nabla \cdot \bar{\mathbf{u}}^s}{\partial t} \right] \\ - \kappa_s \nabla^2 \bar{T}_s - \frac{\gamma}{1 - \eta_0} (\bar{T}_f - \bar{T}_s) = 0 \end{aligned} \quad (42)$$

Equations (37), (38), (39) and (42) form a complete set of equations describing the macroscopic motion of a porous medium saturated with viscous compressible fluid. The variables are $\bar{\mathbf{u}}_s$, $\bar{\mathbf{u}}_f$, \bar{T}_s

and \bar{T}_f denote the average solid displacement, average fluid displacement, average solid temperature and average fluid temperature.

2.4 COMPARISON WITH BIOT'S THEORY

The theory developed by de la Cruz and Spanos (1989a) should be equivalent to the Biot theory (1956a) if the same assumptions are applied. Biot's theory is obtained using macroscopic energy arguments and phenomenological arguments about the macroscopic effects of fluid motions whereas the de la Cruz-Spanos theory originates from specific pore-scale assumptions. However, in both theories the sole attenuation mechanism is due to fluid motions. Since Biot's theory assumes that the fluid motions can be described adequately by Darcy's equation, the attenuation of the wave will be due to momentum loss due to viscous drag of fluid relative to the solid. Therefore the main underlying assumption that would enable one to equate these theories is that the attenuation occurs solely due to the Darcian resistance. Therefore, one must assume that viscous dissipation within the fluid or the Brinkman term and thermo-mechanical coupling are unimportant processes, for the two theories to be equivalent.

The main purpose of comparing the two theories is first as a consistency check and secondly to be able to use the large body of knowledge associated with the Biot theory. This is of importance in determining estimates of empirical parameters, especially δ_s and δ_f , in the de la Cruz Spanos theory.

The relationship in notation between Biot's work and the de la Cruz - Spanos theory is presented in table 1.

Biot	de la Cruz and Spanos
\mathbf{u}	\mathbf{u}_s
\mathbf{U}	\mathbf{u}_f
β	η
k	K
μ	μ_f
p	p_f

Table 1 Relationship in notation between the Biot and de la Cruz - Spanos theory

Biot's (1956a) two equations of motion in terms of de la Cruz and Spanos(1985) notation are

$$\begin{aligned} \frac{\partial^2}{\partial t^2} (\rho_{11}\mathbf{u}^s + \rho_{12}\mathbf{u}^f) = N \nabla^2 \mathbf{u}^s + \nabla[(A + N) \nabla \cdot \mathbf{u}^s + Q \nabla \cdot \mathbf{u}^f] \\ + \frac{\mu_f \eta^2}{K} \frac{\partial}{\partial t} (\mathbf{u}^f - \mathbf{u}^s) \end{aligned} \quad (43)$$

and

$$\frac{\partial^2}{\partial t^2} (\rho_{12}\mathbf{u}^s + \rho_{22}\mathbf{u}^f) = \nabla[Q \nabla \cdot \mathbf{u}^s + R \nabla \cdot \mathbf{u}^f] - \frac{\mu_f \eta^2}{K} \frac{\partial}{\partial t} (\mathbf{u}^f - \mathbf{u}^s) \quad (44)$$

where ρ_{11} , ρ_{12} and ρ_{22} are "mass coefficients" which can be related to the component densities by

$$\rho_{11} + \rho_{12} = (1 - \eta) \rho_s \quad (45)$$

and

$$\rho_{22} + \rho_{12} = \eta \rho_f \quad (46)$$

The parameters A , N , Q and R are Biot's macroscopic elastic coefficients. If we recast (43) and (44) using relationship (45) and (46) respectively one obtains;

$$\begin{aligned} (1 - \eta) \rho_s \frac{\partial^2}{\partial t^2} \mathbf{u}^s &= N \nabla^2 \mathbf{u}^s + \nabla[(A + N) \nabla \cdot \mathbf{u}^s + Q \nabla \cdot \mathbf{u}^f] \\ &+ \frac{\mu_f \eta^2}{K} \frac{\partial}{\partial t} (\mathbf{u}^f - \mathbf{u}^s) - \rho_{12} \frac{\partial^2}{\partial t^2} (\mathbf{u}^f - \mathbf{u}^s) \end{aligned} \quad (47)$$

and

$$\begin{aligned} \eta \rho_f \frac{\partial^2}{\partial t^2} \mathbf{u}^f &= \nabla[Q \nabla \cdot \mathbf{u}^s + R \nabla \cdot \mathbf{u}^f] - \frac{\mu_f \eta^2}{K} \frac{\partial}{\partial t} (\mathbf{u}^f - \mathbf{u}^s) \\ &+ \rho_{12} \frac{\partial^2}{\partial t^2} (\mathbf{u}^f - \mathbf{u}^s) \end{aligned} \quad (48)$$

Assuming that (47) and (48) are identical to (38) and (37) respectively, then one may equate coefficients and the results are presented in table 2

Biot	de la Cruz and Spanos
ρ_{12}	ρ_{12}
Q	$K_f \delta_s$
R	$\eta_0 K_f - K_f \delta_f$
N	$(1 - \eta_0) \mu_s$
A	$(1 - \eta_0) K_s - K_s \delta_s - \frac{2}{3} (1 - \eta_0) \mu_s$

Table 2 Comparison of coefficients for the Biot (1956a) theory and the de la Cruz - Spanos theory (1989a).

In addition, Q and R must satisfy

$$K_f Q + K_s R = \eta_0 K_f K_s \quad (49)$$

which is equivalent to the relation (de la Cruz and Spanos, 1989a)

$$\frac{\delta_s}{\delta_f} = \frac{K_s}{K_f} \quad (50)$$

This final constraint (50) makes the form of the two sets of equations identical and thus the basic physical assumptions in the two theories appear to coincide when this constraint is imposed.

2.5 ROTATIONAL WAVES

Consider the propagation of a rotational wave by taking the curl of the system of equations (37), (38), (39) and (42). Introducing the following symbols

$$\Omega_f \equiv \nabla \times \bar{\mathbf{u}}^f \quad (51)$$

and

$$\Omega_s \equiv \nabla \times \bar{\mathbf{u}}^s \quad (52)$$

the equations of motion are

$$\rho_f \frac{\partial^2 \Omega_f}{\partial t^2} = \mu_f \nabla^2 \frac{\partial \Omega_f}{\partial t} - \frac{\mu_f \eta_0}{K} \frac{\partial}{\partial t} (\Omega_f - \Omega_s) + \frac{\rho_{12}}{\eta_0} \frac{\partial^2}{\partial t^2} (\Omega_f - \Omega_s) \quad (53)$$

$$\begin{aligned} \rho_s \frac{\partial^2 \Omega_s}{\partial t^2} = & \mu_s \nabla^2 \Omega_s + \frac{\mu_f \eta_0^2}{K (1 - \eta_0)} \frac{\partial}{\partial t} (\Omega_f - \Omega_s) - \\ & \frac{\rho_{12}}{(1 - \eta_0)} \frac{\partial^2}{\partial t^2} (\Omega_f - \Omega_s) \end{aligned} \quad (54)$$

and the heat equations are

$$\rho_f c_p^f \frac{\partial \bar{T}_f}{\partial t} - \kappa_f \nabla^2 \bar{T}_f + \frac{\gamma}{\eta_0} (\bar{T}_f - \bar{T}_s) = 0 \quad (55)$$

$$\rho_s c_v^s \frac{\partial \bar{T}_s}{\partial t} - \kappa_s \nabla^2 \bar{T}_s - \frac{\gamma}{1 - \eta_0} (\bar{T}_f - \bar{T}_s) = 0 \quad (56)$$

The equations of motion (53) and (54) are not coupled to the heat equations (55) and (56). This indicates that thermo-mechanical coupling does not affect the rotational waves.

The combination of (53) and (54) describe the motion of a rotational wave as observed at the macroscopic scale. Considering a plane wave , of the form $e^{i(kx - \omega t)}$, propagating in the x-direction with a component along the z-direction only, (53) and (54) become

$$\begin{aligned} & \left[\rho_f \omega^2 + i\omega\mu_f k^2 + i\omega \left(\frac{\mu_f \eta_0}{K} + i\omega \frac{\rho_{12}}{\eta_0} \right) \right] \Omega_f \\ & - i\omega \left(\frac{\mu_f \eta_0}{K} + i\omega \frac{\rho_{12}}{\eta_0} \right) \Omega_s = 0 \end{aligned} \quad (57)$$

and

$$\begin{aligned} & \left[\rho_s \omega^2 - \mu_s k^2 + \frac{i\omega\eta_0}{1 - \eta_0} \left(\frac{\mu_f \eta_0}{K} + i\omega \frac{\rho_{12}}{\eta_0} \right) \right] \Omega_s \\ & - \frac{i\omega\eta_0}{1 - \eta_0} \left(\frac{\mu_f \eta_0}{K} + i\omega \frac{\rho_{12}}{\eta_0} \right) \Omega_f = 0 \end{aligned} \quad (58)$$

Equating the determinant of coefficients to zero, one obtains a dispersion relationship of the form

$$A k^4 + B k^2 + C = 0 \quad (59)$$

where

$$A = \mu_s \mu_f \quad (60)$$

$$B = \frac{\mu_s \mu_f \eta_0}{K} - i\omega \left(\mu_s \rho_f + \frac{\mu_f^2 \eta_0^2}{K(1 - \eta_0)} - \frac{\mu_s \rho_{12}}{\eta_0} \right) - \omega^2 \left(\mu_f \rho_s - \frac{\mu_f \rho_{12}}{(1 - \eta_0)} \right) \quad (61)$$

$$C = i\omega^3 \rho_f \rho_s - \omega^2 \left(\frac{\mu_f \rho_s \eta_0}{K} + \frac{\mu_f \rho_f \eta_0^2}{K(1 - \eta_0)} \right) - i\omega \left(\frac{\rho_{12} \rho_f}{(1 - \eta_0)} + \frac{\rho_{12} \rho_s}{\eta_0} \right) \quad (62)$$

This dispersion relation yields two distinct physical solutions, and is the same as the one presented by de la Cruz and Spanos (1985) but with the addition of a term to account for relative acceleration between the fluid and solid components. It should be emphasized that thermo-mechanical effects do not affect these waves. Numerical examples illustrating the importance of relative acceleration will be presented later.

2.6 DILATATIONAL WAVES

The description of dilatational waves is obtained by taking the divergence of (37), (38), (39) and (42). Introducing the following notation

$$\varepsilon_f \equiv \nabla \cdot \bar{\mathbf{u}}_f \quad (63)$$

and

$$\varepsilon_s \equiv \nabla \cdot \bar{\mathbf{u}}_s \quad (64)$$

the equations of motion are

$$\begin{aligned} \rho_f \frac{\partial^2 \epsilon_f}{\partial t^2} = & -\nabla^2 \left[-K_f \epsilon_f - \frac{K_f}{\eta_0} (\delta_s \epsilon_s - \delta_f \epsilon_f) + K_f \alpha_f (\bar{T}_f - T_0) \right] \\ & + \mu_f \left[\nabla^2 \frac{\partial \epsilon_f}{\partial t} + \frac{1}{3} \nabla \left(\nabla \cdot \frac{\partial \epsilon_f}{\partial t} \right) \right] - \frac{\mu_f \eta_0}{K} \frac{\partial}{\partial t} (\epsilon_f - \epsilon_s) + \frac{\rho_{12}}{\eta_0} \frac{\partial^2}{\partial t^2} (\epsilon_f - \epsilon_s) \end{aligned} \quad (65)$$

$$\begin{aligned} \rho_s \frac{\partial^2 \epsilon_s}{\partial t^2} = & K_s \nabla^2 \epsilon_s - \frac{K_s}{1 - \eta_0} \nabla^2 (\delta_s \epsilon_s - \delta_f \epsilon_f) + \frac{4}{3} \mu_s \nabla^2 \epsilon_s \\ & + \frac{\mu_f \eta_0^2}{K (1 - \eta_0)} \frac{\partial}{\partial t} (\epsilon_f - \epsilon_s) - \frac{\rho_{12}}{1 - \eta_0} \frac{\partial^2}{\partial t^2} (\epsilon_f - \epsilon_s) - K_s \alpha_s \nabla^2 \bar{T}_s \end{aligned} \quad (66)$$

and the heat equations are

$$\begin{aligned} \rho_f c_p^f \frac{\partial \bar{T}_f}{\partial t} - T_0 \alpha_f K_f \frac{\partial}{\partial t} \left[-\epsilon_f - \frac{1}{\eta_0} (\delta_s \epsilon_s - \delta_f \epsilon_f) + \alpha_f \bar{T}_f \right] - \\ \kappa_f \nabla^2 \bar{T}_f + \frac{\gamma}{\eta_0} (\bar{T}_f - \bar{T}_s) = 0 \end{aligned} \quad (67)$$

$$\begin{aligned} \rho_s c_v^s \frac{\partial \bar{T}_s}{\partial t} - T_0 \alpha_s K_s \frac{\partial}{\partial t} \left[-\epsilon_s + \frac{1}{1 - \eta_0} (\delta_s \epsilon_s - \delta_f \epsilon_f) \right] \\ - \kappa_s \nabla^2 \bar{T}_s - \frac{\gamma}{1 - \eta_0} (\bar{T}_f - \bar{T}_s) = 0 \end{aligned} \quad (68)$$

If we assume a plane wave propagating in the x-direction with a component in the z-direction only, $e^{i(kx - \omega t)}$, one constructs a system of four equations with T_s , T_f , ϵ_s , ϵ_f , ω and k as variables. To obtain the dispersion relation (ω vs k) one must equate the determinant of coefficients to zero.

The set of equations may be written in matrix form as follows

$$\begin{bmatrix} A_{11} & A_{12} & A_{13} & A_{14} \\ A_{21} & A_{22} & A_{23} & A_{24} \\ A_{31} & A_{32} & A_{33} & A_{34} \\ A_{41} & A_{42} & A_{43} & A_{44} \end{bmatrix} \begin{bmatrix} \varepsilon_f \\ \varepsilon_s \\ \bar{T}_f - T_0 \\ \bar{T}_s - T_0 \end{bmatrix} = 0 \quad (69)$$

and the determinant as

$$\det \begin{vmatrix} A_{11} & A_{12} & A_{13} & A_{14} \\ A_{21} & A_{22} & A_{23} & A_{24} \\ A_{31} & A_{32} & A_{33} & A_{34} \\ A_{41} & A_{42} & A_{43} & A_{44} \end{vmatrix} = 0 \quad (70)$$

where

$$A_{11} = \left(\rho_f - \frac{\rho_{12}}{\eta_0} \right) \omega^2 - \left(K_f - \frac{K_f \delta_f}{\eta_0} \right) k^2 + \frac{4}{3} i \omega \mu_f k^2 + i \omega \frac{\mu_f \eta_0}{K} \quad (71)$$

$$A_{12} = - \frac{K_f \delta_s}{\eta_0} k^2 - i \omega \frac{\mu_f \eta_0}{K} + \frac{\omega^2 \rho_{12}}{\eta_0} \quad (72)$$

$$A_{13} = - K_f \alpha_f k^2 \quad (73)$$

$$A_{14} = 0 \quad (74)$$

$$A_{21} = - \frac{K_s \delta_f}{1 - \eta_0} k^2 - i \omega \frac{\mu_f \eta_0^2}{K(1 - \eta_0)} + \frac{\omega^2 \rho_{12}}{1 - \eta_0} \quad (75)$$

$$A_{22} = \left(\rho_s - \frac{\rho_{12}}{1 - \eta_0} \right) \omega^2 - \left(K_s - \frac{K_s \delta_s}{1 - \eta_0} \right) k^2 - \frac{4}{3} \mu_s k^2 + i \omega \frac{\mu_f \eta_0^2}{K(1 - \eta_0)} \quad (76)$$

$$A_{23} = 0 \quad (77)$$

$$A_{24} = K_s \alpha_s k^2 \quad (78)$$

$$A_{31} = i\omega T_0 \alpha_f K_f \left(\frac{\delta_f}{\eta_0} - 1 \right) \quad (79)$$

$$A_{32} = - \frac{i\omega T_0 \alpha_f K_f \delta_s}{\eta_0} \quad (80)$$

$$A_{33} = i\omega \left(T_0 \alpha_f^2 K_f - \rho_f c_p^f \right) + \kappa_f k^2 + \frac{\gamma}{\eta_0} \quad (81)$$

$$A_{34} = - \frac{\gamma}{\eta_0} \quad (82)$$

$$A_{41} = - \frac{i\omega T_0 \alpha_s K_s \delta_f}{1 - \eta_0} \quad (83)$$

$$A_{42} = i\omega T_0 \alpha_s K_s \left(\frac{\delta_s}{1 - \eta_0} - 1 \right) \quad (84)$$

$$A_{43} = - \frac{\gamma}{1 - \eta_0} \quad (85)$$

$$A_{44} = - i\omega \rho_s c_v^s + \kappa_s k^2 + \frac{\gamma}{1 - \eta_0} \quad (86)$$

Due to the complexity of this determinant an algebraic solution was determined using Mathematica™. However the algebraic result was very elusive and not physically transparent. Therefore, a numerical solution with numerical consistency checks, in various limiting cases, will be studied.

3. NUMERICAL SOLUTION

The numerical solution was programmed in FORTRANVS and executed on the University of Alberta mainframe computer. For the rotational waves, an algebraic solution for the equations of motion was determined yielding a dispersion relation (59). Therefore, the purpose of the numerical analysis is to illustrate the effects of the various component parameters and ρ_{12} on the phase velocity and attenuation of the rotational waves. The dilatational wave solution is much more complex. The terms in the determinant (70) are polynomials in ω and k and therefore a method of solution based on a cofactor expansion is utilized to obtain the dispersion relationship.

3.1 METHOD OF SOLUTION

The method of obtaining a solution for the dilatational waves is structured on the cofactor expansions of determinants (Campbell, 1977). The determinant of any square matrix can be cofactored into a series of two by two minor determinants by subsequent expansion about given rows or columns. The solution of a two by two determinant is simply the difference of the product of the diagonal elements. The program simply inverts the procedure used to cofactor a four by four determinant using multi-dimensional arrays (see figure 2) to store the coefficients of ω and k of the respective polynomial entries (71-86). The end solution is an array containing numerical values of the coefficients in the dispersion relation.

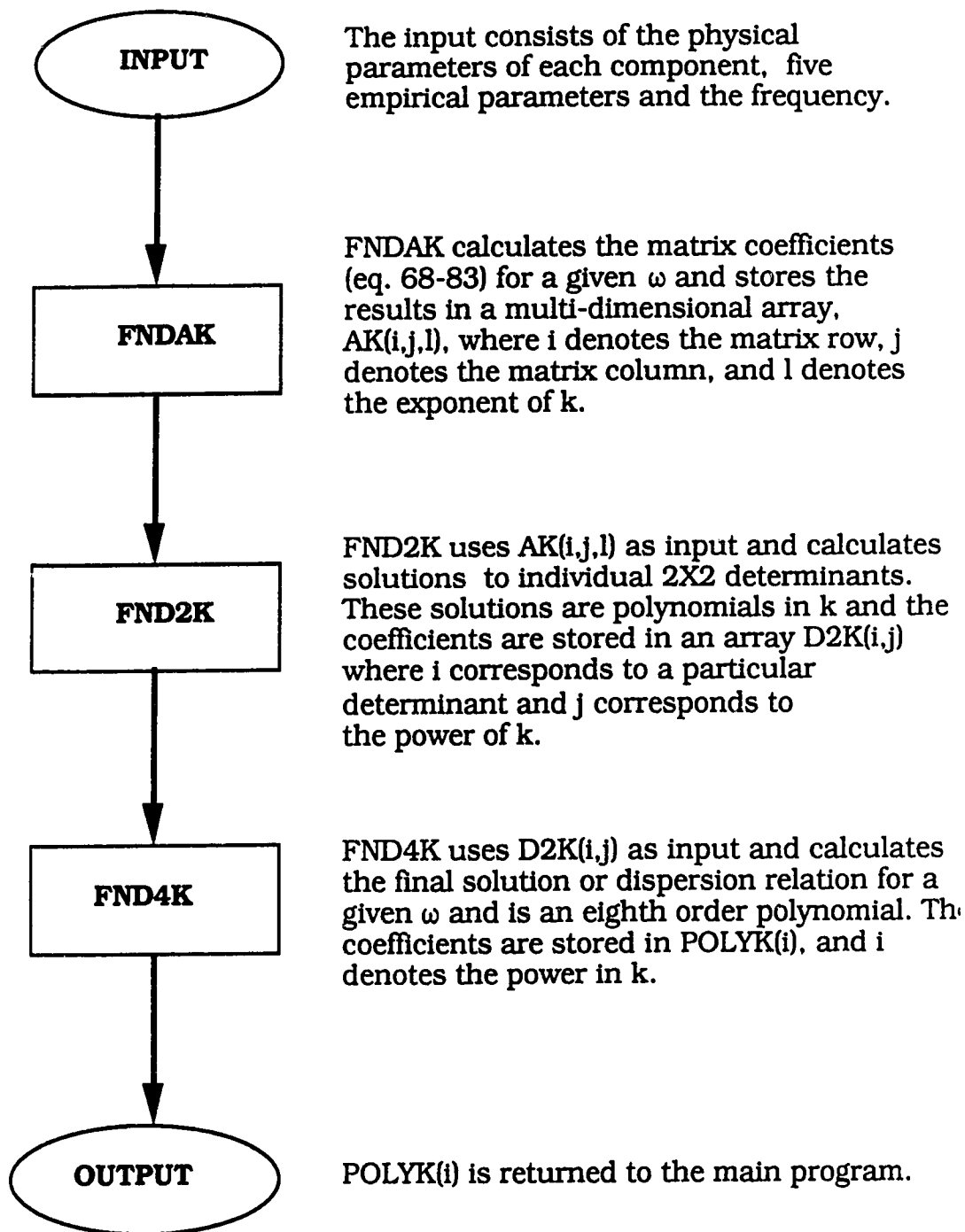


Figure 2 Procedure and array assignment for the numerical calculation of the dispersion relation for dilatational waves.

From this point on, the solution is similar for both dilatation and rotational waves. For a given ω the polynomial in k is determined. The roots to this polynomial are computed using a Newton-Raphson technique and are further refined using a secant method. In the case of the rotational waves and the non-thermal dilatational waves two roots exist, thereby implying the presence of two rotational and two dilational waves. When thermo-mechanical coupling is included four roots exist, suggesting the presence of four dilational waves. Two of these waves are primarily mechanical in nature whereas the other two are primarily thermal. These four waves should converge to two waves, ie first and second sound, in the solid or fluid limits. The rotational solution remains unchanged due to thermo-mechanical coupling.

3.2 EMPIRICAL PARAMETERS

The theory developed by de la Cruz and Spanos (1989a) contains five empirical parameters. They are permeability (K), induced mass coefficient (ρ_{12}), solid compliance factor (δ_s), fluid compliance factor (δ_f) and the inter-component heat conduction coefficient (γ). Ideally these parameters should be determined through some independent experiments. However, the objective of the next several sections is to show explicitly how these empirical parameters enter the theory, place physical constraints, based on analytic and numerical calculations, on the parameters and determine their regime of importance.

3.2.1 Permeability (K)

Permeability is a parameter used to quantify the resistance to flow of a fluid through a porous medium. It is a function of the size, orientation, distribution, and connectivity of the pores. This parameter is not unique to this theory, but has been introduced previously in Darcy's equation,

$$\vec{q} = \frac{-K}{\mu} (\vec{\nabla}p - \rho_f \vec{g}) \quad (87)$$

which is based on a classical experiment performed by Darcy (1856). The fluid pressure is denoted by p and has units Pa, μ is the fluid viscosity in Pa s, \vec{q} is the Darcy velocity in m/s, ρ_f is the density of the fluid in kg/m³, \vec{g} is the acceleration due to gravity in m/s², and K is the permeability in m². There are several methods of measuring permeability based on different forms of Darcy's equation. Most are performed by flowing a fluid of known viscosity through a porous medium at a specified pressure gradient and measuring the flow rate. Utilizing these measured values and the above equation one can calculate the permeability of the medium.

The permeability enters this theory through a physical argument to obtain a solution to a set of surface integrals. When the fluid equation of motion is volume averaged one obtains a surface integral of the form

$$\frac{1}{V} \int_{A_{sf}} [(p_f - p_0) \delta_{ik} - \sigma_{ik}^f] n_k dA \quad (88)$$

and the respective surface integral for the solid is

$$\frac{1}{V} \int_{A_{sf}} [p_0 \delta_{ik} + \sigma_{ik}^s] n_k dA \quad (89)$$

These integrals are opposites of each other and describe the force per unit volume exerted by one continua on the other across the interfaces due to any motion.

If one simplifies the analysis by de la Cruz and Spanos (1983), for two phase flow in a porous medium to account for only one fluid, (26) can be recast as follows

$$\frac{-1}{V} \int_{A_{sf}} [(p_f - p_0) \delta_{ik} - \sigma_{ik}^f] n_k dA = \eta_0 (\vec{\nabla} p_f - \rho_f \vec{g}) \quad (90)$$

Darcy's equation (87) is also a valid description for steady-state, single phase flow, and knowing that the Darcy velocity is equal to the porosity times the velocity at the interface, (90) becomes

$$\frac{-1}{V} \int_{A_{sf}} [(p_f - p_0) \delta_{ik} - \sigma_{ik}^f] n_k dA = -\frac{\eta_0^2 \mu_f}{K} \bar{v}_f \quad (91)$$

In this analysis there is an added complexity. One must allow for motion of the solid, which was not considered by de la Cruz and Spanos (1983). If one uses Stokes flow as an analogous situation then it is clear that (91) must be of the following form

$$\frac{-1}{V} \int_{A_{sf}} [(p_f - p_0) \delta_{ik} - \sigma_{ik}^f] n_k dA = - \frac{\eta_0^2 \mu_f}{K} (\bar{v}_f - \bar{v}_s) \quad (92)$$

where K is a scalar quantity, as long as the volume elements are assumed large enough that the porous medium is macroscopically homogeneous and isotropic.

Physically, (92) represents the momentum transfer between the fluid and solid across the solid-fluid interfaces during wave propagation. This is a significant attenuation mechanism which is known as Darcian resistance. It is dependent on the relative solid-fluid velocity and is therefore also dependent on the relative phase angles. It becomes the dominant attenuation mechanism at low viscosities.

The effect of permeability, K , on the phase velocity and attenuation is determined numerically for a water filled silica sand. The physical parameters for water (Childs, 1939; Weast, 1969) and the properties of a silica sand (Kappelmeyer and Haenel, 1974; Clark, 1966; Forsythe, 1959) are summarized in table 3. As one decreases the permeability it increases the coefficient in (92) therefore increasing the attenuation of the 1st P-wave (figure 3). However, it also changes the phase angle (figure 4) and relative magnitude (figure 5) between the solid and fluid velocities. In the extreme case where this effect (reduced value of $\bar{v}_f - \bar{v}_s$) overshadows the increased value of the coefficient we observe the maximum attenuation. The attenuation of the 1st S wave (figure 6) exhibits a similar dependence on permeability as the 1st P wave. The phase velocity of the 1st P wave

<u>Property</u>	<u>Symbol (units)</u>	<u>Value</u>
temperature	T_0 (°C)	2.0×10^1
porosity	η_0	3.0×10^{-1}
permeability ¹	K (m ²)	1.0×10^{-11}
solid density	ρ_s (kg/m ³)	2.65×10^3
fluid density	ρ_f (kg/m ³)	1.0×10^3
shear modulus	μ_s (Pa)	1.5×10^9
fluid viscosity	μ_f (Pa·s)	1.0×10^{-3}
solid bulk modulus	K_s (Pa)	3.5×10^{10}
fluid bulk modulus	K_f (Pa)	2.14×10^9
solid thermal expansion	α_s (°K ⁻¹)	3.00×10^{-6}
fluid thermal expansion	α_f (°K ⁻¹)	1.50×10^{-4}
solid heat capacity	c_v^s (J/(kg·°K))	7.25×10^2
fluid heat capacity	c_p^f (J/(kg·°K))	4.18×10^3
solid thermal conductivity	κ_s (J/(m·s·°K))	1.50×10^{-0}
fluid thermal conductivity	κ_f (J/(m·s·°K))	5.98×10^{-1}
induced mass coefficient ¹	ρ_{12} (kg/m ³)	0.00×10^0
solid compliance factor ¹	δ_s	4.44×10^{-1}
fluid compliance factor ¹	δ_f	2.71×10^{-2}
conduction coefficient ¹	γ (J/(m ³ ·s·°K))	2.50×10^7

1 - further discussion of these parameters in this section

Table 3 Physical properties properties of water and silica sand and the associated empirical parameters.

1st P-WAVE: Non Thermal Solution

Attenuation vs Log (K) vs f

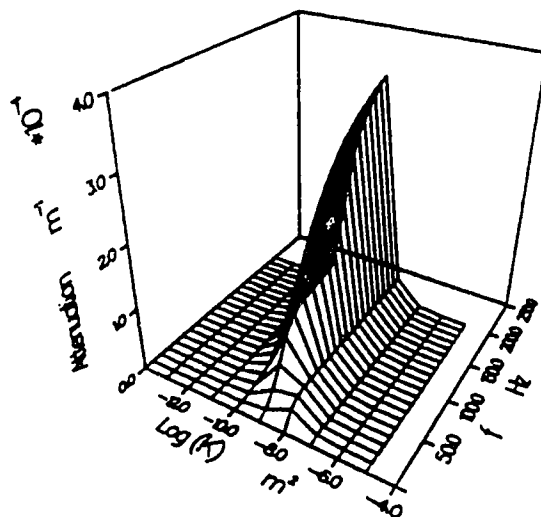


Figure 3 1st P-wave; Attenuation vs. log(K) vs. frequency.

1st P-WAVE: Non Thermal Solution

Phase Angle vs Log (K) vs f

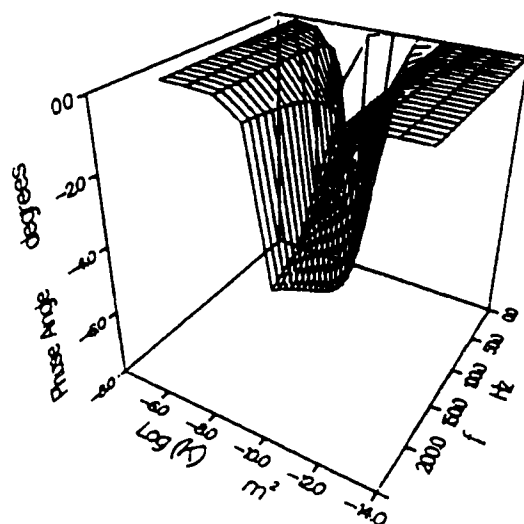


Figure 4 1st P-wave; Phase angle vs. log(K) vs. frequency.

1st P-WAVE: Non Thermal Solution

Relative Magnitude vs $\log(K)$ vs f

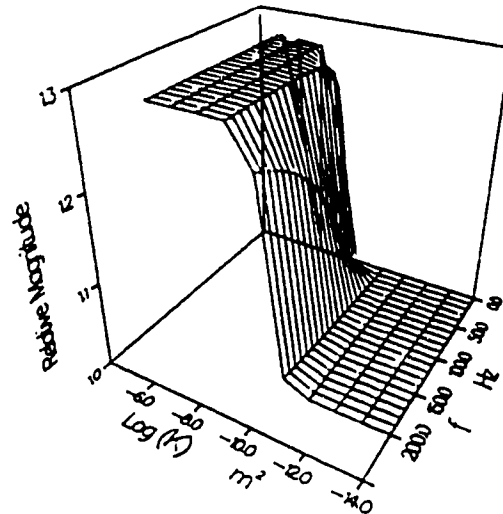


Figure 5 1st P-wave; Relative magnitude vs. $\log(K)$ vs. frequency.

1st S-WAVE:

Attenuation vs $\log(K)$ vs f

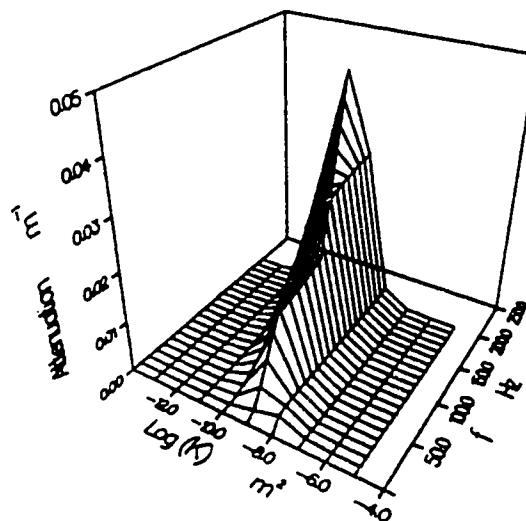


Figure 6 1st S-wave; Attenuation vs. $\log(K)$ vs. frequency.

(figure 7) and the 1st S-wave (figure 8) decreases with a decrease in permeability. The decrease in velocities is due to the interactions with the 2nd P-wave and 2nd S wave respectively.

In reducing the permeability to the zero limit and keeping the porosity constant one is essentially confining the individual pores such that the fluid is no longer a continuous medium. In this limit there should exist only one P wave and one S wave which reflects the convergence of the 1st and 2nd P wave and the 1st and 2nd S wave respectively. Support for only one P wave is evident by the zero phase angle (figure 4) and unity of relative magnitudes (figure 5) at very low permeabilities. The graphs of the 2nd P wave attenuation (figure 9) and phase velocity (figure 10) as a function of permeability conclusively show that this wave vanishes at low permeabilities.

In summary, permeability is an empirical parameter which can be measured by an independent experiment in the laboratory. Due to the assumptions used in the development of this theory, it is a scalar quantity but it need not be. Numerical study illustrates that permeability has a very small effect on the phase velocity of the 1st P-wave and 1st S-wave. However, there is a significant effect on the attenuation of these waves, within the seismic frequency range, for the particular situation studied.

1st P-WAVE: Non Thermal Solution

Phase Velocity vs $\log(K)$ vs f

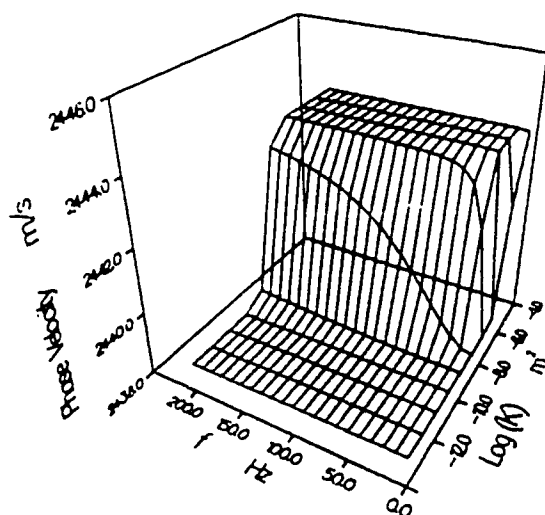


Figure 7 1st P-wave; Phase velocity vs. $\log(K)$ vs. frequency.

1st S-WAVE:

Phase Velocity vs $\log(K)$ vs f

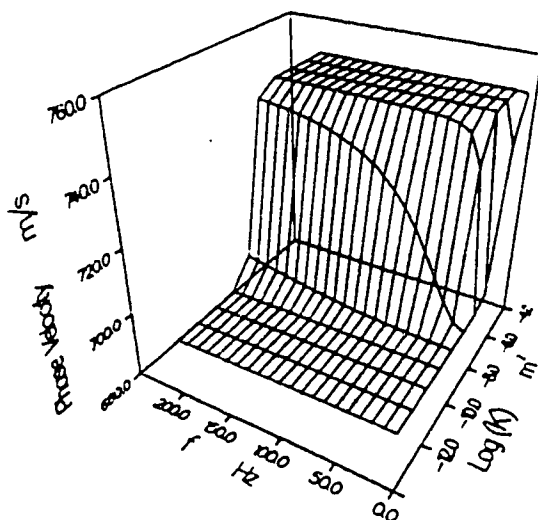


Figure 8 1st S-wave; Phase velocity vs. $\log(K)$ vs. frequency.

2nd P-WAVE: Non Thermal Solution

Attenuation vs Log (K) vs f

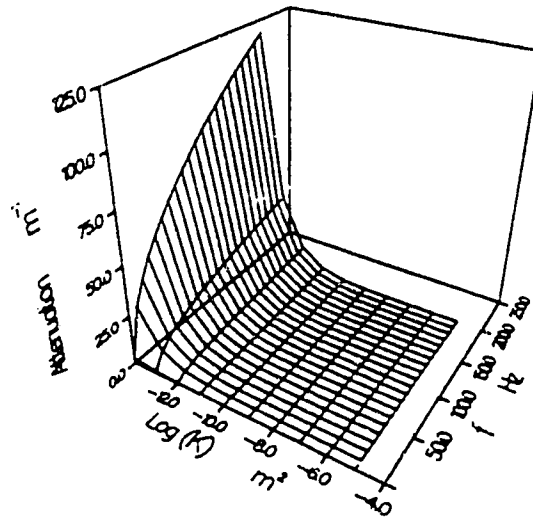


Figure 9 2nd P-wave; Attenuation vs. log(K) vs. frequency.

2nd P-WAVE: Non Thermal Solution

Phase Velocity vs Log (K) vs f

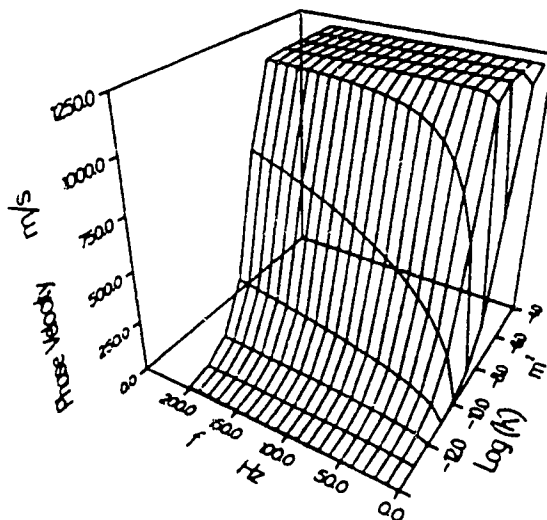


Figure 10 2nd P-wave; Phase velocity vs. log(K) vs. frequency.

3.2.2 Induced Mass Coefficient (ρ_{12})

In the previous description of momentum transfer across the solid-fluid boundary one obtains (92) under the assumption of steady flow. However, when a wave is propagating through a porous medium, inertial coupling between phases will exist. de la Cruz and Spanos (1989a) argue that inertial coupling can be accounted for by an extra term that is proportional to the relative acceleration.

$$\rho_{12} \frac{\partial}{\partial t} (\bar{\mathbf{v}}^f - \bar{\mathbf{v}}^s) \quad (93)$$

They have used the symbol ρ_{12} because when comparison with Biot's (1956a) theory is meaningful (cf 2.3) it is exactly the induced mass coefficient, ρ_{12} , of Biot.

Landau and Lifshitz (1975a) derived an expression for ρ_{12} based on a model of a rigid sphere oscillating in an incompressible perfect fluid. This discussion yields an upper bound for ρ_{12} , namely $\rho_{12} < 0$ which is determined by the directions of the applied forces and should therefore extend to more general cases. Berryman (1983) utilizes an approach similar to Landau and Lifshitz to arrive at the following expression:

$$\rho_{12} = -(\alpha - 1) \eta_0 \rho_f \quad (94)$$

for a model consisting of glass beads and helium gas. The coefficient, α , is restricted to be greater than unity and depends on the topology of the interconnected pore spaces. It is important to note that it is

straightforward to construct a gedanken experiment in which the roles of the fluid and solid are interchanged (a highly viscous fluid and a solid with a zero shear modulus). However, since equation (94) does not reflect this inherent symmetry it is unlikely it can be used for highly viscous fluids with a finite bulk modulus. Eastwood et al. (1990) conclude that a more general form for ρ_{12} is required which may depend on ρ_f , ρ_s , K_f , K_s , μ_f , δ_f and δ_s , and which incorporates the inherent symmetry.

The effect of the induced mass coefficient, ρ_{12} , on the phase velocity and attenuation is determined for a water filled silica sand. The limits on ρ_{12} values used are $\rho_{12}=0.0$ and $\rho_{12}= - \eta_0 \rho_f$. Choosing $\rho_{12}= - \eta_0 \rho_f$ is a common expression used for ρ_{12} in the literature (Eastwood et al., 1990).

The phase velocity of the 1st P-wave (figure 11), 1st S-wave (figure 12), 2nd P-wave (figure 13) and the 2nd S-wave (figure 14) decreases with a decreasing ρ_{12} . However, these changes are very small and are only evident when the frequencies are larger than about 10^4hz . Also at these higher frequencies the phase velocity becomes frequency dependent.

The attenuation of the 1st P-wave (figure 15), 1st S-wave (figure 16), and 2nd P-wave (figure 17) decreases with decreasing ρ_{12} , but is analogous to the velocity data. The changes only occur when the frequency is about 10^4hz or larger. The 2nd S-wave attenuation (figure 18) is very large and increases with decreasing ρ_{12} for frequencies larger than 10^4hz .

Similar results were observed in the study by Eastwood et al. (1990). They also investigated an oil filled silica sand, and reported that the frequency before ρ_{12} is important becomes much larger.

1st P-WAVE: Non Thermal Solution

Phase Velocity vs Log (f) vs ρ_{12}

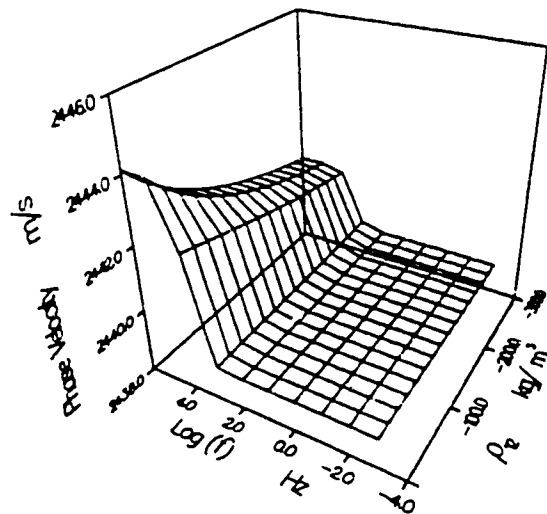


Figure 11 1st P-wave; Phase velocity vs. log(f) vs. ρ_{12} .

1st S-WAVE:

Phase Velocity vs Log (f) vs ρ_{12}

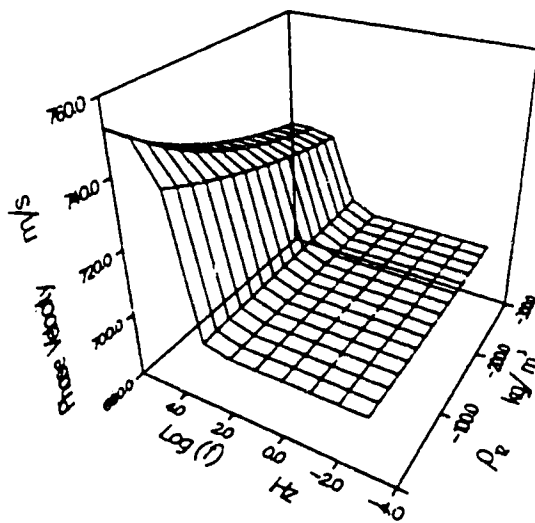


Figure 12 1st S-wave; Phase velocity vs. log(f) vs. ρ_{12} .

2nd P-WAVE: Non Thermal Solution

Phase Velocity vs $\text{Log}(f)$ vs ρ_{12}

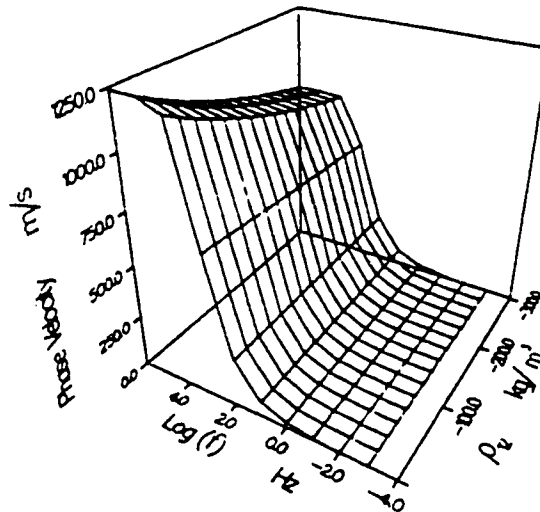


Figure 13 2nd P-wave: Phase velocity vs. $\text{log}(f)$ vs. ρ_{12} .

2nd S-WAVE:

Phase Velocity vs $\text{Log}(f)$ vs ρ_{12}

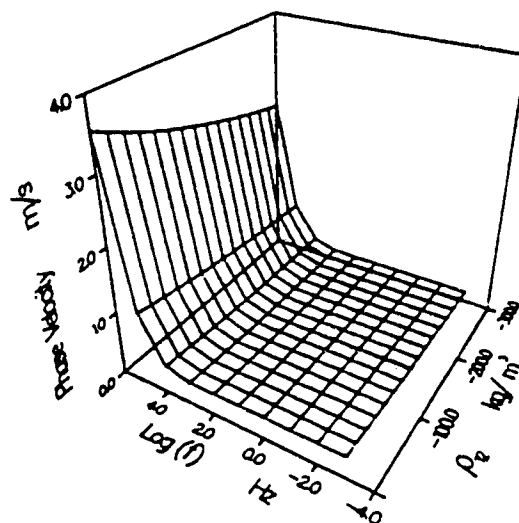


Figure 14 2nd S-wave: Phase velocity vs. $\text{log}(f)$ vs ρ_{12} .

1st P-WAVE: Non Thermal Solution

Attenuation vs Log (f) vs ρ_{12}

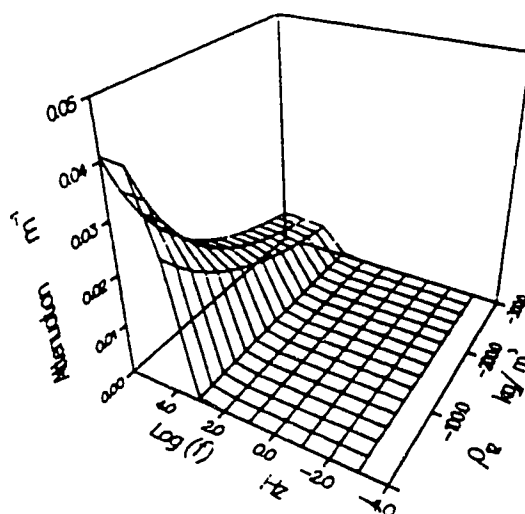


Figure 15 1st P-wave; Attenuation vs. log(f) vs. ρ_{12} .

1st S-WAVE:

Attenuation vs Log (f) vs ρ_{12}

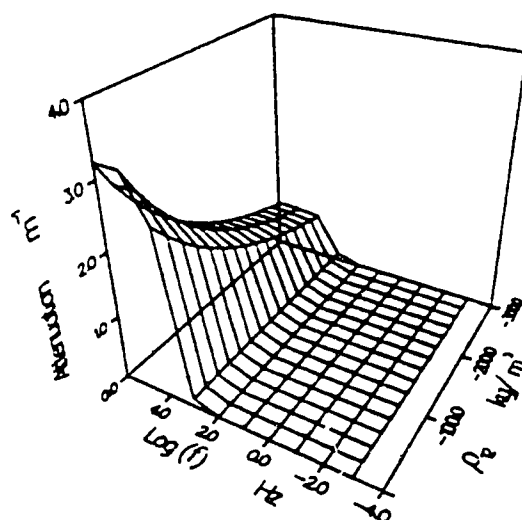


Figure 16 1st S-wave; Attenuation vs. log(f) vs. ρ_{12} .

2nd P-WAVE: Non Thermal Solution

Attenuation vs $\log(f)$ vs ρ_{12}

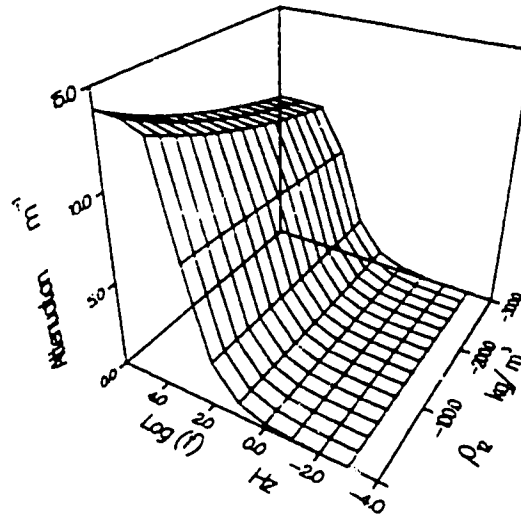


Figure 17 2nd P-wave: Attenuation vs. $\log(f)$ vs. ρ_{12}

2nd S-WAVE:

Attenuation vs $\log(f)$ vs ρ_{12}

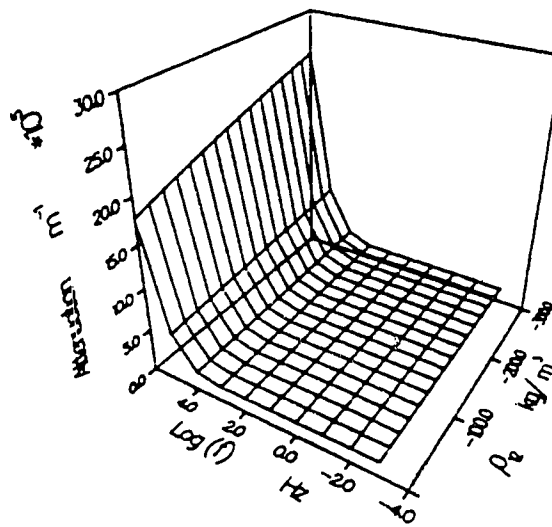


Figure 18 2nd S-wave: Attenuation vs. $\log(f)$ vs. ρ_{12}

The general result observed is that ρ_{12} can affect the phase velocity (very small) and the attenuation of P and S-waves. However, these changes occur at frequencies in excess of 10^4 hz for a water filled silica sand and at larger values for an oil filled silica sand. Therefore it can be concluded that ρ_{12} is an unimportant parameter when dealing with seismic waves.

A point of interest is that, if ρ_{12} is unimportant in the seismic frequency range and can be neglected, the S-wave solution obtained from the de la Cruz and Spanos (1989a) theory has only one empirical parameter, the permeability (K). This parameter was discussed in the previous section and there exists methods for measuring this parameter independently. Therefore, the resulting phase velocities and attenuation for the S-waves calculated using this theory are dependent only on the physical parameters of component materials.

3.2.3 Solid compliance factor (δ_s) and fluid compliance factor (δ_f)

In order to obtain a complete set of equations describing the propagation of a dilatational wave de la Cruz and Spanos (1989a) adopted relation (36)

$$\frac{\partial \eta}{\partial t} = \delta_s \nabla \cdot \bar{v}_s - \delta_f \nabla \cdot \bar{v}_f$$

where δ_s and δ_f are dimensionless empirical parameters. This dynamic relation is constructed at the macroscale since porosity is a macroscopic variable with no pore-scale meaning. If we consider a wave of the form $e^{-i\omega t}$ then equation (36) can be written as

$$\eta - \eta_0 = \delta_s \nabla \cdot \bar{\mathbf{u}}_s - \delta_f \nabla \cdot \bar{\mathbf{u}}_f \quad (95)$$

which appears to define the change in porosity, within a volume element, as the difference in the product of δ_s and the fractional change in volume of the solid and δ_f and the fractional change in volume of the fluid. The fractional change in volume of the solid is basically the dilatation due to the wave but the fractional change in volume of the fluid is the dilatation of the fluid and flow of the fluid in or out of the volume element.

A previous comparison with Biot's theory (1956a) provided a correlation between coefficients (cf table 2) and the additional constraint (50)

$$\frac{\delta_s}{\delta_f} = \frac{K_s}{K_f}$$

for the two theories to describe equivalent physical systems. This constraint (50) specifies uniquely one empirical parameter in terms of the other. Using this relationship (50) de la Cruz and Spanos (1989a) considered the case where the two average pressures, \bar{p}_s and \bar{p}_f , are regarded as approximately equal. Neglecting thermal effects in (32) and (33) they obtain a relationship for $\frac{\partial \eta}{\partial t}$ but with the following definite expressions for δ_s and δ_f

$$\delta_s = \frac{\eta_0 (1 - \eta_0)}{K_f \left[\frac{\eta_0}{K_f} + \frac{1 - \eta_0}{K_s} \right]} \quad (96)$$

and

$$\delta_f = \frac{\eta_0 (1 - \eta_0)}{K_s \left[\frac{\eta_0}{K_f} + \frac{1 - \eta_0}{K_s} \right]} \quad (97)$$

A numerical analysis illustrating the significance of δ_s and δ_f was carried out using the parameters for a water filled silica sand. There was a restriction imposed in the plot routines, which stipulates that adjacent points of opposite sign not be connected. Therefore, unconnected regions represent domains of attenuation or phase velocities of opposite sign. The attenuation as a function of δ_s and δ_f for 100 hz 1st P wave (figure 19) and a 100 hz 2nd P wave (figure 20) exhibits regions of positive and negative attenuations. Since negative attenuations are unphysical, the boundaries of such regions must represent a physical limit on the chosen combination of δ_s and δ_f for the given parameter set. The projection of these boundaries onto the δ_s - δ_f plane (figure 21) confines the region where physical combinations of δ_s and δ_f exist and is indicated by the shaded region. The two strongest constraints on δ_s and δ_f are observed in the 1st P wave solution. Also relationship (50) obtained from comparison with the Biot theory is not a sufficient condition for physical solutions to exist.

Further study indicates that the constraints on δ_s and δ_f discussed above are not affected by thermo-mechanical coupling. Comparing the attenuation as a function of δ_s and δ_f for a 5000 hz 1st P wave (figure 22) and a 5000 hz 2nd P wave (figure 23) with the 100 hz solution (figures 19 and 20) it is apparent that the constraint common to both the 1st and 2nd P waves is frequency dependent. However, the

1st P-WAVE: Non Thermal Solution

Attenuation vs δ_r vs δ_s

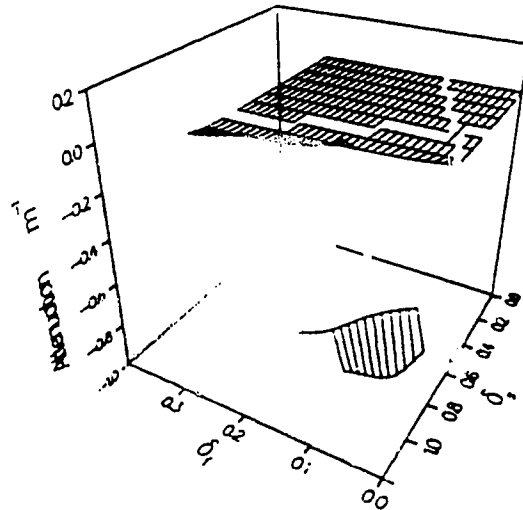


Figure 19 1st P-wave @ 100 hz; Attenuation vs. δ_s vs. δ_r

2nd P-WAVE: Non Thermal Solution

Attenuation vs δ_r vs δ_s

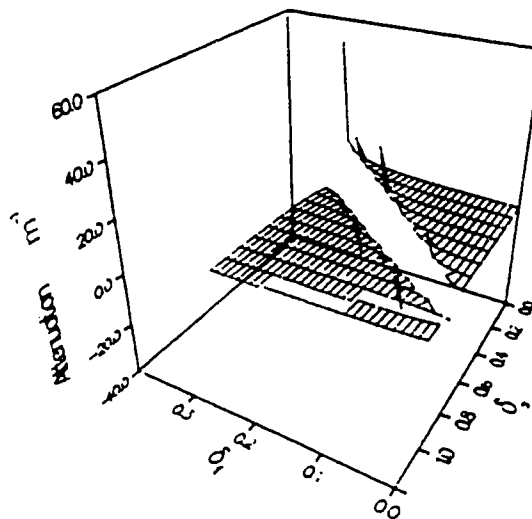


Figure 20 2nd P-wave @ 100 hz; Attenuation vs. δ_s vs. δ_r

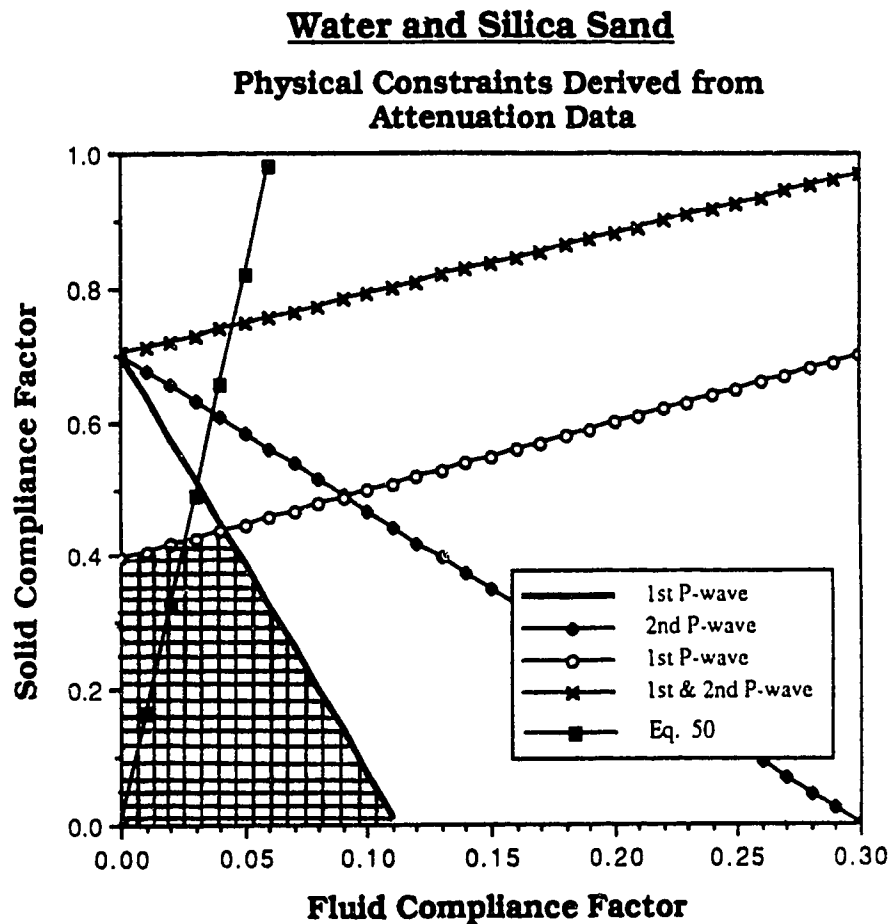


Figure 21 Projection of the constraints on the δ_s and δ_f plane. The line originating at the origin with positive slope is the line representing δ_s and δ_f values which concur with the Biot theory (cf equation (50)).

1st P-WAVE: Non Thermal Solution

Attenuation vs δ_r vs δ_s

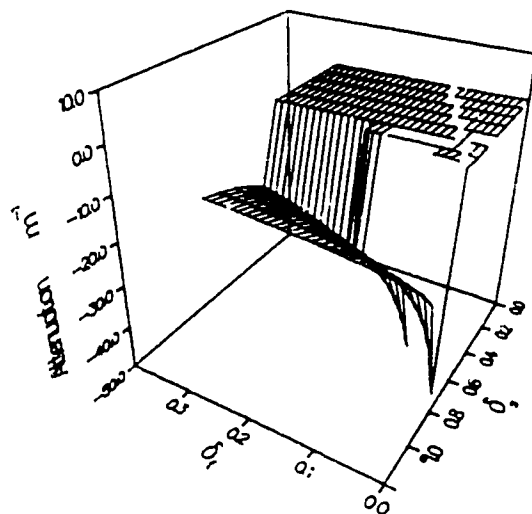


Figure 22 1st P-wave @ 5000 hz; Attenuation vs. δ_s vs. δ_r

2nd P-WAVE: Non Thermal Solution

Attenuation vs δ_r vs δ_s

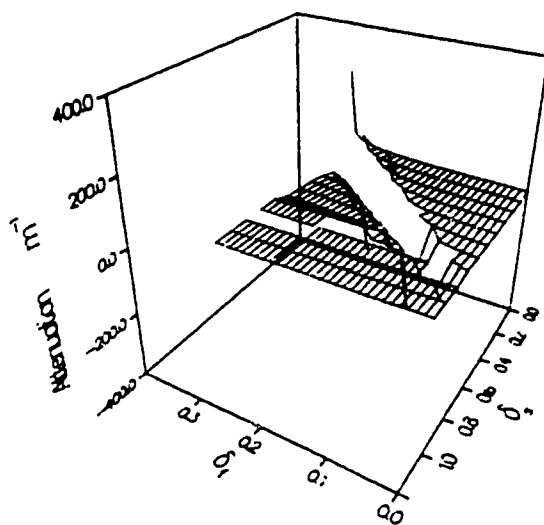


Figure 23 2nd P-wave @ 5000 hz; Attenuation vs. δ_s vs. δ_r

strongest constraints confining δ_s and δ_f are frequency independent.

Remaining within the physical region defined by the 1st P wave constraints and increasing the parameter δ_s and δ_f being calculated using constraint (50), causes a decrease in the 1st P wave phase velocity independent of frequency (figure 24). Increasing the parameter δ_s also causes a decrease in attenuation independent of frequency (figure 25). The parameter δ_s has a negligible effect on the 2nd P wave phase velocity (figure 26) and attenuation (figure 27) for this parameter set.

Numerical studies have constrained δ_s and δ_f to a narrow range of values on the basis that the theory yield solutions for waves with positive attenuation. However, these constraints may not necessarily be the strongest constraints. It has been illustrated that δ_s and δ_f have an effect on the phase velocity and attenuation of the P-waves within the seismic frequency range. They do not have any effect on the S-waves. Several definite expressions for δ_s and δ_f have been derived under particular assumptions. However, there is a great need for independent experiments which can measure δ_s and δ_f .

3.2.4 Intercomponent Conduction Coefficient (γ) .

The intercomponent conduction coefficient is introduced when de la Cruz and Spanos (1989a) explicitly take into account thermo-mechanical coupling. The physical argument for its introduction is very similar to that for the permeability aside from the fact that it deals with heat conduction rather than momentum transfer across the solid-fluid interfaces.

1st P-WAVE: Non Thermal Solution

Phase Velocity vs f vs δ_s

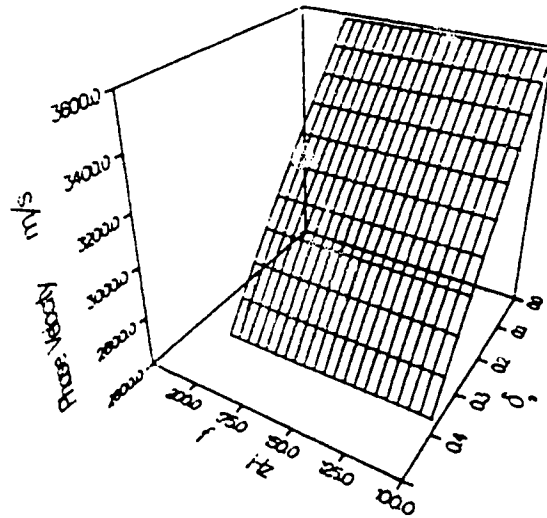


Figure 24 1st P-wave; Phase velocity vs. δ_s vs. frequency

1st P-WAVE: Non Thermal Solution

Attenuation vs f vs δ_s

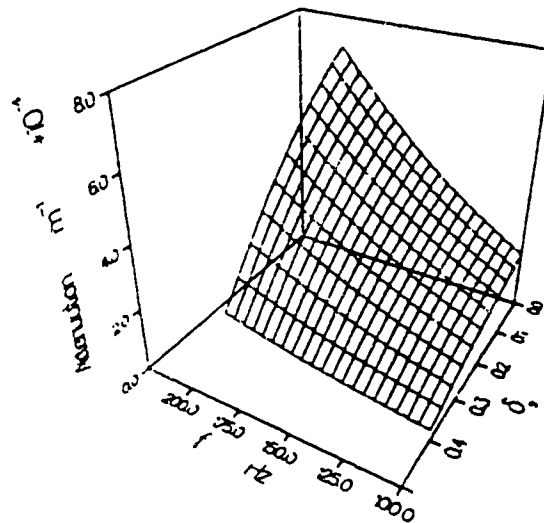


Figure 25 1st P-wave; Attenuation vs. δ_s vs. frequency

2nd P-WAVE: Non Thermal Solution

Phase Velocity vs f vs δ_s

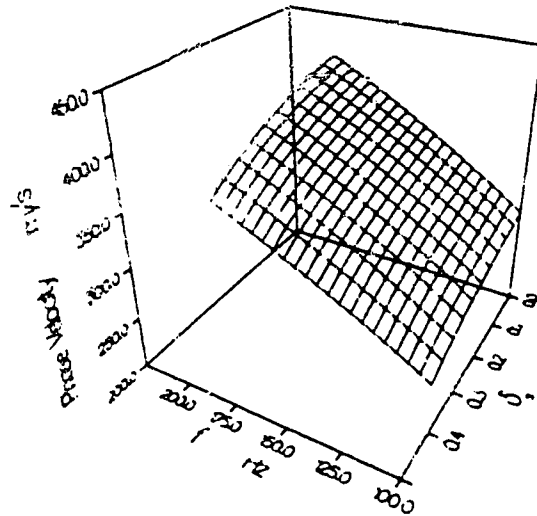


Figure 26 2nd P-wave: Phase velocity vs. δ_s vs. frequency

2nd P-WAVE: Non Thermal Solution

Attenuation vs f vs δ_s

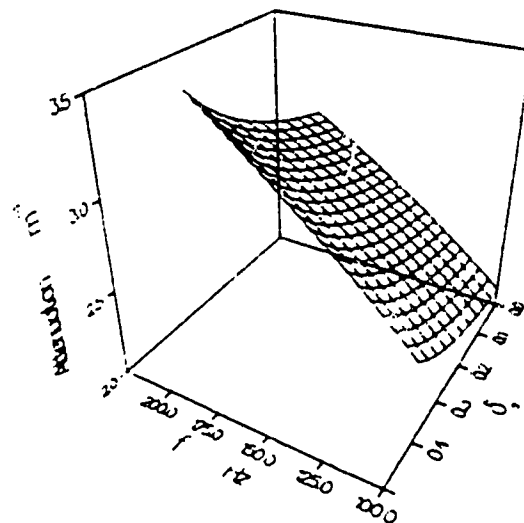


Figure 27 2nd P-wave: Attenuation vs. δ_s vs. frequency

When the equations describing the thermodynamics of the components (fluid and solid) are volume averaged de la Cruz and Spanos obtain a pair of surface integrals. For the fluid the surface integral is

$$\int_{A_{fs}} \kappa_f \nabla T_f \cdot d\vec{A} \quad (98)$$

and owing to the heat boundary condition (14) the surface integral for the solid is

$$\int_{A_{fs}} \kappa_s \nabla T_s \cdot d\vec{A} \quad (99)$$

These two integrals are equal and opposite and represent the heat transfer from one component to the other across the microscopic interfaces. It is discussed by de la Cruz and Spanos (1989a) that these heat exchange terms between components should vanish if and only if the macroscopic component temperatures are equal ($\bar{T}_f = \bar{T}_s$). It is therefore argued by de la Cruz and Spanos (1989a) that these terms may be represented by a first order scalar proportional to $(\bar{T}_s - \bar{T}_f)$ and therefore they obtain

$$\int_{A_{fs}} \kappa_f \nabla T_f \cdot d\vec{A} = \gamma (\bar{T}_s - \bar{T}_f) \quad (100)$$

where γ is the positive empirical parameter. The heat transfer,

between components, represented by this term should contribute to the attenuation of the dilatational waves. γ may be approximated as follows (de la Cruz and Spanos, 1989a)

$$\gamma \approx \frac{\bar{\kappa} A}{\ell V} \approx \frac{\bar{\kappa}}{\ell^2} \quad (101)$$

where $\bar{\kappa}$ is some average thermal conductivity, A is the area of the microscopic interfaces within volume element V and ℓ is a characteristic microscopic length.

When heat conduction is a "slow process", under certain conditions the local temperatures will be equal ($\bar{T}_s = \bar{T}_f$). Let $f^{-1} = \frac{2\pi}{\omega}$ be the period of disturbance then

$$\frac{\partial \bar{T}_f}{\partial t} \approx \frac{\Delta \bar{T}_f}{f^{-1}} \quad (102)$$

For the temperatures to be equalized through conduction one must have

$$\Delta \bar{T}_f \approx |\bar{T}_s - \bar{T}_f| \quad (103)$$

Substituting into the fluid heat equation (30) and neglecting the two middle terms, one finds

$$\rho_f c_p^f \eta_0 \frac{|\bar{T}_s - \bar{T}_f|}{f^{-1}} \approx \gamma |\bar{T}_s - \bar{T}_f| \quad (104)$$

and for the solid

$$\rho_s c_v (1 - \eta_0) \frac{|\bar{T}_s - \bar{T}_f|}{f^1} \approx \gamma |\bar{T}_s - \bar{T}_f| \quad (105)$$

A general estimate of the frequency below which there will be equality of local temperatures can be determined by cancelling $|\bar{T}_s - \bar{T}_f|$ from the equations and is

$$\omega \approx \frac{2\pi\gamma}{\rho c} \quad (106)$$

where ρc is some average heat capacity per unit volume.

The changes in attenuation (figure 28) of the 1st P-wave, for a water filled silica sand, due to γ can be explained using a similar argument as was previously used for permeability. However, this situation consists of a transfer of energy (heat) from one component to the other across the microscopic boundaries. If the heat is transferred from the solid to the fluid, ie $\bar{T}_s > \bar{T}_f$, it will promote motion in the fluid due to the thermal expansion. This added motion of the fluid will therefore create a larger attenuation. Therefore as one increases γ the attenuation increases but as γ increases the minimum frequency needed to equalize the component temperatures increases and can be approximated by (106). As the component temperatures approach each other it is obvious that $|\bar{T}_s - \bar{T}_f| \rightarrow 0$. There will exist a value for γ at a given frequency such that the value of $(\bar{T}_s - \bar{T}_f)$ will overshadow the importance of γ . At this point one observes a maximum in the attenuation. Further increases in γ make $(\bar{T}_s - \bar{T}_f)$ approach zero and will cause the change in attenuation due to the transfer of heat to decrease. The phase velocity (figure 29) also

1st P-WAVE: Thermal Solution
Attenuation vs f vs $\text{Log}(\gamma)$

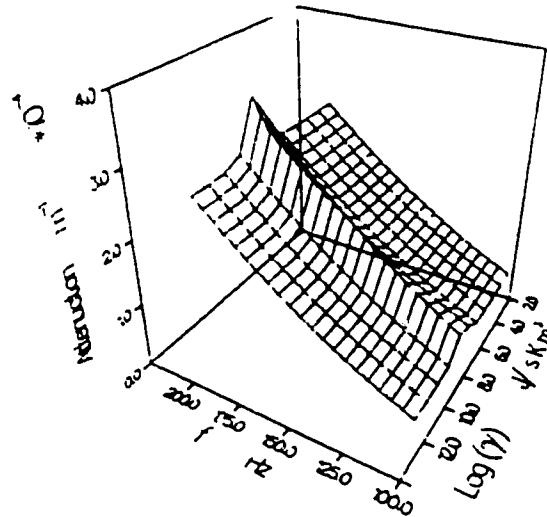


Figure 28 1st P-wave: Attenuation vs. $\log(\gamma)$ vs. frequency

1st P-WAVE: Thermal Solution
Phase Velocity vs f vs $\text{Log}(\gamma)$

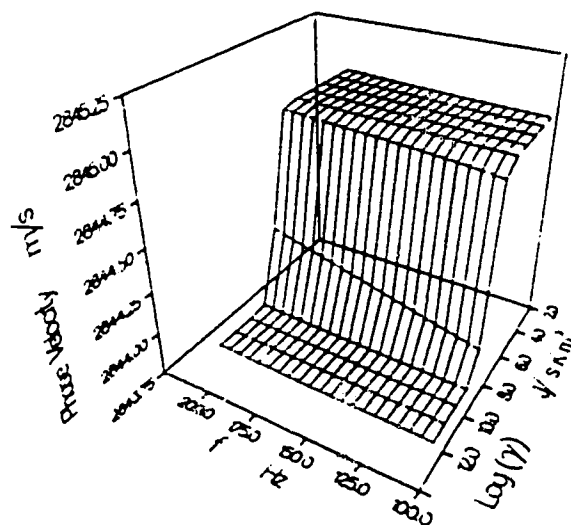


Figure 29 1st P-wave: Phase velocity vs. $\log(\gamma)$ vs. frequency

exhibits a very small change with changes in γ . This change is due to the interaction with the associated thermal wave.

Intercomponent heat conduction is present only when thermo-mechanical coupling is included and induces significant changes in attenuation of the 1st P-wave within the seismic frequency range. It can be approximated by (101) and becomes more important for small pore sizes. The frequency at which the equality of component temperatures exists depends on γ . No independent experiment for measuring this parameter exists at this time.

3.3 LIMITING CASES

The solution for waves propagating in an elastic solid or a compressible viscous fluid have been developed and are well established in the literature. The range of applicability of the de la Cruz - Spanos theory is illustrated by subjecting the theory to constraints indicative of such solid and fluid limits. These limiting cases also serve as numerical consistency checks on the computer algorithm.

3.3.1 Solid Limit.

The solid or elastic limit is obtained by equating the porosity of the porous medium to zero. In doing so, one must also consider the change in permeability, K , induced mass coefficient, ρ_{12} , and the intercomponent conduction coefficient, γ . As $\eta \rightarrow 0$ the permeability must also tend to zero. The induced mass coefficient, ρ_{12} , was shown

previously to be unimportant in the seismic frequency range and is therefore set to zero. An approximation for the intercomponent conduction coefficient, γ , was determined (cf. 3.2.4) and is dependent on the amount of solid - fluid interface and therefore as $\eta \rightarrow 0$ the amount of solid - fluid interface must also go to zero. Hence, as porosity goes to zero the intercomponent conduction coefficient, γ , must also go to zero.

Subjecting the macroscopic equations (37,38,39,42) to such a limit ($\eta=0$), one can show algebraically that the fluid equations vanish and the solid equations become

$$\rho_s \frac{\partial^2 \bar{\mathbf{u}}_s}{\partial t^2} = K_s \nabla (\nabla \cdot \bar{\mathbf{u}}_s) + \mu_s \left[\nabla^2 \bar{\mathbf{u}}_s + \frac{1}{3} \nabla (\nabla \cdot \bar{\mathbf{u}}_s) \right] - K_s \alpha_s \nabla \bar{T}_s \quad (107)$$

and

$$\rho_s c_v^s \frac{\partial \bar{T}_s}{\partial t} + T_0 K_s \alpha_s \frac{\partial \nabla \cdot \bar{\mathbf{u}}_s}{\partial t} - \kappa_s \nabla^2 \bar{T}_s = 0 \quad (108)$$

which are simply the equation of motion and equation of heat transfer in an elastic solid. For a wave propagating in an elastic solid (ignoring thermo-mechanical coupling), explicit expressions for the phase velocity of the mechanical and thermal waves can be obtained. For the mechanical P wave the velocity is calculated as

$$v_p^s = \sqrt{\frac{K_s + \frac{4}{3} \mu_s}{\rho_s}} \quad (109)$$

and for the mechanical S wave it is

$$v_s^s = \sqrt{\frac{\mu_s}{\rho_s}} \quad (110)$$

The phase velocity of the thermal wave is represented (Chadwick, 1970) as

$$v_{\text{thermal}}^s = \sqrt{\frac{2 \kappa_s \omega}{\rho_s c_v^s}} \quad (111)$$

and the attenuation per meter as

$$\xi_{\text{thermal}}^s = \sqrt{\frac{\rho_s c_v^s \omega}{2 \kappa_s}} \quad (112)$$

Using the physical parameters of a silica sand the calculated phase velocities for the mechanical motions are $v_p^s=3736$ m/s and $v_s^s=752$ m/s and the attenuation of these waves is zero. The phase velocity and attenuation of the thermal wave is $v_{\text{thermal}}^s = 3.1 \times 10^{-2}$ m/s and $\xi_{\text{thermal}}^s = 2.0 \times 10^4$ m⁻¹, respectively.

If one now includes the effect of heat conduction, ie. thermo-mechanical coupling, then there should be transfer between heat energy and mechanical energy associated with compressions and extensions of the medium. The compressed part becomes hot which leads to heat flow into the extended region. As a consequence this results in damping or attenuation of the waves. Furthermore, through thermal expansion, the temperature distribution will induce mechanical motions. If heat conduction is described as a wave propagation phenomenon (Achenbach, 1973), there will exist two P waves referred to as first and second sound. An analytic solution to

this coupled thermoelastic problem was determined by Chadwick (1960). Assuming a plane wave he obtained explicit expressions for the phase velocity and attenuation of the the two P waves, namely first and second sound. The phase velocities are represented by

$$v_{1P}^S = v_P^S \left[1 + \frac{\epsilon}{2(1 + \chi^2)} \right] \quad (113)$$

and

$$v_{2P}^S = v_P^S (2\chi)^{\frac{1}{2}} \left[1 - \frac{\epsilon(1 + \chi)}{2(1 + \chi^2)} \right] \quad (114)$$

and the attenuations (ξ) are given by

$$\xi_{1P}^S = \frac{\omega^*}{v_P^S} \left[\frac{\epsilon \chi^2}{2(1 + \chi^2)} \right] \quad (115)$$

and

$$\xi_{2P}^S = \frac{\omega^*}{v_P^S} \left(\frac{1}{2}\chi \right)^{\frac{1}{2}} \left[1 + \frac{\epsilon(1 - \chi)}{2(1 + \chi^2)} \right] \quad (116)$$

where

$$\omega^* = \frac{(v_P^S)^2 \rho_s c_v}{\kappa_s} \quad (117)$$

$$\chi = \frac{\omega}{\omega^*} \quad (118)$$

and

$$\varepsilon = \frac{9 K_s^2 \alpha_s^2 T_0}{\left(K_s + \frac{4}{3} \mu_s\right) \rho_s c_v^s} \quad (119)$$

v_p^s is the mechanical wave velocity when thermo-mechanical coupling is ignored and is calculated using expression (109).

The speed of the fast wave front is greater than the larger of the mechanical, v_p^s , or thermal, v_{thermal}^s wave velocity calculated when thermo-mechanical coupling is ignored. The speed of the slow wave is less than the smaller of the mechanical, v_p^s , or thermal, v_{thermal}^s wave velocity. The attenuation of the first sound (115) is an increasing function of the reduced frequency, χ , and will reach a finite value at frequencies approaching the characteristic value ω^* (Chadwick, 1960).

Expression (119) defines a dimensionless thermoelastic coupling constant and in most applications of thermoelasticity it will be a small number. For $\frac{v_{\text{thermal}}^s}{v_p^s} < \sqrt{1 + \varepsilon}$ the slow wave is essentially thermal and the fast wave is mechanical. For $\frac{v_{\text{thermal}}^s}{v_p^s} > \sqrt{1 + \varepsilon}$ the opposite is the case and the slow and fast waves are essentially mechanical and thermal respectively (Achenback, 1973).

Using the parameters of a silica sand (at a frequency of 100 hz) the fast wave will be the mechanical wave and the slow will be essentially the thermal wave. The phase velocity and attenuation of the fast wave, calculated using expressions (113) and (115), are $v_{1p}^s = 3755 \text{ m/s}$ and $\xi_{1p}^s = 3.0 \times 10^{-14} \text{ m}^{-1}$. The phase velocity and attenuation of the thermal wave, calculated using (114) and (116), are $v_{2p}^s = 3.10 \times 10^{-2}$

m/s and $\xi_{2P}^S = 2.0 \times 10^4 \text{ m}^{-1}$ respectively.

When thermo-mechanical coupling is included in the wave description for a porous medium (de la Cruz and Spanos, 1989a) the theory predicts four P waves. However, in the limiting case of an elastic solid two of these waves should vanish and the resulting waves should be the first and second sound discussed previously. The results of the numerical solution for the de la Cruz - Spanos (1989a) theory (with thermo-mechanical coupling included) is in agreement with the work of Chadwick (1960) and Achenbach (1973).

It can be shown algebraically that the de la Cruz - Spanos (1985, 1989a) theory simplifies to the elastic limit. When thermo-mechanical coupling is included the theory predicts the two P waves commonly referred to as first and second sound. These represent a modified elastic wave and a modified thermal wave associated with the energy transfer due to thermal conduction.

3.3.2 Fluid Limit

The fluid limit is obtained by equating the porosity of the porous medium to one. In doing so, one must again consider the change in permeability, K , induced mass coefficient, ρ_{12} , and the intercomponent conduction coefficient, γ . As $\eta \rightarrow 1$ the permeability must go to infinity. The induced mass coefficient, ρ_{12} , was shown previously to be unimportant in the seismic frequency range and is once again set to zero. An approximation for the intercomponent conduction coefficient, γ , (cf. 3.2) was determined which is dependent on the amount of solid - fluid interface. Hence, as porosity goes to one the intercomponent conduction coefficient, γ , must go to

zero.

Equating the porosity to one ($\eta=1$) in the macroscopic equations (37,38,39,42), one can algebraically show that the solid equations vanish and the fluid equation of motion is

$$\rho_f \frac{\partial^2 \bar{\mathbf{u}}^f}{\partial t^2} = -\nabla[-K_f \nabla \cdot \bar{\mathbf{u}}^f + K_f \alpha_f T_f] + \mu_f \left[\nabla^2 \frac{\partial \bar{\mathbf{u}}^f}{\partial t} + \frac{1}{3} \nabla \left(\nabla \cdot \frac{\partial \bar{\mathbf{u}}^f}{\partial t} \right) \right] \quad (120)$$

and the equation of heat transfer is

$$(\rho_f c_p^f - T_0 \alpha_f^2 K_f) \frac{\partial \bar{T}_f}{\partial t} + T_0 \alpha_f K_f \frac{\partial}{\partial t} \nabla \cdot \bar{\mathbf{u}}^f - \kappa_f \nabla^2 \bar{T}_f = 0 \quad (121)$$

These are simply the equations for a viscous compressible fluid. Unlike perfect fluids, a viscous fluid can sustain both dilatational and rotational waves. Also, due to internal friction, a part of the mechanical energy is converted to heat thereby attenuating the wave. The solution for waves propagating in a viscous compressible fluid is presented by Bhatia and Singh (1986). The phase velocity of the P wave is given by

$$v_p^f = \sqrt{\frac{K_f}{\rho_f}} \quad (122)$$

and the attenuation per meter is

$$\xi_p^f = \frac{\omega^2}{2 v_p^f \omega_v} \quad (123)$$

where

$$\omega_v = \frac{\rho_f v_p^f}{\frac{4}{3} \mu_f} \quad (124)$$

is known as the viscosity relaxation frequency. In order for the above expression for phase velocity and attenuation to be valid,

$$\frac{\omega}{\omega_v} \ll 1. \quad (125)$$

It is important to note that for highly viscous fluids, ie. larger values of μ_f , ω_v will become smaller such that condition (125) is no longer satisfied at particular frequencies. The results obtained using the Navier - Stokes equation (120) will not be correct, therefore condition (125) is a built in limitation for the Navier - Stokes equation (Bhatia and Singh, 1986).

Considering the rotational motion or vorticity of a viscous fluid gives rise to shear waves which are usually known as viscous waves (Bhatia and Singh, 1986). Taking the curl of the Navier - Stokes equation (120) and assuming a plane wave the velocities of propagation and attenuations are

$$v_s^f = \sqrt{\frac{2 \mu_f \omega}{\rho_f}} \quad (126)$$

and

$$\xi_s^f = \sqrt{\frac{\rho_f \omega}{2 \mu_f}} \quad (127)$$

indicating that these viscous waves are dispersive and very highly attenuated. However, for fluids of high viscosity they will be less damped and propagate at higher velocity.

The phase velocity of the thermal wave, without thermo-mechanical coupling, travelling in viscous compressible fluid is denoted by

$$v_{\text{thermal}}^f = \sqrt{\frac{2 \kappa_f \omega}{\rho_f c_p^f - T_0 \alpha_f^2 K_f}} \quad (128)$$

and attenuation per meter is

$$\xi_{\text{thermal}}^f = \sqrt{\frac{(\rho_f c_p^f - T_0 \alpha_f^2 K_f) \omega}{2 \kappa_f}} \quad (129)$$

Using the physical parameters for water, the calculated phase velocity and attenuation for the P wave is $v_p^f = 1462.873$ m/s and $\xi_p^f = 8.407 \times 10^{-11}$ m⁻¹. The phase velocity and attenuation of the viscous wave is $v_s^f = 3.5449 \times 10^{-2}$ m/s and $\xi_s^f = 1.77245 \times 10^4$ m⁻¹ respectively. The phase velocity and attenuation of the thermal wave is $v_{\text{thermal}}^f = 1.34 \times 10^{-2}$ m/s and $\xi_{\text{thermal}}^f = 4.7 \times 10^4$ m⁻¹. The latter two waves are very highly attenuated and would probably not be observed in most physical situations.

Including thermo-mechanical coupling in the analysis will not affect the S wave. However there will now exist two P waves, first and second sound, and the previously described P wave should be altered due to energy transfer by thermal conduction. Solving the coupled differential equations (120 and 121) one obtains the following expressions for the phase velocity and attenuation of the pseudo-

mechanical wave

$$(v_{1P}^f)^2 = \gamma^* (v_P^f)^2 \quad (130)$$

and

$$\xi_{1P}^f = \frac{2 \mu_f \omega^2}{3 \rho_f (v_P^f)^3} + \frac{\kappa_f (\gamma^* - 1) \omega^2}{2 \rho_0 c_p^f (v_P^f)^2 v_{1P}^f} \quad (131)$$

and for the pseudo-thermal wave

$$v_{2P}^f = \sqrt{\frac{2 \kappa_f \omega}{\rho_0 c_p^f}} \quad (132)$$

and

$$\xi_{2P}^f = \sqrt{\frac{\rho_0 c_p^f \omega}{2 \kappa_f}} \quad (133)$$

where

$$\gamma^* = \frac{c_p}{c_v} \quad (134)$$

is the ratio of heat capacities. The attenuation due to heat conduction in solids will be less than for fluids since $\gamma_{\text{solid}}^* < \gamma_{\text{fluid}}^*$ (Bhatia and Singh, 1986). The attenuation of 1st P wave (131) is the sum of attenuation due to viscosity (123) and attenuation due to thermal conduction and is called classical absorption (Bhatia and Singh, 1986). Once again using parameters indicative of water one can calculate the phase

velocities and attenuations for the two P waves. The phase velocities are $v_{1P}^f = 1465.35$ m/s, $v_{2P}^f = 1.34081 \times 10^{-2}$ m/s and the attenuations are $\xi_{1P}^f = 8.41019 \times 10^{-11}$ m⁻¹ and $\xi_{2P}^f = 4.68611 \times 10^4$ m⁻¹ for the pseudo-mechanical wave and pseudo-thermal wave, respectively, assuming a frequency of 100 Hz. The phase velocity of the first sound v_{1P}^f and attenuation ξ_{1P}^f are slightly greater than the respective phase velocity v_p^f and attenuation ξ_p^f calculated without thermo-mechanical coupling as is expected.

3.3.3 Numerical Calculation of Limits.

In performing the numerical calculations for the solid and fluid limiting cases the induced mass coefficient, ρ_{12} , is set to zero since it was shown previously to be unimportant in the seismic frequency range. The intercomponent conduction coefficient, γ , is set to be very small (order of 10^{-15}) since it is dependent on the amount of solid - fluid interface which becomes non-existent in the solid and fluid limits. The solid, δ_s , and fluid, δ_f , compliance factors describe the change in relative proportions of the constituent materials to the change volume of these materials, therefore, in the solid limits these parameters should tend to zero and are given small values of the order of 10^{-10} . Hence, with the above mentioned constraints and the properties of water and silica sand the phase velocities and attenuations of the P and S waves are calculated as functions of porosity and permeability. It is important to recognize that the de la Cruz-Spanos theory predicts two P and two S waves without thermo-mechanical coupling and four P waves and two S wave when thermo-

mechanical coupling is included.

The phase velocity (figure 30) of the 1st P wave is illustrated as a function of porosity and permeability, calculated without thermo-mechanical coupling. The phase velocity of the 2nd P wave is shown in figure 31. This 2nd P wave is not the pseudo-thermal wave (second sound) described previously, since thermo-mechanical coupling is not included in this calculation. It is the other mechanical wave present due to the interaction of the fluid and solid continua. If one now chooses values of permeability and porosity indicative of the solid and fluid limits one observes that the 1st P wave velocity tends to the phase velocity calculated for the elastic limit, whereas the 2nd P-wave phase velocity tends to the phase velocity calculated in the fluid limit. Therefore, one sees that the numerical the solution becomes decoupled in these limits and the 1st P wave represents the solid limit and the 2nd P wave represents the fluid limit. The attenuation of the 1st and 2nd P waves behave similarly.

The phase velocity of the 1st S (figure 32) and 2nd S (figure 33) behave in a similar fashion. For values of porosity and permeability characteristic of the solid and fluid limits the phase velocity of the 1st S wave is equal the shear wave velocity propagating in an elastic solid with the properties of silica sand. The 2nd S wave phase velocity is very close to zero since it is basically the viscous wave propagating in the fluid which in this case is water.

When thermo-mechanical coupling is included analogous character of the phase velocity and attenuation of the of the was is observed. The numerically calculated values of the phase velocity and attenuation of the S waves and P waves (both mechanical and thermal) are in agreement with the values calculated in the solid (cf. 3.31) and fluid

1st P-WAVE: Non Thermal Solution

Phase Velocity vs η vs Log (K)

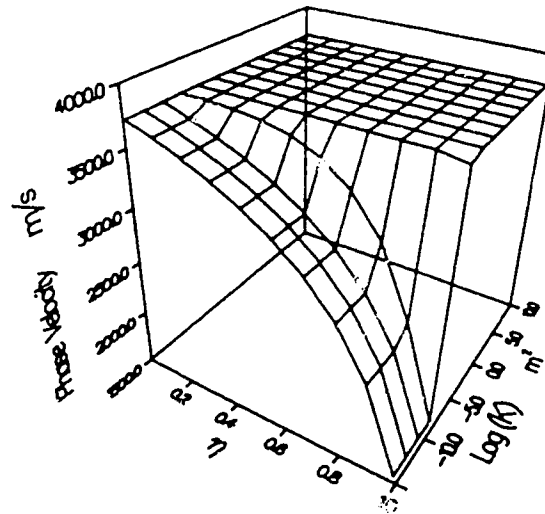


Figure 30 1st P wave; Phase velocity vs. porosity vs. permeability, illustrating the convergence of the numerical solution in the solid and fluid limits.

2nd P-WAVE: Non Thermal Solution

Phase Velocity vs η vs Log (K)

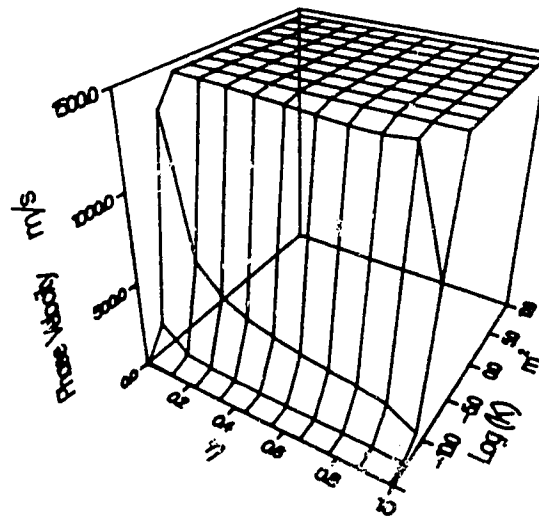


Figure 31 2nd P wave; Phase velocity vs. porosity vs. permeability, illustrating the convergence of the numerical solution in the solid and fluid limits.

1st S-WAVE:

Phase Velocity vs η vs Log (K)

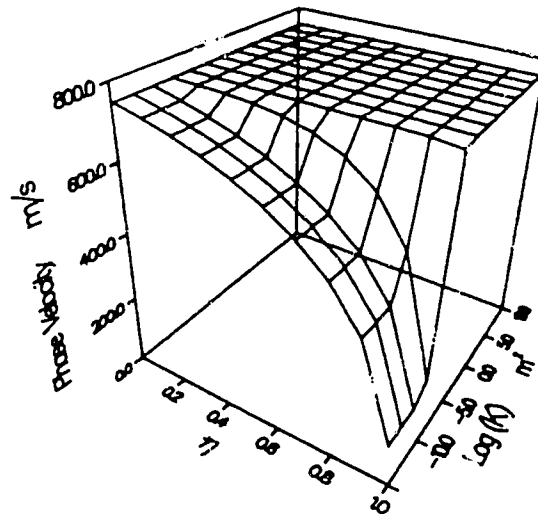


Figure 32 1st S wave; Phase velocity vs. porosity vs. permeability, illustrating the convergence of the numerical solution in the solid and fluid limits.

2nd S-WAVE:

Phase Velocity vs η vs Log (K)

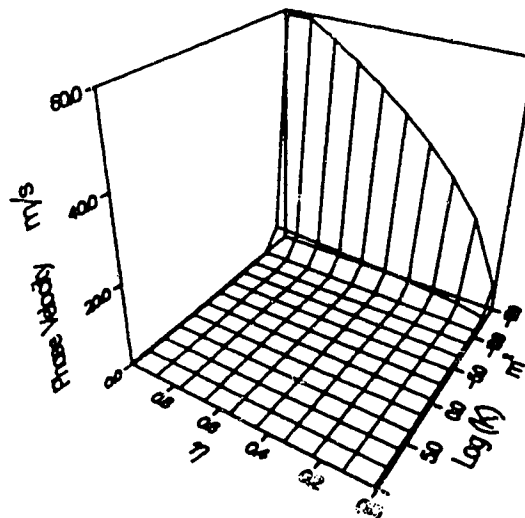


Figure 33 2nd S wave; Phase velocity vs. porosity vs. permeability, illustrating the convergence of the numerical solution in the solid and fluid limits.

(cf. 3.32) limits. The decoupling of the numerical solution in the limits still exists.

The adopted method of solution based on the cofactor expansion becomes decoupled in the solid and fluid limits. However, it is important that one specify proper functional forms for the empirical parameters when constructing such limiting cases. Values of phase velocity and attenuation calculated using the numerical algorithm and algebraic expressions are in good agreement for both the solid and fluid limit. When thermo-mechanical coupling is included the theory predicts two dilational waves in these limits commonly known as first

and sound. The S wave or viscous wave and the 2nd P-wave (second sound) have very low propagation velocities and high attenuations. These waves would not be detected for this given case; however, their importance might be visible due to their coupling effect with the observed waves propagating in a porous medium.

4. CASE STUDIES

Seismic studies are used extensively to image structures beneath the earth's surface. Hydrogeologists and engineers use seismic techniques to define near surface features needed in groundwater exploration and geotechnical investigations. They are used extensively by the petroleum industry for the delineation of features which could be indicative of possible oil or gas reservoirs and more recently in monitoring recovery techniques used in heavy oil reservoirs. They are also used for exploring the deep interior of the earth by interpretation of global seismic events such as earthquakes or large explosions.

The theory commonly used in the modelling of seismic data is based on the fundamental assumption that the encompassing material is a perfectly elastic solid. However, it is evident that this assumption is not valid for the majority of materials within the earth. For instance the near surface material, studied by hydrogeologists and engineers, is better characterized as a porous matrix whose pores are primarily saturated with air and water above the water table and fully saturated with water below the water table. Also petroleum reservoirs can be more accurately modelled using a porous medium. In this case the pores are filled by various saturations of gas, oil and water. The composition and characteristics of materials within the deep earth is a topic of present day research. The solids may not behave elastically, but in a plastic or viscoelastic fashion and the fluids may or may not behave as Newtonian fluids. Although the theory discussed here does not account for such behavior, the presence of fluids within a solid matrix may help explain observed anomalies within the deep earth

(e.g. low velocity zone). The change in physical character, such as viscosity, of the fluid within the solid matrix may have a significant effect on the seismic signal, for example attenuation. Conventional elastic theory cannot account for such changes. However, these deviations could be of major importance when seismic techniques are used as a monitoring tool.

The application of the de la Cruz - Spanos theory to several physical situations related to various disciplines will be compared with predictions obtained from conventional elastic theory. Furthermore, a comparison of the de la Cruz - Spanos theory with and without thermo-mechanical coupling will be examined.

4.1 AIR FILLED SILICA SAND

This model consists of a porous elastic matrix fully saturated with air. This type of model may be used for near surface layers, if one can neglect any water saturation. It is also a possible model for natural gas reservoirs assuming the in-situ properties of the gas are similar to air. The physical parameters for air are readily available (Weast, 1969; Childs, 1939) and are presented along with the associated empirical parameters in table 4. Values for the empirical parameters are such that they obey previously discussed restrictions which are necessary for the solution to yield physically consistent results. The solid is assumed to have the properties of a silica sand (Kappelmeyer and Haenel, 1974; Clark, 1966; Forsythe, 1959) and are listed in table 3. In all the models discussed in this work the sand grains will not be allowed to slip relative to each other. This assumption has been shown by a number of authors to be fully justified since grain slippage results in nonlinear wave propagation (Mindlin and Dersiewicz, 1953;

Knopoff and McDonald, 1960; White, 1966; Walsh, 1966; Mavko, 1979) while experimental evidence, at least in the presence of fluids with viscosities indicative of water and light oil, indicates that at seismic strains, attenuation is dominated by linear processes (Pandit and Savage, 1973; Brennan and Stacey, 1977).

<u>Property</u>	<u>Symbol</u>	<u>Value</u>
temperature	T_0	2.00×10^1
porosity	η_0	3.00×10^{-1}
permeability	K	1.00×10^{-11}
fluid density	ρ_f	1.21×10^0
fluid viscosity	μ_f	1.82×10^{-5}
fluid bulk modulus	K_f	9.00×10^4
fluid thermal expansion	α_f	3.43×10^{-3}
fluid heat capacity	c_p^f	1.00×10^3
fluid thermal conductivity	κ_f	2.52×10^{-2}
induced mass coefficient	ρ_{12}	0.00×10^0
solid compliance factor	δ_s	3.70×10^{-1}
fluid compliance factor	δ_f	9.51×10^{-7}
conduction coefficient	γ	5.00×10^7

Table 4 Properties of air and the associated empirical parameters

The phase velocity and attenuation of dilatational and rotational waves were calculated previously for the elastic limit (c.f. 3.3.1). In the case considered here, the porosity is assumed to be 30%.

The phase velocity of the 1st P-wave (figure 34) is frequency

independent and is approximately 35% lower than the value calculated in the elastic limit. This degree of change in phase velocity would be easily detected in seismic studies. The attenuation of the 1st P-wave (figure 35) increases with increasing frequency but the magnitude of the attenuation is small for the frequency range (0 - 200 hz) considered. The 2nd P-wave exhibits a frequency dependent phase velocity (figure 36) and attenuation (figure 37). The magnitude of the phase velocity is small but the attenuation is several orders of magnitude larger than the 1st P-wave. This wave might be detected in a controlled laboratory experiment but is unlikely to be observed in field data. It is important to point out that this wave is not the thermal wave (i.e. second sound) which is described when thermo-mechanical coupling is included in the elastic limit. It is primarily a mechanical disturbance propagating through the fluid which is modified by interactions with the solid component. The de la Cruz - Spanos theory does predict two more P-waves, when thermo-mechanical coupling is included, which are analogous to second sound in the elastic limit. Each thermal wave is associated with one of the respective mechanical waves; however, there is an interaction between all four P-waves. The attenuation of these latter two P waves is extremely large ($\sim 10^4 \text{ m}^{-1}$). Thermo-mechanical coupling does not effect the 1st P wave for the case considered here since the non-thermal and thermal solutions overlay one another in figures 34 and 35.

The phase velocity of the 1st S-wave (figure 38) is frequency independent and is equal to the value calculated in the elastic limit. Due to the low viscosity of air, the solid - fluid coupling is almost non-existent and therefore the fluid effect on the 1st S wave travelling

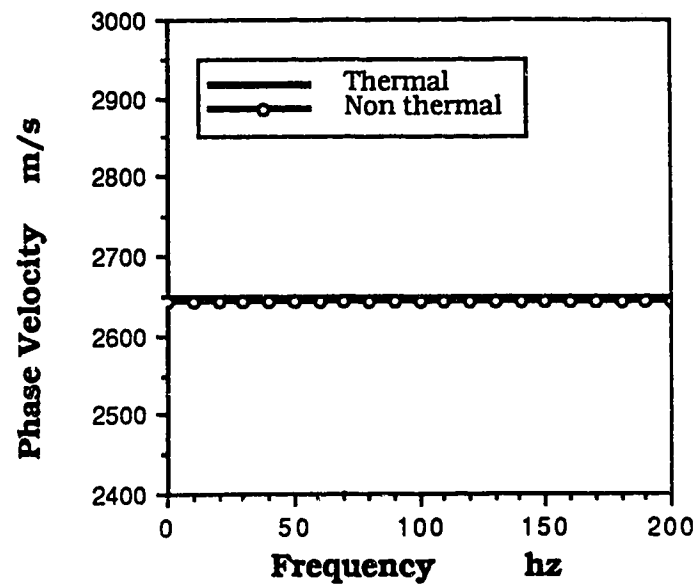


Figure 34 1st P-wave; Phase velocity vs. frequency for an air filled silica sand with 30% porosity. Thermal solution includes thermomechanical coupling.

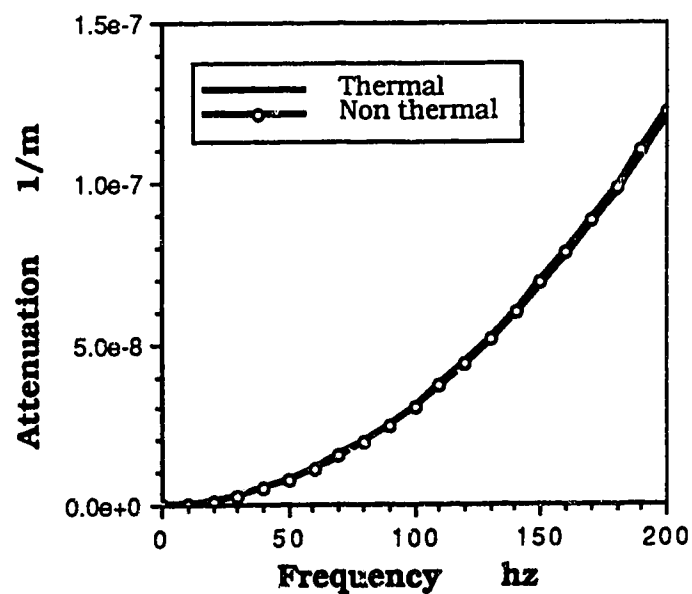


Figure 35 1st P-wave; Attenuation vs. frequency for an air filled silica sand with 30% porosity. Thermal solution includes thermomechanical coupling.

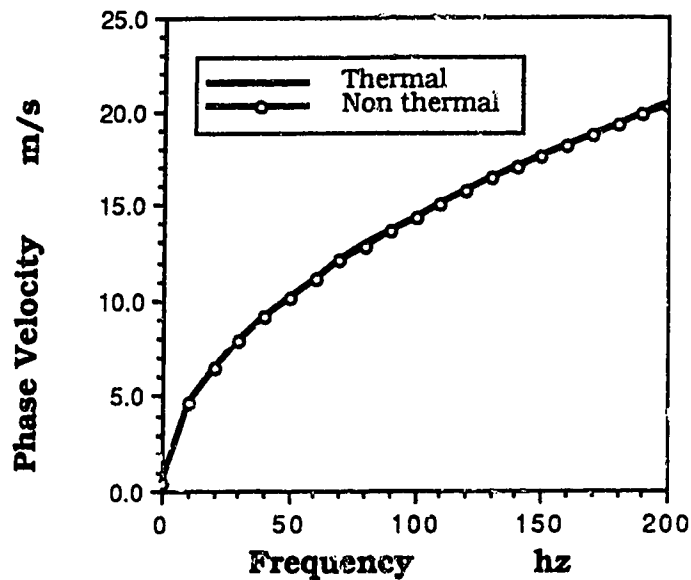


Figure 36 2nd P-wave; Phase velocity vs. frequency for an air filled silica sand with 30% porosity. Thermal solution includes thermomechanical coupling.

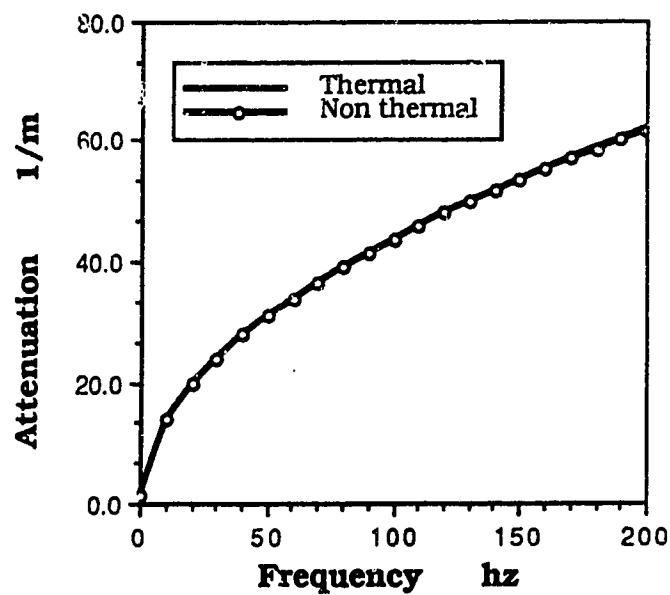


Figure 37 2nd P-wave; Attenuation vs. frequency for an air filled silica sand with 30% porosity. Thermal solution includes thermomechanical coupling.

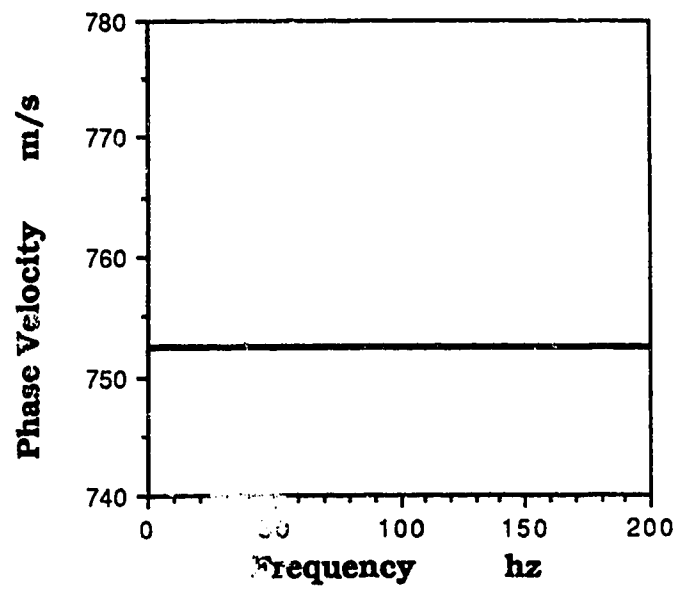


Figure 38 1st S-wave; Phase velocity vs. frequency for an air filled silica sand with 30% porosity.

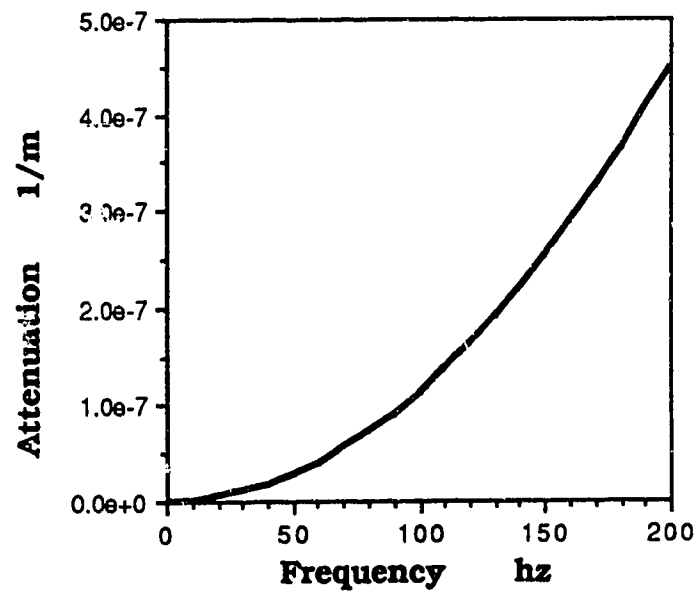


Figure 39 1st S-wave; Attenuation vs. frequency for an air filled silica sand with 30% porosity.

primarily in the solid is very small. However the amplitude of such a wave should be much less in the porous case than in the elastic case. The attenuation of the 1st S-wave (figure 39) increases with increasing frequency but the magnitude is small for the frequency range considered. The 2nd S-wave is mainly a viscous wave altered by interactions with the solid. It is characterized by a very low phase velocity and high attenuation ($\sim 10^5 \text{ m}^{-1}$). Although it probably will never be observed, it is important to know that it might have an effect on the 1st S wave.

For an air filled silica sand the phase velocities of the 1st P and 1st S waves are frequency independent for frequencies up to 200 hz. The phase velocity of the 1st S wave is the same as calculated in the elastic cases; however, the amplitude of this wave should be considerably smaller. The attenuation of the 1st P and 1st S waves increases with increasing frequency, but the magnitudes are small. Thermo-mechanical coupling is not important for this given parameter set.

4.2 WATER FILLED SILICA SAND

This model is of primary importance in the search for groundwater aquifers and possibly in the monitoring of water floods for enhanced or secondary oil recovery techniques. The parameters indicative of this model were used to illustrate numerical consistencies in limiting cases as well as discussing empirical parameters and were presented in table 3. The model is analogous to the air filled model with the exception that the voids or pores are now fully saturated with water. Therefore a comparison of the two models should illustrate the effect of different pore fluids on the propagation of a wave.

The phase velocity (figure 40) of the 1st P wave is not dependent on frequencies in the range of 0 to 200 hz. It is approximately 10% larger than the phase velocity calculated in the air filled case but it is still much lower than the value calculated in the elastic limit. This increase in phase velocity as compared to the air filled case is due to the lower compressibility of water. The presence of water helps restrict compression of the pores thereby making the porous medium less compressible and as a consequence the 1st P wave will propagate at a higher velocity. The attenuation (figure 41) of the 1st P wave is frequency dependent and is about three orders of magnitude larger than calculated in the air filled case. This increase in attenuation is due to the greater transfer of mechanical to thermal energy through viscous dissipation which is associated with the larger viscosity of water.

The 2nd P wave, which can be thought of as the mechanical motions propagating primarily in the fluid but influenced by the solid, has a larger phase velocity (figure 42) and smaller attenuation (figure 43) as compared to the air filled model. The increased phase velocity can be accounted for mainly by the lower compressibility of water as compared to air. The attenuation cannot be explained by changes in the fluid character alone but one must consider the interaction between the component materials. Along with the attenuation of the 2nd P wave the difference in phase velocity (figure 44) and attenuation (figure 45) of 1st S waves determined for the water filled model and air filled model must also be explained in terms of the solid - fluid interaction. First, an increase in viscosity increases the coupling between the solid and fluid components thereby amplifying the characteristic contribution of that component to the wave. In the case of the 2nd P wave the

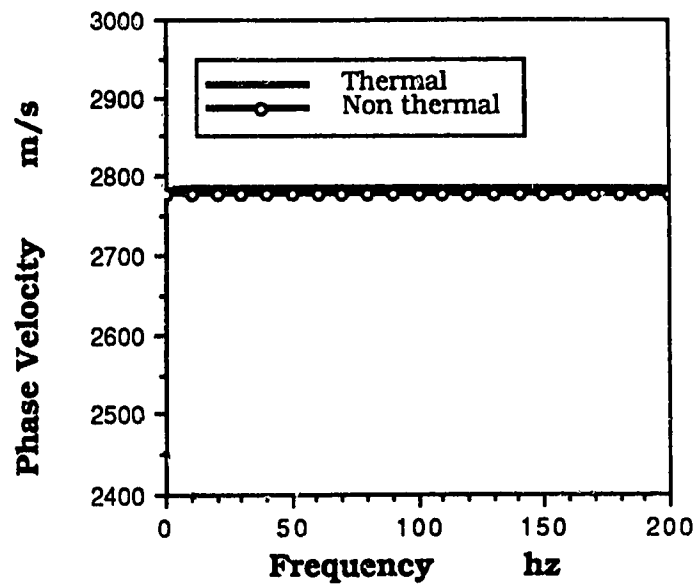


Figure 40 1st P-wave; Phase velocity vs. frequency for a water filled silica sand with 30% porosity. Thermal solution includes thermomechanical coupling.

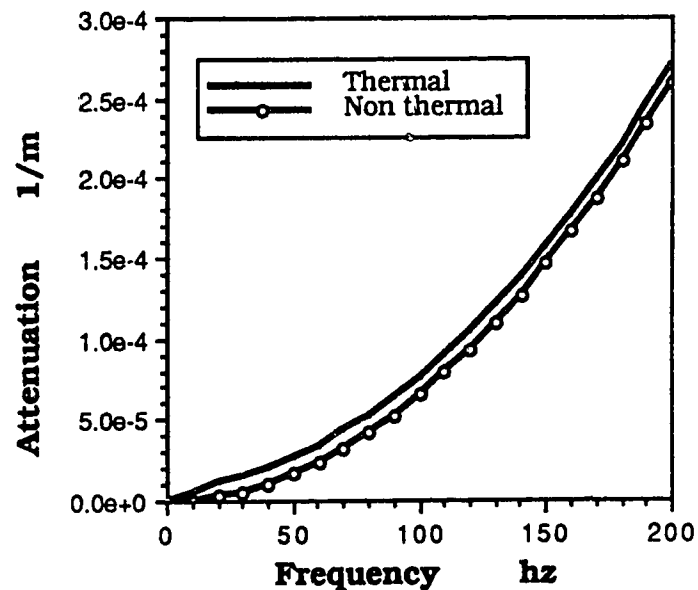


Figure 41 1st P-wave; Attenuation vs. frequency for a water filled silica sand with 30% porosity. Thermal solution includes thermomechanical coupling.

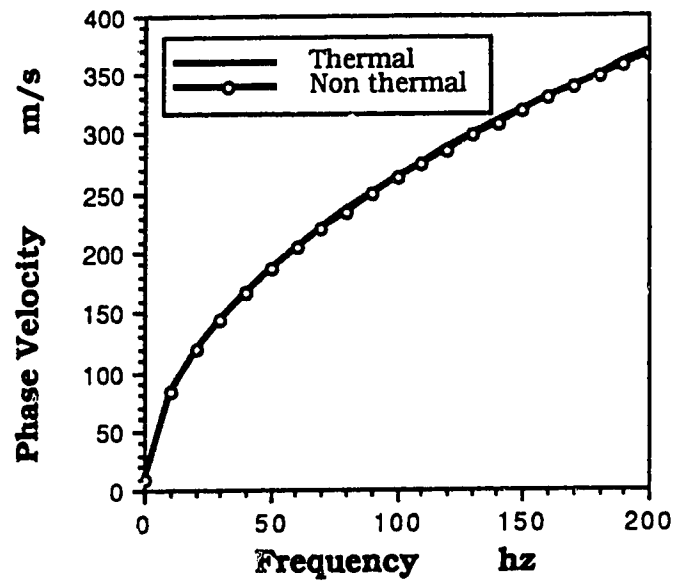


Figure 42 2nd P-wave; Phase velocity vs. frequency for a water filled silica sand with 30% porosity. Thermal solution includes thermomechanical coupling.

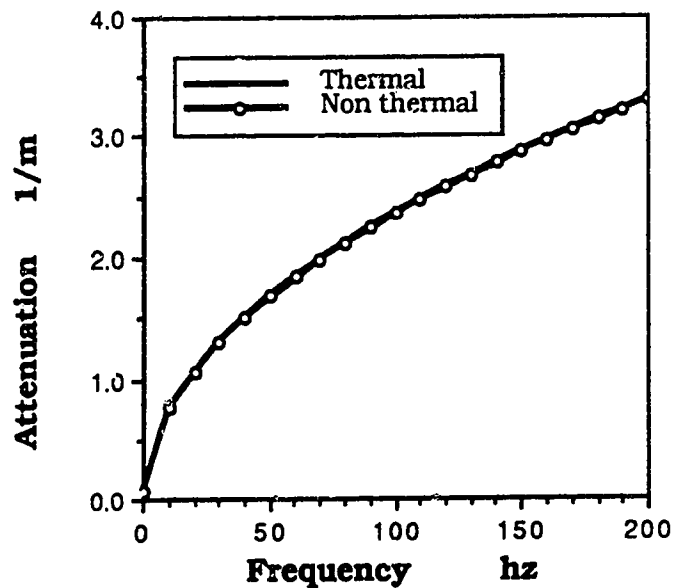


Figure 43 2nd P-wave; Attenuation vs. frequency for a water filled silica sand with 30% porosity. Thermal solution includes thermomechanical coupling.

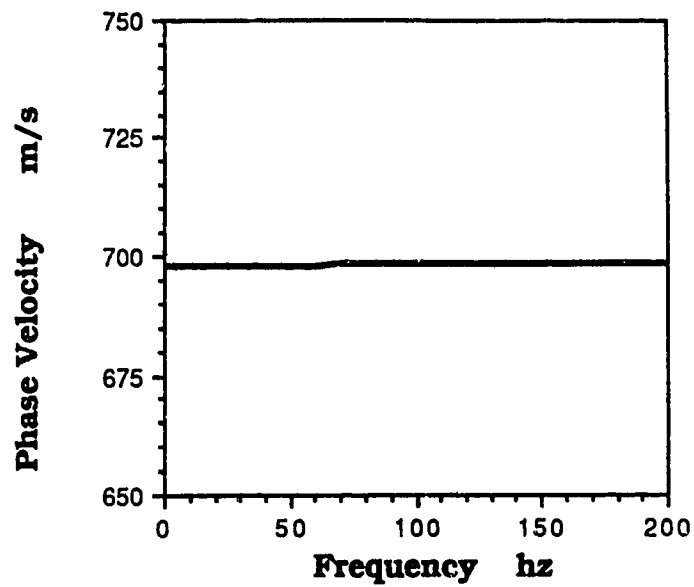


Figure 44 1st S-wave; Phase velocity vs. frequency for a water filled silica sand with 30% porosity.

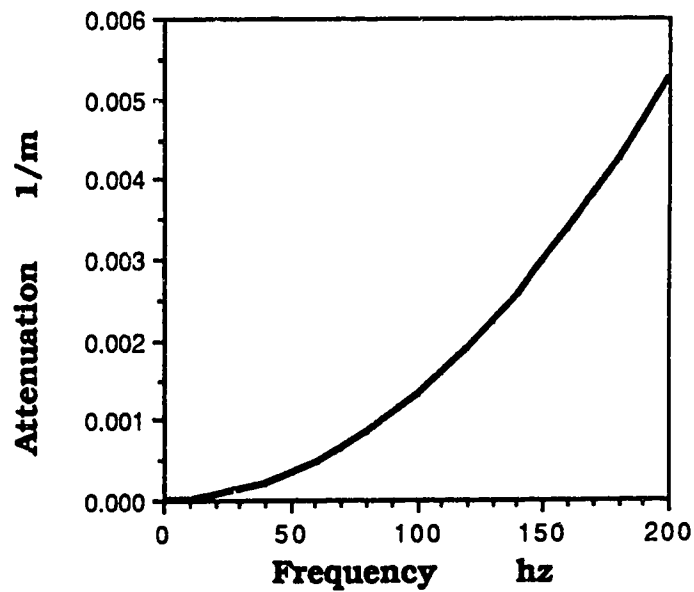


Figure 45 1st S-wave; Attenuation vs. frequency for a water filled silica sand with 30% porosity.

contribution due to the solid is increased thereby reducing the attenuation. The 1st S wave on the other hand has an increased contribution by the fluid. This contribution can be thought of as a viscous drag by the fluid onto the solid motion. This influence will impede the wave thereby decreasing the phase velocity and due to viscous dissipation will increase the attenuation.

The deviation between the "thermal" and "non thermal" curves in figure 41 indicates a small increase in attenuation of the 1st P wave when thermo-mechanical coupling is included. Such a small deviation in attenuation would not be recognizable in seismic investigations.

The increase in viscosity of the pore fluid increases the coupling between motions in the solid and fluid components. This coupling can have different effects on the different waves depending on the component dependence of that wave. When the water filled model is compared to the air filled model, the phase velocity and attenuation of the 1st P wave is increased. The phase of the 1st S wave is decreased; however, its attenuation is increased. It appears that thermo-mechanical coupling can be neglected for a water filled silica sand.

4.3 BITUMEN FILLED SILICA SAND

Sand deposits which are impregnated with dense, viscous petroleum are commonly referred to as tar sands (also known as oil sand and bituminous sands). The largest deposits in the world are located in the Athabasca area in the northeast part of the province of Alberta (Baughman, 1978). The depleting reserves of light crude oil has generated interest in exploitation of these tar sands. Due to the highly viscous nature, the mobility of the fluid is very low under ambient reservoir conditions and therefore recovery methods are

being developed to deal with such problems. Seismic techniques would be very valuable in the monitoring of these recovery methods and therefore it is important to investigate the effect such material has on seismic wave propagation.

Oil sands exist in both consolidated and unconsolidated form, depending on the degree of cementation. The solid matrix in the majority of oil sands consists mainly of quartz grains and clay minerals. The sand grains range downward in size from a maximum diameter of about 1 mm, however, about 99.9% of the mineral matter is finer than 100 μm (Baughman, 1978). The quartz component was found to be subangular to subrounded with good sorting. The primary cementing material was found to be calcite (Camp, 1970,1974). The porosity of selected Athabasca oil sands was measured by Camp (1970,1974) and has a range of 30 to 40 percent. The permeability ranged from 10^{-14} to 10^{-12} m^2 .

The pore fluids consist of bitumen, water, and gas. The gas is usually air but some test borings in Alberta have reported methane (Baughman, 1978). Several of the physical and thermal parameters for bitumen were determined by Camp (1970,1974) using Athabasca tar sand. The bitumen was removed from core samples using a solvent extraction technique. There are some problems associated with this technique. For example, Camp (1970,1974) associates the large variability in viscosity with small amounts of solvent left in the bitumen sample or by a small portion of the lighter end fractions of the bitumen being lost during stripping of the extraction solvent. Many authors (Dusseault and Morgenstern,1978; Agar, 1984; Agar *et al.*, 1987) dealing with bulk investigations of tar sands emphasize the implications of sample disturbance on the stress - strain parameters.

Therefore, it is possible that laboratory measured properties of bitumen will be somewhat altered as compared to the in - situ values. These studies involving the bulk properties are not directly relevant to this theory, since one needs the physical properties of the individual component materials.

The model considered here will consist of an elastic matrix having the properties of silica sand and the pores will be assumed to be fully saturated with bitumen. The saturations of gas and water will be assumed negligible. There is some evidence that bitumen exhibits viscoelastic properties (Dealy, 1980). However, additional experimental studies are required under in-situ conditions and at the strain rates involved in seismic wave propagation before including such effects into seismic studies would be justified.

The physical parameters for the solid component are the same as for the previous models (c.f. table 3.) and the bitumen parameters and choice of empirical parameters are listed in table 5.

The phase velocity (figure 46) and attenuation (figure 47) for the 1st P wave were calculated for a frequency range of 0 to 200 hz with, "thermal", and without, "non thermal", thermo-mechanical coupling. The phase velocity is less than the value calculated for the water filled silica sand but greater than the value calculated for the air filled silica sand. This was expected since the compressibility of bitumen lies between the compressibility of water and air. The phase velocity is slightly larger and frequency dependent when thermo-mechanical coupling is included.

The non-thermal attenuation of the 1st P-wave (figure 47) is about an order of magnitude larger than determined for the water filled model. In order to explain this difference in attenuation it is important to understand which mechanisms are responsible. In the

<u>Property</u>	<u>Symbol</u>	<u>Value</u>
temperature	T_0	2.00×10^1
porosity	η_0	3.00×10^{-1}
permeability	K	1.00×10^{-11}
fluid density	ρ_f	1.02×10^3
fluid viscosity	μ_f	5.00×10^4
fluid bulk modulus	K_f	4.30×10^8
fluid thermal expansion	α_f	$3.40 \times 10^{-3} ?$
fluid heat capacity	c_p^f	2.00×10^3
fluid thermal conductivity	κ_f	1.60×10^{-1}
induced mass coefficient	ρ_{12}	0.00×10^0
solid compliance factor	δ_s	3.60×10^{-1}
fluid compliance factor	δ_f	4.41×10^{-3}
conduction coefficient	γ	5.00×10^8

Table: 5 Properties of bitumen and associated empirical parameters.

de la Cruz - Spanos (1989a) theory there are basically two attenuation mechanisms. They are "Darcian resistance" and viscous dissipation within the fluid itself. The "Darcian resistance" is dependent on the relative motion between the solid and fluid components and is therefore dependent on the fluid viscosity. A higher viscosity is responsible for a greater transfer of mechanical to heat energy. However, it also reduces the relative fluid-solid motion thereby producing a competing effect. This competing effect has been observed experimentally as a peak in attenuation as a function of the product of frequency and pore-fluid viscosity (Jones, 1986, Jones and

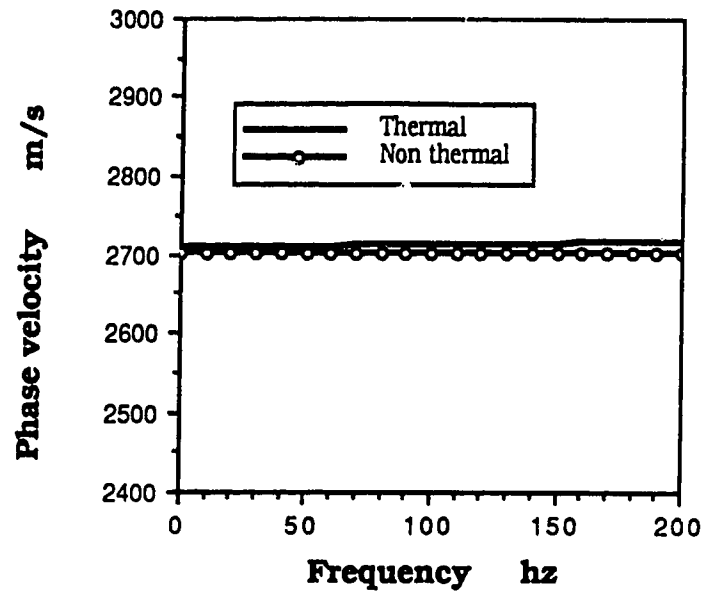


Figure 46 1st P-wave; Phase velocity vs. frequency for a bitumen filled silica sand with 30% porosity. Thermal solution includes thermomechanical coupling.

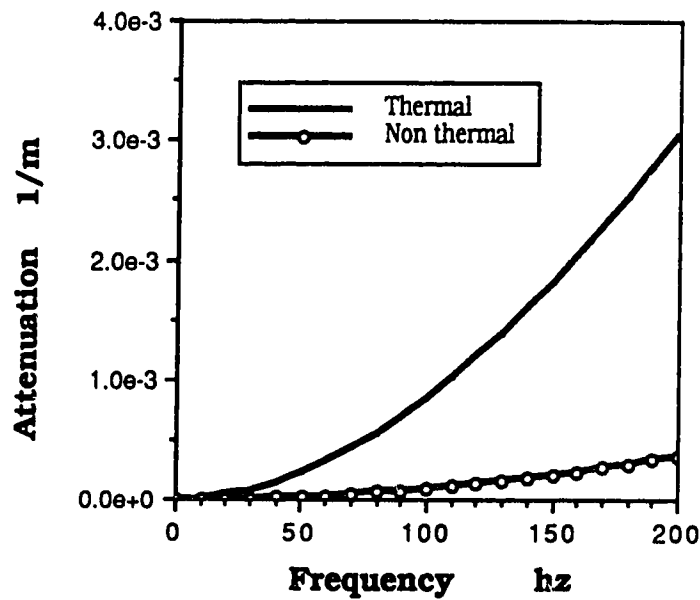


Figure 47 1st P-wave; Attenuation vs. frequency for a bitumen filled silica sand with 30% porosity. Thermal solution includes thermomechanical coupling.

Nur, 1983, Tittmann et al., 1983). At very large viscosities, velocity gradients in the fluid itself will cause a large transfer in energy while the "Darcian resistance" will be reduced due to reduction in relative motion of solid and fluid. Therefore, for very large viscosities the attenuation mechanism within the fluid itself will dominate; however, both mechanisms still contribute to the attenuation in all cases. In the bitumen filled case, viscous dissipation within the fluid itself can be considered the dominant attenuation mechanism. The attenuation of the 1st P wave in the bitumen filled silica sand is not only larger than for the water filled silica sand but is due to a different mechanism.

When thermo-mechanical coupling is included, the attenuation (figure 47) of the 1st P-wave increases much more rapidly as a function of frequency as compared to the non-thermal case. This increase in attenuation is due to the transfer of heat from the solid to the fluid components across the pore scale interfaces. This heat is then converted to mechanical motions through the thermal expansion of the fluid and since the viscous dissipation within the fluid itself is the dominating attenuation mechanism it causes a large increase in attenuation. It is evident from this discussion that thermo-mechanical coupling may enhance attenuation but is not an important attenuation mechanism in itself.

The 1st S wave phase velocity (figure 48) and attenuation (figure 49) illustrate similar behavior as predicted by the previous models. The phase velocity is frequency independent and similar in magnitude to that calculated for the water filled case. The increase in fluid-solid coupling which is associated with an increase in viscosity does not appear to alter further the phase velocity of the rotational waves. The attenuation is frequency dependent, increasing in magnitude with

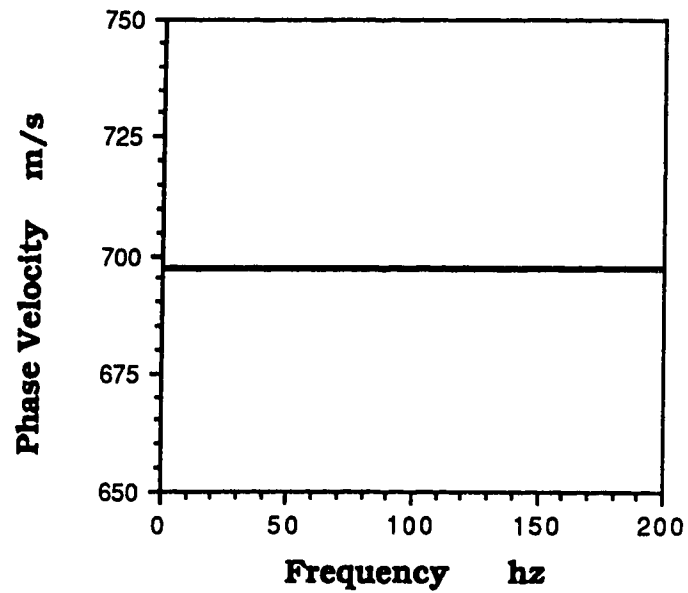


Figure 48 1st S-wave; Phase velocity vs. frequency for a bitumen filled silica sand with 30% porosity.

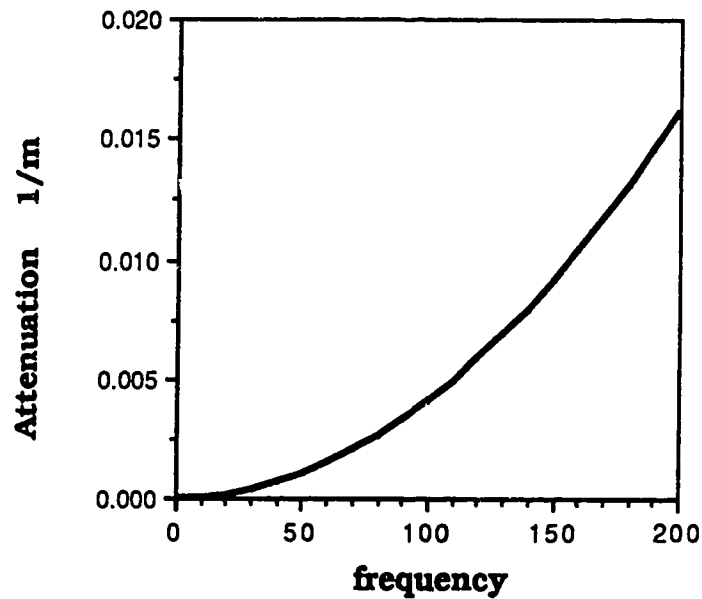


Figure 49 1st S-wave; Attenuation vs. frequency for a bitumen filled silica sand with 30% porosity.

increasing frequency, and much larger than calculated in previous cases. It should be emphasized that thermo-mechanical coupling does not affect the rotational waves.

Phase velocity for the other P waves predicted by the de la Cruz - Spanos (1989a) theory is frequency dependent and is about five orders of magnitude less than the 1st P wave phase velocity. The attenuation of the other P waves is of the order of 10^5 m^{-1} . The extremely large attenuation and low phase velocity of these waves indicate that they will not be observed.

The phase velocity and attenuation of a wave propagating in a bitumen filled silica sand are much different than would be expected in an elastic solid as well as in a water filled silica sand. The phase velocity of the 1st P wave is usually less; however, the greatest difference is in the increase in attenuation of this wave. The 1st S wave has the same phase velocity for both a bitumen filled silica sand and a water filled silica sand; however, the attenuation is about five times larger for the bitumen case. More important is the effect of thermo-mechanical coupling for a bitumen filled silica sand. Although its effect on phase velocity is minimal, it has been shown that within the seismic frequency range it can increase the attenuation of the 1st P wave by five times the value calculated without thermal effects.

4.4 STRUCTURES OF THE DEEP EARTH

Observations of records of elastic waves generated by earthquakes and large explosions provide the main source of information about the Earth's deep interior. These records contain the movement of the ground produced by the passing of various elastic waves and are displayed as a function of time. The travel time depends on how the

velocities of the different seismic waves change as they pass through materials having different elastic properties. The velocity generally increases with depth, however, there are some observations, such as shadow zones, which can be best explained by layers of lower velocity. Using an iterative least-squares method (Jeffreys, 1939, 1959) it is possible to obtain velocity-depth curves from observed data. One of the first velocity-depth curves (figure 50) was determined by Jeffreys (1939) for S and P waves.

The attenuation of seismic waves may also provide a possible technique for exploring the internal properties of the Earth (Anderson and Archambeau, 1964; Knopoff, 1964). The intrinsic attenuation is usually measured by the quality factor Q^* , defined as

$$Q^* = \frac{2\pi E}{\Delta E} \quad (138)$$

where ΔE is the energy dissipated per wave cycle and E is the total elastic energy of a wave cycle. Assuming a plane wave propagating in the x-direction with amplitude in the z-direction only, one can rewrite (138) as

$$Q^* = \frac{\pi f}{v \xi} \quad (139)$$

where ξ is the attenuation coefficient and v is the phase velocity at the frequency f . The attenuation in dry rocks is very small and frequency independent (Spencer, 1981). Experimental studies have shown, however, that attenuation is strongly affected by the fluid saturation, properties of the pore fluid and the frequency (Toksoz et al. 1979; Spencer, 1981; Winkler and Nur, 1982; Murphy; 1983; Jones and

This figure has been removed because of the unavailability of copyright permission.

Figure 50 P and S wave velocity distribution in the Earth's interior (from Bullen, 1963).

Nur, 1983; Tittmann et al., 1983; Winkler, 1985; Jones, 1986). Therefore, the attenuation in partially melted rocks, which involves contributions from both liquid and solid phases, should show such characteristics (Kampfmann and Berckhemer, 1985; Walsh, 1968; Anderson and Spetzler, 1970). It is very important to point out that apparent attenuation measured from records of elastic waves can be caused by interference effects and scattering from velocity and density heterogeneities (Jones, 1986). Therefore, it maybe difficult to discern apparent attenuation from intrinsic attenuation which is discussed here.

More recently the preliminary reference earth model, PREM, was developed by Dziewonski and Anderson (1981) by inverting a large set of P, S and surface wave observations. The attenuation was also taken into consideration but since published data on attenuation is of variable quality a small set of data based on measurements by various authors (Buland et al., 1979; Geller and Stein, 1979; Stein and Dziewonski, 1980) was used. It was further assumed that the seismic quality factor is independent of frequency.

Dziewonski and Anderson could not justify the assumption of isotropy because a large amount of important data could not be fit adequately with an isotropic Earth model. They therefore adopted anisotropy and inelastic dispersions as essential complexities for the depth interval of 25 km to 220 km; however, results for the "equivalent" isotropic Earth are also present. "Equivalent" means that the model has approximately the same bulk modulus and shear modulus as the anisotropic model, not that it provides an equivalent, or satisfactory, fit to the data (Dziewonski and Anderson, 1981). The parameters of the final model are presented in Table 6. It contains

the velocities, density and Q^* as a function of radius, where Q_μ^* and Q_K^* represent the isotropic dissipation of the shear and compressional energy, respectively. The parameters listed are valid for a reference period of 1s. This model divides the Earth into several principal regions:

- 1) Ocean layer
- 2) Upper and lower crust
- 3) Region above the low velocity zone (LID), considered to be the main part of the seismic lithosphere.
- 4) Low velocity zone (LVZ)
- 5) Transition zone spacing from the LVZ to the 670 km discontinuity.
- 6) Lower mantle which is subdivided into three parts
- 7) Outer core
- 8) Inner core

which are strongly dependent on the starting model.

The Earth's internal composition is deduced from numerical calculations of elastic parameters from the given phase velocities and attenuations. These calculations and final compositions are very hypothetical and dependent on the theory used. Primarily, elastic theory is used where the bulk and shear moduli are assumed to be complex valued in order to account for the attenuation aspect. Expressions for these moduli are derived using various viscoelastic models (Gordon and Davis, 1968; Walsh, 1968). The Biot theory could also be used; however, a clear understanding of Biot's phenomenological parameters in terms of component parameters would be needed. The de la Cruz-Spanos (1989a) theory is developed in terms of the component properties and would therefore be very useful in determining the composition of the Earth's interior.

This table has been removed because of the
unavailability of copyright permission.

Table: 6 The parameters describing the Preliminary Reference Earth Model (PREM)
The variable x is the normalized radius: $x=r/a$ where $a=6371$ km. The parameters listed
are valid at a reference period of 1 s. The effective isotropic velocities between 24.4 and
220 km can be approximated by $V_P=4.1875 + 3.9382x$ and $V_S=2.1519 + 2.3481x$
(Dziewonski and Anderson, 1981).

In order to identify the actual materials present one must incorporate high-temperature, high-pressure experiments as well as thermodynamical and geochemical constraints, indicative of the location within the Earth's interior. These types of studies have been carried out by numerous authors; Ringwood (1970), Kushiro et al. (1968), Ringwood (1975), Manghnani and Akimoto (1977), and Manghnani and Syono (1987). From this type of study they conclude that the crust consists mainly of granitic rocks underlain by more dense basalt or gabbro. The mantle below the Mohorovicic consists primarily of dense ultrabasic rock called peridotite. The lower mantle is believed to consist of perovskite, $(\text{Mg,Fe})\text{SiO}_3$. Shock wave and laser heated diamond anvil experiments on iron appear to indicate that both densities and bulk moduli in the liquid outer core are less than those of iron under equivalent conditions (Williams et al., 1987; Jacobs, 1981). In order to comply with these observations it is assumed there exists a lighter more compressible element or compound. There is no firm evidence as to the identity of the light element in the outer core. It must, however, be reasonably abundant, miscible with iron and posses chemical properties that would allow it to enter the core. The prime candidates are silicon and sulphur and more recently oxygen. The inner core is believed to consist of iron and nickel.

Major advances in controlled static type experiments have come about in the past few years due to the advent of the diamond anvil press and the uniaxial split-sphere multi-anvil press or "Superpress". These experiments are still limited to pressures of about 25 GPa which is believed to be indicative of depths of about 700 km. Simulation of higher pressures and temperatures can be attained using shock wave experiments; however, these experiments involve

measurements over very short periods of time and many assumptions are needed in order to interpret these measurements in terms of actual mineral composition and structure.

Assembling the seismological and high pressure-temperature knowledge, various authors have constructed models for the Earth (Jacobs, 1981). Although these models are somewhat elaborate, one must remember they contain many uncertainties and assumptions which still need to be resolved or justified.

Two regions which have received much attention in the recent literature are the low-velocity layer and the core-mantle boundary. These two regions exhibit very anomalous seismic behavior such as negative velocity gradients and very high attenuations. The de la Cruz-Spanos (1989a) theory will be used to calculate the phase velocities and intrinsic attenuation for these zones. The available data for the proposed constituent material in these zones is very sparse, therefore, the trends of the solutions will be emphasized rather than actual values.

4.4.1 Asthenosphere, LVZ.

The asthenosphere or low-velocity zone, LVZ, is characterized by lower velocities and more rapid attenuation of seismic waves than adjacent regions. The upper boundary is located just below the solid lithosphere at a depth of about 60 km from the continental surface. The lower boundary is assumed to be at a depth of about 250 km. Within this zone one observes the maximum decrease in velocity, about 3 to 5% of the initial velocity, at a depth of about 150 km. The attenuation increases by a factor of 3 or more (Anderson and Sammis,

1970). At depths between 150 and 250 km the phase velocity increases again with depth. The thickness and velocity of the zone can, to some extent, be traded off against each other so that the details of this region cannot be unambiguously determined (Anderson and Sammis, 1970).

Peridotite and eclogite are two principle candidates for the composition of the asthenosphere. Peridotite is a heavy dark green igneous rock composed primarily of olivine with pyroxene and/or amphibole (hornblende) usually present. Eclogite is composed primarily of pyroxene and a reddish garnet and is more dense than peridotite. There are favorable arguments for both of these candidates (Cailleux, 1968); however, a variety of peridotite is regarded as the most probable composition (Birch, 1970; Lambert and Wyllie, 1970; Anderson and Sammis, 1970; Anderson and Bass, 1986).

Several mechanisms based on the peridotite composition have been suggested to explain the anomalous velocity gradients and larger attenuations of seismic waves in the asthenosphere. These include temperature and pressure effects, with or without relaxation of elasticity, partial melting, or phase changes associated with the pressure-temperature environment. Some solutions (Gutenberg, 1959) of velocity-depth curves are roughly consistent with a homogeneous layer of peridotite affected only by temperature and pressure. However, the preferred explanation of more recent velocity-depth models is based on the presence of a partial melt (Anderson and Bass, 1986). There is some basis for arguing that the temperature in the upper most asthenosphere (~60 km) would not be sufficient to melt peridotite and that the presence of small amounts of water is needed (Lambert and Wyllie, 1970).

The parameters used in the calculation of phase velocity and

attenuation for the LVZ are presented in table 7. The parameters for the solid are primarily of forsterite, Mg_2SiO_4 . Very little is known about the properties of the melt within the LVZ and therefore a large uncertainty exists in the values presented. The melted zones are assumed to be pore-like structures of random sizes, shapes and orientations. The pores are restricted to be interconnected in such a manner that the assumed permeability is obtained. The majority of the fluid parameters are from Jacoby and Schmeling (1982).

The phase velocity, at 1 hz, (figure 51) of the 1st P wave decreases with an increase in partial melt. The attenuation (figure 52) increases with an increase in partial melt. Thermo-mechanical coupling does not change the phase velocity or attenuation of the 1st P wave. The presence of a 6% melt produces about a 7% change in the 1st P wave velocity and a Q_K^* value of 7856 m^{-1} . The de la Cruz - Spanos (1989a) theory predicts a much larger effect on the phase velocity and attenuation than has been quoted previously by other authors (Birch, 1970; Anderson and Sammis, 1970) for this amount of melt. The change in phase velocity is in agreement with the PREM model; however, the Q_K^* value is about an order of magnitude smaller. The phase velocity, at a 1 hz frequency, (figure 53) of the 1st S wave decreases with an increase in partial melt. The attenuation (figure 54) increases with an increase in partial melt. A 6% melt produces about a 3% decrease in S wave velocity which is somewhat smaller than expected. The Q_μ^* value for a 6% melt is about 3494 m^{-1} which is considerably larger than is quoted in the PREM model. This difference can be accounted for easily by the uncertainty in the determination of the PREM model combined with the uncertainty in selection of the constituent parameters used in the de la Cruz -Spanos

<u>Property</u>	<u>Symbol</u>	<u>Value</u>
temperature	T_0	1.0×10^3
porosity	η_0	5.0×10^{-2}
permeability	K	1.0×10^{-17}
solid density	ρ_s	3.5×10^3
fluid density	ρ_f	3.0×10^3
shear modulus	μ_s	7.0×10^{10}
fluid viscosity	μ_f	1.0×10^8
solid bulk modulus	K_s	1.5×10^{11}
fluid bulk modulus	K_f	1.2×10^{10}
solid thermal expansion	α_s	2.6×10^{-8}
fluid thermal expansion	α_f	3.7×10^{-5}
solid heat capacity	c_v^s	1.2×10^3
fluid heat capacity	c_p^f	5.0×10^3
solid thermal conductivity	κ_s	2.0×10^0
fluid thermal conductivity	κ_f	1.2×10^0
induced mass coefficient	ρ_{12}	0.0×10^0
solid compliance factor	δ_s	2.2×10^{-1}
fluid compliance factor	δ_f	1.8×10^{-2}
conduction coefficient	γ	1.0×10^3

Table 7 Physical properties properties of the asthenosphere and the associated empirical parameters.

(1989a) theory.

Further numerical studies, assuming a 5% partial melt, indicate that the phase velocity of the 1st P wave (figure 55) and 1st S wave

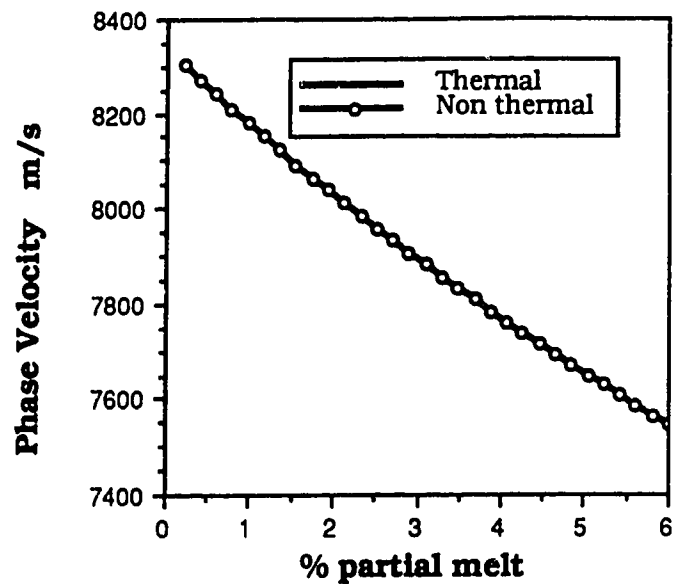


Figure 51 1st F wave; Phase velocity vs. % partial melt for a model of the asthenosphere at a frequency of 1 hz. Thermal solution includes thermomechanical coupling.

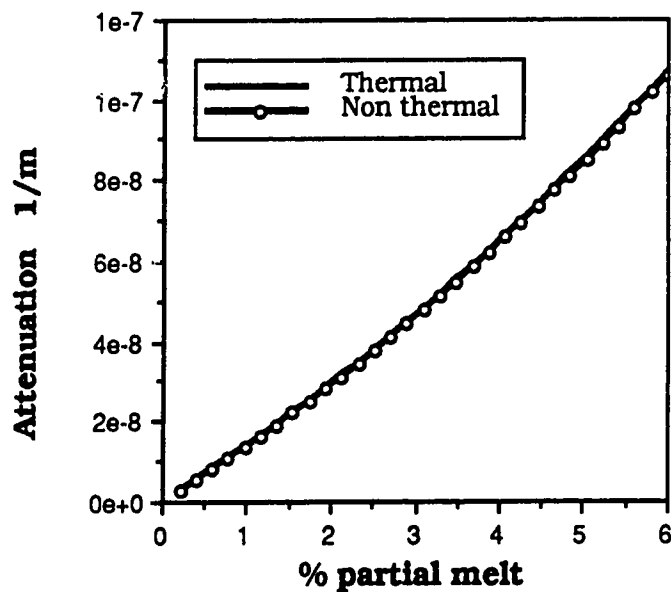


Figure 52 1st P wave; Attenuation vs. % partial melt for a model of the asthenosphere at a frequency of 1 hz. Thermal solution includes thermomechanical coupling.

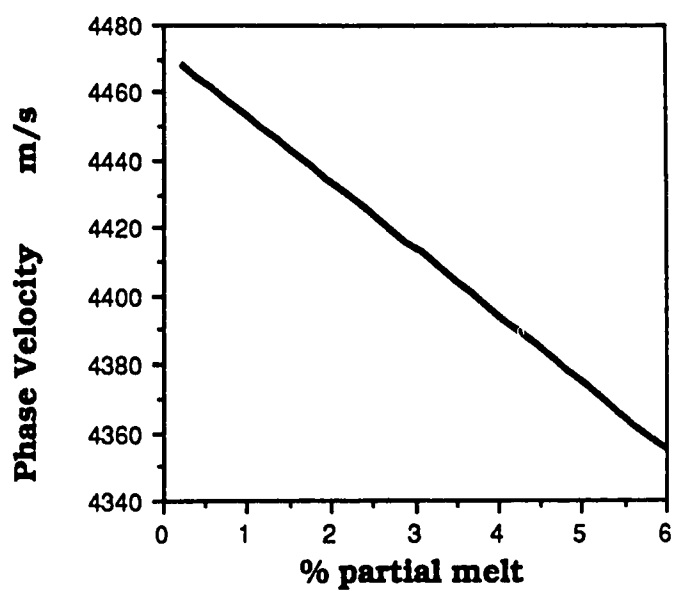


Figure 53 1st S wave; Phase velocity vs. % partial melt for a model of the asthenosphere at a frequency of 1 hz.

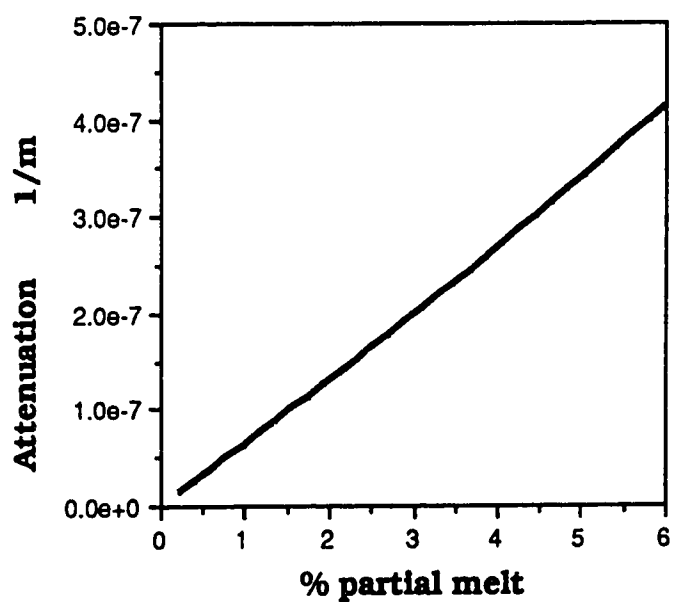


Figure 54 1st S wave; Attenuation vs. % partial melt for a model of the asthenosphere at a frequency of 1 hz.

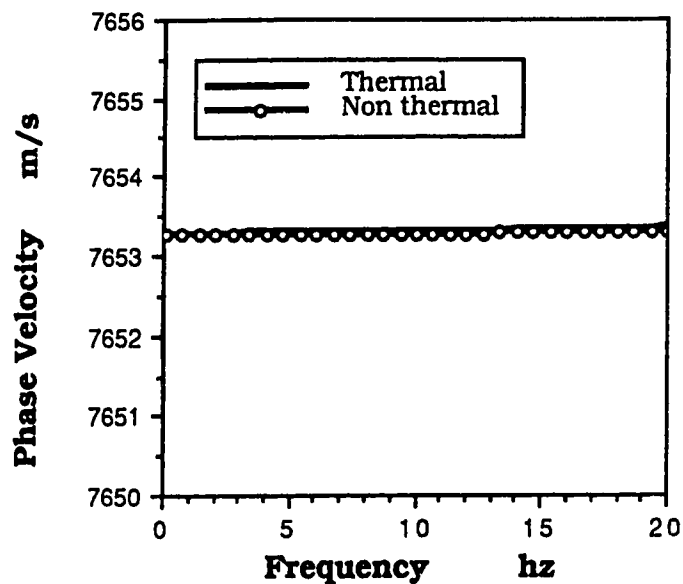


Figure 55 1st P wave; Phase velocity vs. frequency for a model of the asthenosphere with 5% partial melt. Thermal solution includes thermomechanical coupling

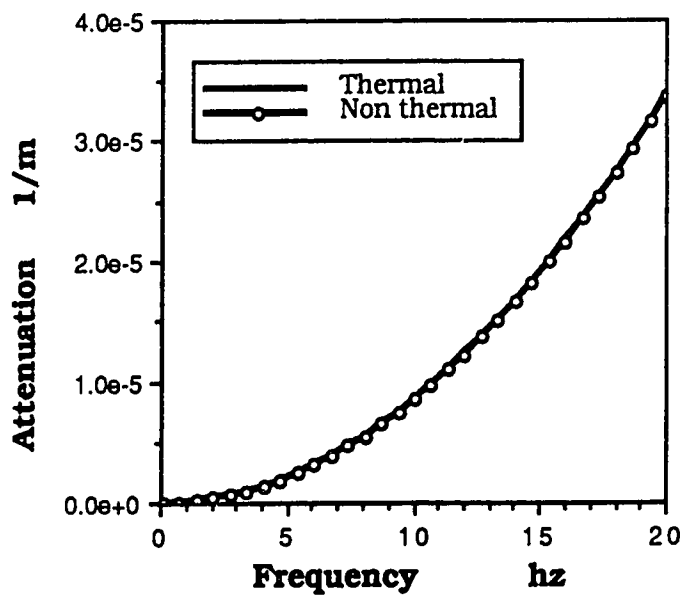


Figure 56 1st P wave; Attenuation vs. frequency for a model of the asthenosphere with 5% partial melt. Thermal solution includes thermomechanical coupling

(figure 57) are frequency independent for frequencies up to 20 Hz. The attenuation of these waves (figures 56,58) increases considerably with frequency within 0 to 20 Hz. This increase in attenuation is non-linear; therefore, this theory does not support a frequency independent Q^* which is assumed in the construction of PREM. This could be another possible explanation for the differences in the calculated Q^* and PREM.

The de la Cruz - Spanos (1989a) theory can explain the observed negative velocity gradients and high attenuation within the LVZ in terms of a partial melt. The differences in magnitude of the observed and calculated phase velocity and Q^* could be eliminated by varying the physical parameters of the component materials to obtain a best fit. However, the frequency dependence of Q^* would probably remain. The de la Cruz (1989a) theory could, however, be used in conjunction with measured parameters from high pressure experiments to calculate independently phase velocities and attenuation of waves propagating in materials of known compositions, temperatures and pressures. These composition, temperatures and pressures could be chosen to be indicative of particular locations within the Earth

4.4.2 Core-mantle boundary, D".

The core-mantle boundary (CMB) is the largest discontinuity in composition and material properties within the Earth. It is located at a depth of about 2900 km and separates the outer core from the lower mantle. Shock wave and laser heated diamond anvil experiments on iron appear to indicate that both densities and bulk moduli in the liquid outer core are less than those of iron under equivalent conditions (Williams *et al.*, 1987; Jacobs, 1981). In order to comply

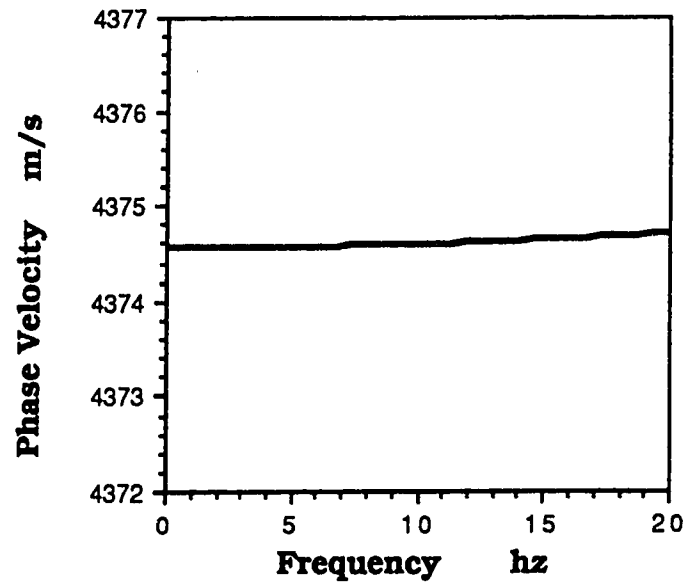


Figure 57 1st S wave; Phase velocity vs. frequency for a model of the asthenosphere with 5% partial melt.

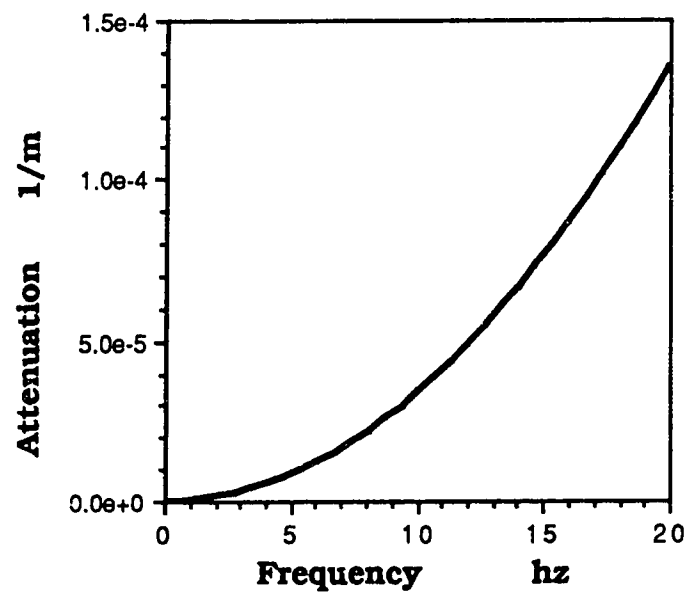


Figure 58 1st S wave; Attenuation vs. frequency for a model of the asthenosphere with 5% partial melt.

with these observations it is assumed there exists a lighter more compressible element or compound. The prime candidates are silicon, sulphur and more recently oxygen (Ahrens, 1982). Experiments conducted in a laser heated diamond anvil cell have recently provided evidence supporting perovskite, $(\text{Fe,Mg})\text{SiO}_3$, as the dominant phase in the lower mantle; however, the relative abundance of Fe and Mg and presence of other possible phases are not well resolved (Ahrens and Jeanloz, 1988; Knittle and Jeanloz, 1987; Heinz and Jeanloz, 1987; Knittle *et al.*, 1986). The properties of the lower mantle, denoted as the solid component, and the outer core, denoted as the fluid component, are presented in table 8. The empirical parameters are calculated such that physical results are obtained.

The large change in material properties between the lower mantle and outer core is believed to be responsible for transition zones adjacent to the core-mantle boundary. The lower-most 200-300 km of the mantle was recognized for a long time to have anomalous seismic properties and was labeled the D" boundary by Bullen (1949). The D" region is characterized by a decrease in P and S wave velocities with depth in radially symmetric earth models such as PREM (see table 6). Models of the quality factor, Q^* , tend to indicate low values in D" as compared to the rest of the deep mantle (Anderson and Given, 1982). Young and Lay (1987) review many of the models based on seismological observations. They conclude that present day quantitative models are becoming more consistent; however, there is still no definite model for the D" region.

The two prominent explanations for the observed anomalous behavior of the D" transition zone are the presence of a chemical and/or a thermal boundary layer. The large density contrast between

the outer core and lower mantle lends strong support for a chemical boundary layer. Further support is the strength of lateral velocity gradients and experiments indicating chemical reactivity between molten iron and perovskite. However, these latter two areas are rather controversial.

Estimates of the heat flux out of the core indicate that the 200 km thick D" region at the base of the mantle is a major thermal boundary layer (Young and Lay, 1987). Stacey and Loper (1983) accredit the anomalous velocity gradients in radially symmetric earth models to a thermal boundary layer with an 800 K temperature contrast. Recent estimates of mean lower mantle adiabats range from 2600 K to 3100 K (Jeanloz and Morris, 1986) so that any strong temperature increases in the D" region may approach the solidus of perovskite, leading to the possibility of the existence of partial melt. More elaborate models comprised of the superposition of various chemical and thermal boundaries, at varying scales, have been proposed (Lay, 1989).

An attempt is made at calculating the phase velocity and attenuation for a simple core-mantle transition zone model using the de la Cruz-Spanos (1989a) theory. The model consists of an elastic matrix, with the properties of perovskite, containing zones of partial melt. The zones of melt are assumed to be of random shapes, sizes and orientations. There is assumed to be sufficient convection within the outer core that the melt is a mixture of perovskite melt and outer core material. Therefore the properties of the fluid within the pores will be similar to the properties of the liquid outer core. The physical parameters are presented in table 8.

The phase velocity (figure 59) and attenuation (figure 60) of the 1st P wave are altered by changes in the degree of partial melt. For a wave at a frequency of 1 hz the phase velocity decreases linearly with an

<u>Property</u>	<u>Symbol</u>	<u>Value</u>
temperature	T_0	3.9×10^3
porosity	η_0	5.0×10^{-2}
permeability	K	1.0×10^{-17}
solid density	ρ_s	5.57×10^3
fluid density	ρ_f	9.9×10^3
shear modulus	μ_s	2.9×10^{11}
fluid viscosity	μ_f	1.0×10^6
solid bulk modulus	K_s	6.85×10^{11}
fluid bulk modulus	K_f	6.35×10^{11}
solid thermal expansion	α_s	1.0×10^{-5}
fluid thermal expansion	α_f	8.0×10^{-6}
solid heat capacity	c_v^s	2.0×10^3
fluid heat capacity	c_p^f	5.0×10^3
solid thermal conductivity	κ_s	4.0×10^0
fluid thermal conductivity	κ_f	2.5×10^1
induced mass coefficient	ρ_{12}	0.0×10^0
solid compliance factor	δ_s	3.64×10^{-2}
fluid compliance factor	δ_f	3.38×10^{-2}
conduction coefficient	γ	1.0×10^9

Table 8 Physical properties properties of the core-mantle transition zone, D", and the associated empirical parameters. The solid is assumed to be perovskite and the fluid is the molten iron alloy of the outer core.

increase in partial melt at a rate of about 90 m/s per % partial melt. The attenuation of the wave increases with an increase in partial melt.

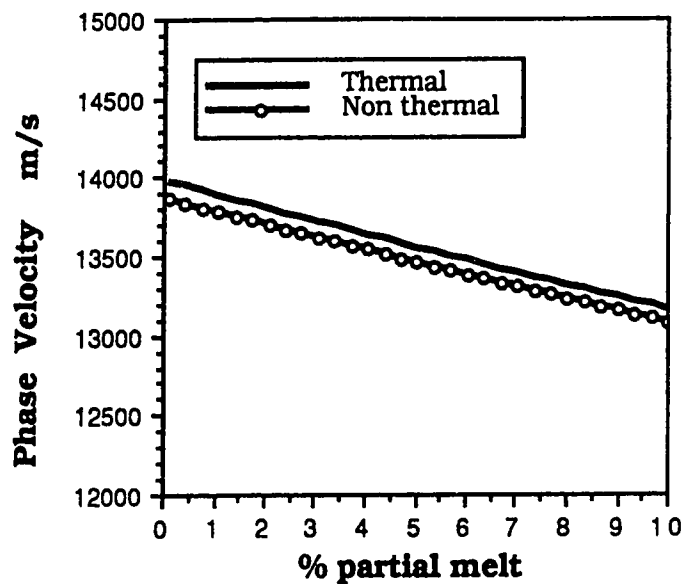


Figure 59 1st P wave; Phase velocity vs. % partial melt for a model of the core-mantle transition zone at a frequency of 1 hz. Thermal solution includes thermomechanical coupling.

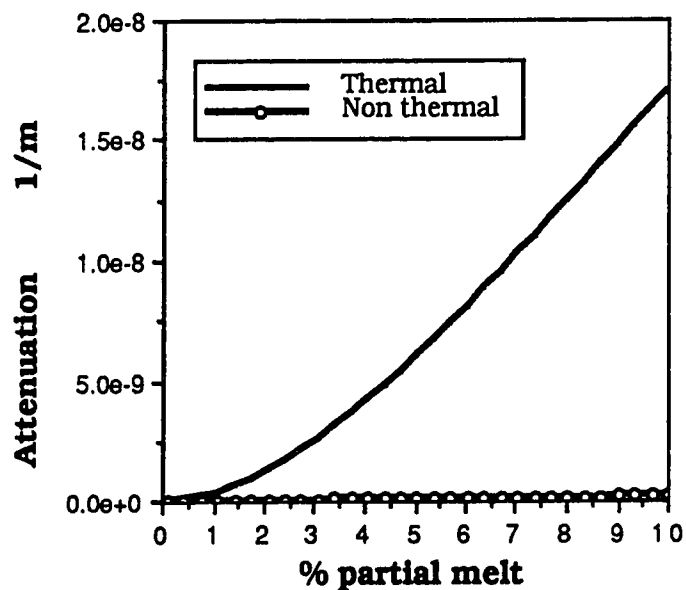


Figure 60 1st P wave; Attenuation vs. % partial melt for a model of the core-mantle transition zone at a frequency of 1 hz. Thermal solution includes thermomechanical coupling.

When thermo-mechanical coupling is included, the attenuation increases much more rapidly. The attenuation calculated with 7% partial melt is approximately two orders of magnitude greater when thermo-mechanical coupling is included as compared to the non-thermal solution. Thermo-mechanical coupling also produces a slight increase in phase velocity.

The phase velocity (figure 61) and attenuation (figure 62) for the 1st S-wave have a similar dependence on the amount of partial melt as for the first P-wave. Thermo-mechanical coupling does not affect the rotational waves. The phase velocity of the 1st S-wave at a frequency of 1 hz decreases at a rate of about 60 m/s per % partial melt. The attenuation increases linearly by about two orders of magnitude over a 10% range in partial melt. The Q^* value determined in the PREM is still significantly larger than the value calculated here with a 10 % partial melt.

The frequency dependence of the 1st P-wave phase velocity and attenuation is illustrated in figures 63 and 64, respectively, for frequencies of 0 to 5 hz. There is assumed to be a 5% partial melt. The phase velocity is independent of frequency within this range and the thermal velocity is slightly greater than the non-thermal velocity. The attenuation due to non-thermal effects increases only slightly as illustrated by the non-thermal solution. However, when thermo-mechanical coupling is included the attenuation increases by several orders of magnitude over the given frequency range. Furthermore, the increase occurs in a non-linear fashion and a frequency independent phase velocity indicates that Q^* would be a frequency dependent value. The phase velocity of the 1st S-wave (figure 65) also shows a frequency independence for frequencies of 0 to 5 hz. The attenuation (figure 66) increases in a non-linear fashion with an increase in

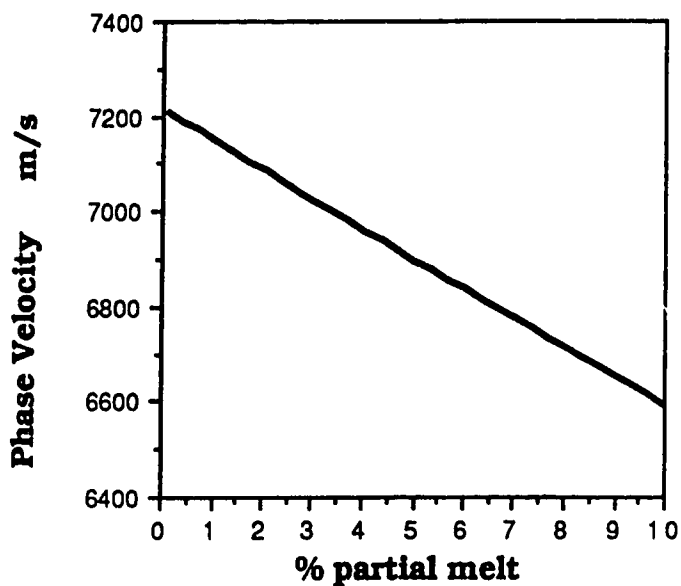


Figure 61 1st S wave; Phase velocity vs. % partial melt for a model of the core-mantle transition zone at a frequency of 1 hz.

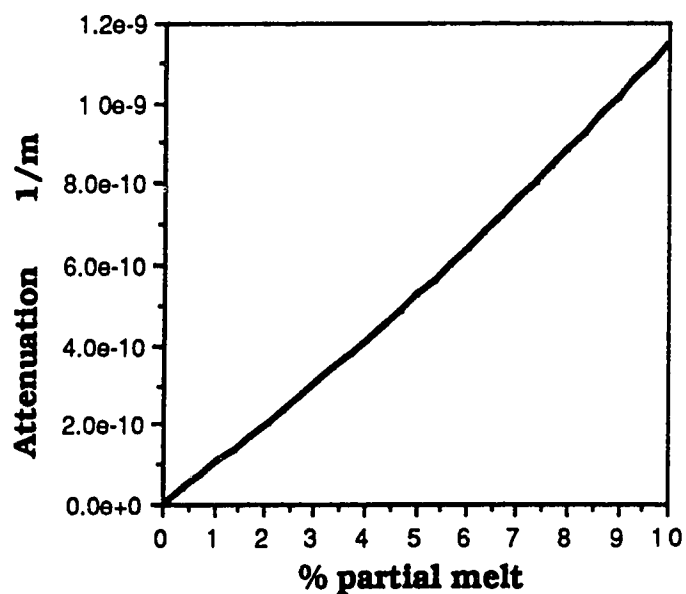


Figure 62 1st S wave; Attenuation vs. % partial melt for a model of the core-mantle transition zone at a frequency of 1 hz..

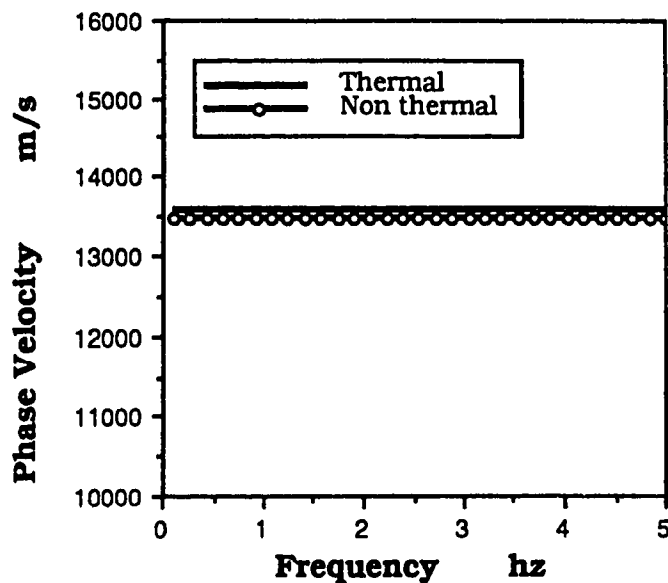


Figure 63 1st P wave; Phase velocity vs. frequency for a model the of core-mantle transition zone with 5% partial melt. Thermal solution includes thermomechanical coupling.

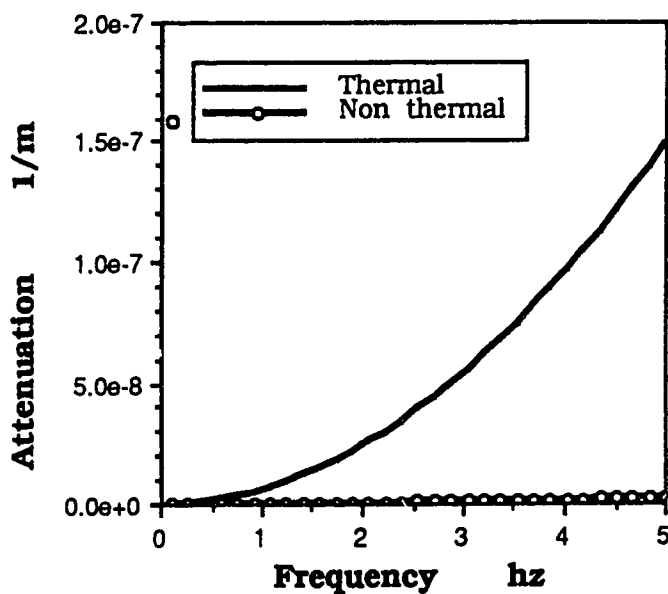


Figure 64 1st P wave; Attenuation vs. frequency for a model the of core-mantle transition zone with 5% partial melt. Thermal solution includes thermomechanical coupling.

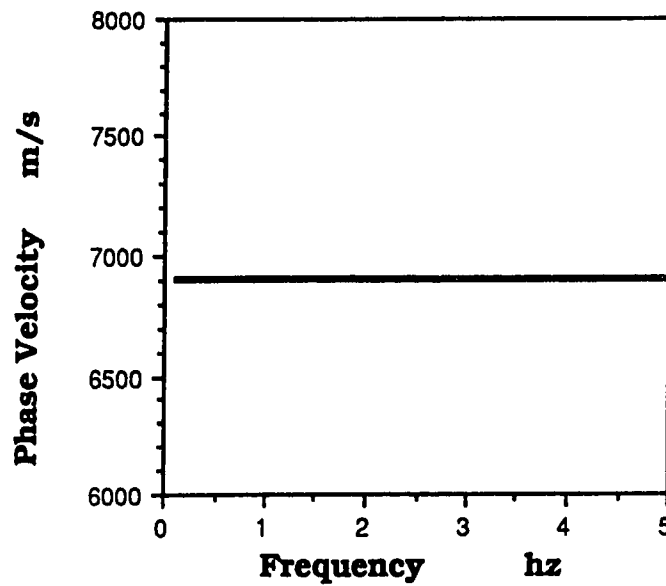


Figure 65 1st S wave; Phase velocity vs. frequency for a model of the core-mantle transition zone with 5% partial melt.

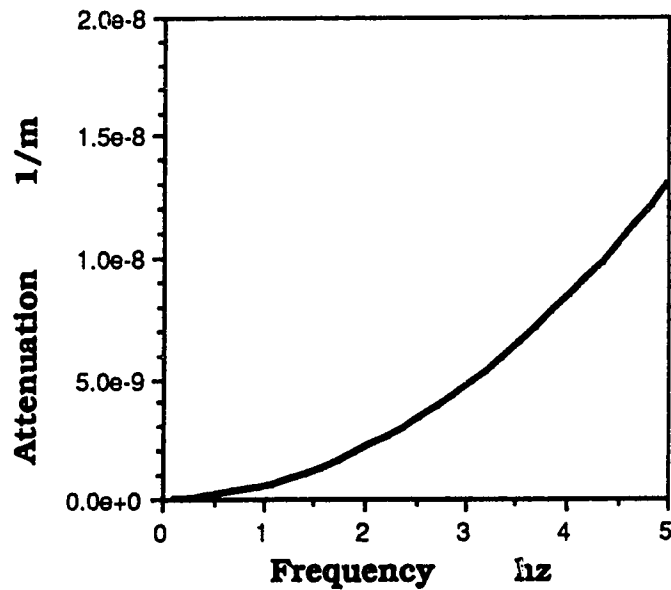


Figure 66 1st S wave; Attenuation vs. frequency for a model of the core-mantle transition zone with 5% partial melt.

frequency.

If the core-mantle transition zone can be approximated by the given parameter set, then increases in partial melt or fluid within a solid framework can account for decreases in phase velocity and Q^* . The phase velocity of both P and S-waves appear to be frequency independent unlike Q^* , which will decrease with increases in frequency. It is evident that thermo-mechanical coupling will be an important process and should be considered when seismic observations are used to investigate this region. However, one should remember that it affects only the P-waves.

5. CONCLUSIONS

The theory for wave propagation in porous media developed by de la Cruz and Spanos (1985, 1989a) is based on the fundamental equations governing each component at the pore scale. Assuming the structures are much smaller than the wavelength of the disturbance, the macroscopic equations are obtained by volume averaging the component equations and appropriate boundary conditions. The complete set of coupled macroscopic equations contains five empirical parameters, namely; permeability, K , induced mass coefficient, ρ_{12} , solid compliance factor, δ_s , fluid compliance factor, δ_f and the intercomponent conduction coefficient, γ . When the main underlying assumptions equating the de la Cruz - Spanos theory and the Biot (1956a) theory are imposed one obtains an interpretation of Biot's phenomenological parameters in terms of the pore scale quantities, δ_f and δ_s . However, δ_f can be determined uniquely by δ_s through (50).

The de la Cruz - Spanos theory predicts two rotational and four dilatational waves when thermo-mechanical coupling is included. The rotational waves are unaffected by thermo-mechanical coupling. Assuming a plane wave, propagating in the x direction with an amplitude in the z direction only, algebraic expressions for the dispersion relations were obtained for both rotational and dilatational waves. However, the dispersion relation for the dilatational waves is very elusive and not physically transparent and therefore a numerical solution must be used.

The adopted method of solution based on cofactor expansion yields the correct results in the solid and fluid limits. However it is

important that one specify proper functional forms for the empirical parameters when constructing such cases. Values of phase velocity and attenuation calculated using the numerical algorithm and algebraic expressions are in good agreement for both the solid and fluid limit. When thermo-mechanical coupling is included the theory predicts two dilatational waves in the solid and fluid limits which are commonly known as first and second sound.

Investigation of empirical parameters using a water filled silica sand model, illustrates that the permeability, K , has a significant effect on the attenuation of both rotational and dilational waves within the seismic frequency range. However, changes in phase velocities can be neglected for the case studied. The induced mass coefficient, ρ_{12} , only becomes important at frequencies in excess of 10^4 hz and therefore can be considered unimportant for seismic waves. The solid and fluid compliance factors (δ_f and δ_s) have been constrained to a narrow range of values. However, values chosen within this range still have an affect on the phase velocity and attenuation of the dilatational waves. Furthermore, the relation between δ_s and δ_f derived from a comparison with Biot's theory (eq. 50) is not a sufficient condition for physical results to exist. Further work is needed to fully understand the importance of the solid and fluid compliance factors and significance of the observed constraints. The intercomponent conduction coefficient, γ , is present only when thermo-mechanical coupling is included. This thermal empirical parameter, γ , can change the attenuation of the P waves but has little effect on the phase velocity for the model considered. The frequency at which component temperatures are equal ($T_s = T_f$) is dependent on this parameter.

The character of the seismic waves propagating through porous

media is dependent on the properties of the fluid and solid components and the coupling between the two. For an air filled silica sand the phase velocities of the 1st P and 1st S waves are frequency independent, for all practical purposes, for frequencies up to 200 Hz. The attenuation of the 1st P and 1st S waves increase with increasing frequency. The phase velocity of the 1st S wave is the same as calculated in the elastic case due to the small coupling between components at the pore-scale. However, the amplitude of this wave should be considerably smaller as compared to the elastic case. This coupling can have different effects on the different waves depending on the component dependence of that wave. Increasing the viscosity of the pore fluid increases the coupling between motions of the solid and fluid components.

For a water filled silica sand model, the phase velocity and attenuation of the 1st P wave is larger than values calculated for the air filled model. The phase of the 1st S wave decreased and its attenuation is increased for the water filled model. This is due to the increased coupling between component material due to the increase in viscosity. It appears that thermo-mechanical coupling can be neglected for a water or air filled silica sand.

The phase velocity and attenuation of a wave propagating in a bitumen filled silica sand are significantly different than is predicted for an elastic solid or a water filled silica sand. The phase velocity of the 1st P wave is usually less; however, the greatest difference is in the increase in attenuation of this wave. The 1st S wave has the same phase velocity for both a bitumen filled silica sand and a water filled silica sand however; the attenuation is about five times larger for the bitumen case. More important is the effect of thermo-mechanical

coupling for a bitumen filled silica sand. Although its effect on phase velocity is minimal, it has been shown that within the seismic frequency range it can increase the attenuation of the 1st P wave by five times the value calculated without thermal effects.

For the above cases, the phase velocities of the 1st S and 1st P waves are frequency independent within the seismic frequency range. The attenuation of the 1st S and P waves is usually a non-linear function of frequency and can be increased significantly by thermo-mechanical coupling.

The de la Cruz-Spanos (1989a) theory supports the hypothesis that the observed negative velocity gradients and high attenuation within the LVZ are due to the presence of a partial melt. Also if the core-mantle transition zone can be approximated by the given parameter set, then increases in partial melt or fluid within a solid framework can account for decreases in phase velocity and Q^* . The phase velocity of both P and S-waves appear to be frequency independent unlike Q^* , which will decrease with increases in frequency. Thermo-mechanical coupling is an important process and should be considered when seismic observations are used to investigate this region. The actual magnitudes of the observed (PREM) and calculated phase velocity and Q^* differ. These differences are most likely due to the uncertainty of the physical parameters of the models and could be eliminated by varying the physical parameters of the component materials to obtain a best fit. However, the frequency dependence of Q^* would probably remain. A vast number of high pressure experiments are being conducted on materials of compositions and at temperatures and pressures believed to be indicative of particular locations within the Earth. If one can adapt these experiments to measure the physical

properties of the constituent materials, then the de la Cruz-Spanos (1989a) theory could be used to calculate phase velocities and attenuation of waves propagating within these zones.

REFERENCES

- Achenbach, J.D., 1973. *Wave Propagation in Elastic Solids*, North-Holland Publishing Co., Amsterdam.
- Agar, J.G., 1984. Geotechnical behavior of oil sands at elevated temperatures and pressures, Ph.D. thesis, The University of Alberta, Edmonton, Alta.
- Agar, J.G., Morgenstern, N.R., and Scott, J.D., 1987. Shear strength and stress-strain behavior of Athabasca oil sand at elevated temperatures and pressures, *Can. Geotech. J.*, **24**, 1-10.
- Ahrens, T.J., 1982. Constraints on core composition from shock wave data, *Philos. Trans. R. Soc. London, Ser. A*, **306**, 37-47.
- Ahrens, T.J. and Jeanloz, R., 1988. Properties of the lower mantle and core materials from high pressure experiments, in *Proceedings of the first SEDI Symposium*, Blanes, Spain.
- Anderson, D.L. and Archambeau, C.B., 1964. The anelasticity of the Earth, *J. Geophys. Res.*, **69** (10), 2017-2084
- Anderson, D.L. and Bass, J., 1986. Transition region of the Earth's upper mantle, *Nature*, **320**, 321-328.
- Anderson, D.L. and Given, J.W., 1982. Absorption band Q model for the Earth, *J. Geophys. Res.*, **87**, 3893-3904.

- Anderson, D.L. and Sammis, C., 1970. Partial melting in the upper mantle, *Phys. Earth Planet. Interiors*, **3**, 41-50.
- Anderson, D.L. and Spetzler, H., 1970. Partial melting and the low-velocity zone, *Phys. Earth Planet. Interiors*, **4**, 62-64.
- Baughman, G.L., 1978. *Synthetic Fuels Data Handbook*, Cameron Eng., Inc., Denver, Colorado.
- Berryman, J. G., 1981. Elastic wave propagation in fluid-saturated porous media, *J. Acoust. Soc. Am.*, **69** (2), 360-373.
- Berryman, J. G., 1983. Effective conductivity by fluid analogy for a porous insulator filled with a conductor, *Phys. Rev. B*, **27** (12), 7789-7792.
- Bhatia, A. B., and Singh, R. N., 1986. *Mechanics of Deformable Media*, Addam Hilger, Bristol and Boston.
- Biot, M. A., 1956a. Theory of propagation of elastic waves in a fluid saturated porous solid, I, Low-frequency range, *J. Acoust. Soc. Am.*, **28**, 168-178.
- Biot, M. A., 1956b. Theory of propagation of elastic waves in a fluid saturated porous solid, II, High-frequency range, *J. Acoust. Soc. Am.*, **28**, 179-191.
- Birch, F., 1970. Interpretations of the low-velocity zone, *Phys. Earth Planet. Interiors*, **3**, 178-181.

- Brennan, B.J. and Stacey, F.D., 1977. Frequency dependence of elasticity of rock-test of seismic velocity dispersion, *Nature*, **268**, 220-222.
- Buland, R., Berger, J., and Gilbert, F., 1979. Observations from the IDA network of attenuation and splitting during a recent earthquake, *Nature(London)*, **277**, 358-362.
- Bullen, K.E., 1963. *An Introduction to the Theory of Seismology*, Cambridge University Press, London.
- Burridge, R. and Keller, J.B., 1981. Poroelasticity equations derived from microstructure, *Journ. Acoust. Soc. Am.*, **70**, 1140-1146.
- Cailleux, A., 1968. *Anatomy of the Earth*, McGraw-Hill, New York.
- Camp, F.W., 1970. *The Tar Sands of Alberta Canada*, 1st edition Cameron Eng.,Inc., Denver, Colorado.
- Camp, F.W., 1974. *The Tar Sands of Alberta Canada*, 2nd edition Cameron Eng.,Inc., Denver, Colorado.
- Campbell, H.G., 1977. *An Introduction to Matrices, Vectors, and Linear Programming*, Prentice-Hall, New Jersey.
- Chadwick, P., 1960. Thermoelasticity and dynamical theory. In: *Progress in Solid Mechanics*, ed. Sneddon, I.N. and Hill, R., North-Holland, Amsterdam.

- Childs, W.H.J., 1939. *Physical Constants*, Methuen & Co., London.
- Clark, S.P. Jr, 1966. *Handbook of Physical Constants*, Memoir **97**, The Geological Society of America, New York.
- Darcy, H., 1856. *Les Fontaines Publiques de la Ville de Dijon*, Victor Dalmont, Paris.
- de la Cruz, V. and Spanos, T.J.T., 1983. Mobilization of oil ganglia, *AIChE J.* **29** (7), 854-858.
- de la Cruz, V., and Spanos, T.J.T., 1985. Seismic wave propagation in a porous medium, *Geophysics*, **50** (10), 1556-1565.
- de la Cruz, V., and Spanos, T.J.T., 1989a. Thermo-mechanical coupling during seismic wave propagation in a porous medium, *J. Geophys. Res.*, **94**, 637-642.
- de la Cruz, V., and Spanos, T.J.T., 1989b. Seismic boundary conditions for porous media, *J. Geophys. Res.*, **94**, 3025-3029.
- Dusseault, M.B. and Morgenstern, N.R., 1978. Shear strength of Athabasca oil sands, *Can. Geotech. J.*, **15**, 216-238.
- Dziewonski, A.M. and Anderson, D.L., 1981. Preliminary reference Earth model, *Phys. Earth Planet. Interiors*, **25**, 297-356.
- Eastwood, J.E., Hickey, C.J. and Spanos, T.J.T., 1990. An analysis of the parameters required to describe seismic wave propagation in porous media, submitted to *J. Acoust. Soc. Am.*

- Forsythe, W.E., 1959. *Smithsonian Physical Tables*, The Smithsonian Institute, Baltimore.
- Gassman, F., 1951a. Über die elastizität poroser medien: Ver der Natur. *Gesellschaft*, **96**, 1-23.
- Gassman, F., 1951b. Elastic waves through a packing of spheres, *Geophys*, **16**(4), 673-685.
- Geertsma, J. and Smit, D.C., 1961. Some aspects of elastic wave propagation in fluid saturated porous solids, *Geophysics*, **26** (2), 169-181.
- Geller, R.J., and Stein, S., 1979. Time domain measurements of attenuation of fundamental spherical modes (${}_0S_6$ - ${}_0S_{28}$) for the 1977 Indonesian earthquake, *Bull. Seismol. Soc. Am.*, **69**, 1671-1691.
- Gordon, R.B. and Davis, D.L., 1968. Velocity and attenuation of seismic waves in imperfectly elastic rock, *J. Geophys. Res.*, **73**, 3917-3935.
- Gutenberg, B, 1959. *Physics of the Earth's interior*, International Geophysics Series, V. 1, Academic Press, New York.
- Heinz, D.L. and Jeanloz, R., 1987. Measurements of the melting curve of $Mg_{0.9}Fe_{0.1}SiO_3$ at lower mantle conditions and its geophysical implications, *J. Geophys. Res.*, **92**(11), 437

- Hubbard, M.K., 1956. Darcy's law and field equations of flow of underground fluids, *Am. Inst. Min. Metall. and Petrol. Eng.*, **207**, 222-239.
- Jacobs, J.A., 1981. Seismology and deep structure of the Earth. In: *Cambridge Encyclopedia of Earth Sciences*, ed. Smith, D.G., Crown Publisher, Cambridge University Press, New York.
- Jacoby, W.R. and Schmeling, H., 1982. On the effects of the lithosphere on mantle convection and evolution, *Phys. Earth Planet. Interiors*, **29**, 305-319.
- Jeanloz, R. and Morris, S., 1986. Temperature distribution in the crust and mantle, *Annu. Rev. Earth Planet. Sci.*, **14**, 377- 415.
- Jeffreys, Sir, H., 1939. The times of P, S, and SKS and the velocities of P and S, *Mon. Not. R. Astr. Soc., Geophys. Suppl.*, **4**, 498-533.
- Jeffreys, Sir, H., 1959 *The Earth*, Cambridge University Press.
- Johnson, D. L., and Plona, T. J., 1982. Acoustic slow waves and the consolidation transition, *J. Acoust. Soc. Am.*, **72** (2), 556-565.
- Johnston, D. H., Toksoz, M. N., and A. Timur, 1979, Attenuation of seismic waves in dry and saturated rocks: II. Mechanisms, *Geophysics*, **44** (4), 691-711.

- Jones, J. D., 1986. Pore fluids and frequency dependent wave propagation in rocks, *Geophysics*, **51** (10), 1939-1953.
- Jones, T.D., and Nur, A., 1983. Velocity and attenuation in sandstone at elevated temperatures and pressures, *Geophys. Res. Lett.*, **10**, 140-143.
- Kampfmann, W. and Berckhemer, H., 1985. High temperature experiments on the elastic and anelastic behavior of magmatic rocks, *Phys. Earth Planet. Interiors*, **40**, 223-247.
- Kappelmeyer, O. and Haenel, R., 1974. *Geothermics, with Special Reference to Application*, Geophysical monograph series 1-4, Geopublication Associates, Gebruder Borntraeger, Berlin.
- Knittle, E. and Jeanloz, R., 1987. Synthesis and equation of state of (Mg,Fe)SiO₃ perovskite to over 100 Gigapascals, *Science*, **235**, 668-670
- Knittle, E., Jeanloz, R. and Smith, G.L., 1986, Thermal expansion of silicate perovskite and stratification of the Earth's mantle, *Nature*, **319**, 214-215
- Knopoff, L., 1964. *Q*, *Rev. Geophys.*, **2**, 625-660.
- Knopoff, L. and Mac Donald, G.J.F., 1960. Models for acoustic loss in solids, *J. Geophys. Res.*, **65**, 2191-2197.

- Kushiro, I., Syono, Y. and Akimoto, S., 1968. Melting of a peridotite nodule at high pressures and high water pressures, *J. Geophys. Res.*, **73** (18), 6023-6029.
- Lamb, Sir, H., 1932. *Hydrodynamics*, Dover, New York.
- Lambert, I.B. and Wyllie, P.J., 1970. Melting in the deep crust and upper mantle and the nature of the low-velocity layer, *Phys. Earth Planet. Interiors*, **3**, 316-322.
- Landau, L.D., and Lifshitz, E.M., 1975a. *Fluid Mechanics*, Pergamon, New York.
- Landau, L.D., and Lifshitz, E.M., 1975b. *Theory of Elasticity*, Pergamon, New York.
- Lay, T., 1989. Structure of the core mantle transition zone: A chemical and thermal boundary layer, *EOS Trans. Am. Geophys. Union*, **70**(4), 49-50
- Manghnani, M.H. and Akimoto, S., 1977. *High Pressure Research: Application in Geophysics*, Academic Press, New York.
- Manghnani, M.H. and Syono, Y., 1987. *High Pressure Research in Mineral Physics*, Geophysical monograph, **39**, American Geophysical Union, Washington, D.C.
- Mavko, G. M. and Nur, A., 1979. Wave attenuation in partially saturated rocks, *Geophys.*, **44**, 161-178.

- Mindlin, R.D. and Deresiewicz, H., 1953. Elastic spheres in contact under varying oblique forces, *J. Appl. Mech.*, **20**, 327-344.
- Murphy, W.F., 1982. Effects of partial water saturation on attenuation in partially saturated rocks, *Geophysics*, **44**, 1458-1468.
- Murphy, W.M., 1983. Effects of partial water saturation on attenuation in Massillon sandstone and Vycor porous glass, *J. Acoust. Soc. Am.*, **71**, 1458-1468.
- Pandit, B.I. and Savage, J.C., 1973. An experimental test of Lomnitz's theory of internal friction in rocks, *J. Geophys. Res.*, **78**, 6092-6099.
- Ringwood, A.E., 1970. Phase transformations and the constitution of the mantle, *Phys. Earth Planet. Interiors*, **3**, 109-155.
- Ringwood, A.E., 1975. *Composition and Petrology of the Earth's Mantle*, McGraw-Hill, New York.
- Slattery, J.C., 1969. Single phase flow through porous media, *J. Am. Inst. Chem. Eng.*, **15**, 866-872.
- Spanos, T.J.T., Eastwood, J.E., Hickey, C.J. and Udey, N., 1990. Seismic wave propagation in oilsands, unpublished.
- Spencer, J.W., Jr, 1979. Bulk and shear attenuation in Berea sandstone: The effects of pore fluids, *J. Geophys. Res.*, **84**, 7521-7523

- Spencer, J.W., Jr, 1981. Stress relaxations at low frequencies in fluid saturated rocks: Attenuation and modulus dispersion, *J. Geophys. Res.*, **86**, 1803-1812.
- Stacey, F.D. and Loper, D.E., 1983 The thermal boundary-layer interpretations of D" and its role as a plume source, *Phys. Earth Planet. Inter.*, **33**, 45-55.
- Steim, J.M. and Dziewonski, A.M., 1980. A new approach to measurements of dispersion and attenuation of mantle waves, *EOS Trans. Am. Geophys. Union*, **61**, 298 (abstract).
- Tittmann, B.R., Bulua, J.R. and Abdel-Gawad, M., 1983. Dissipation of elastic waves in fluid saturated rock, *Am. Inst. Phys. conference on physics and chemistry of porous media*, Schlumberger-Doll Research, Johnson, D.L. and Sen, P.N., Ed., Am. Inst. Phys., 131-143.
- Toksoz, M. N., Johnston, D. H., and A. Timur, 1979. Attenuation of seismic waves in dry and saturated rocks: I. Laboratory measurements, *Geophysics*, **44** (4), 681-690.
- Walsh, J.B., 1966. Seismic attenuation in rock due to friction, *J. Geophys. Res.*, **71**, 2591-2599.
- Walsh, J.B., 1968. Attenuation in partially melted material, *J. Geophys. Res.*, **73** (6), 2209-2216.
- Weast, R.C., 1969. *C.R.C. Handbook of Chemistry and Physics*, The Chemical Rubber Co., Ohio.

- Whitaker, S., 1966. The equations of motion in porous media, *Chem. Eng. Sci.*, **21**, 291-300.
- Whitaker, S., 1969. Advances in the theory of fluid motion in porous media, *Ind. Eng. Chem.*, **61** (12), 14-28.
- White, J.E., 1966. *Seismic Waves*, Mc Graw-Hill Book Co., Inc, New York.
- White, J. E., 1986. Biot- Gardner theory of extensional waves in porous rods, *Geophys.*, **51**, 742-745.
- Williams, Q., Knittle, E. and Jeanloz, R., 1987. High temperature experiments on liquid iron alloys: Applications to the Earth's core, *EOS Trans. Am. Geophys. Union*, **68**(44), 1493 (abstract).
- Winkler, K. W., 1983. Frequency dependent ultrasonic properties of high-porosity sandstones, *J. Geophys. Res.*, **88**, 9493-9499.
- Winkler, K.W., 1985. Dispersion analysis of velocity and attenuation in Berea sandstone, *J. Geophys. Res.*, **90**, 6793-6800.
- Winkler, K.W., 1986. Estimates of velocity dispersion between seismic and ultrasonic frequencies, *Geophysics*, **51** (1), 183-189.
- Winkler, K.W., and Nur, A., 1982. Seismic attenuation: Effects of pore fluids and frictional sliding, *Geophysics*, **47** (1), 1-15.

- Winkler, K.W. and Plona, T.J., 1982. Technique for measuring ultrasonic velocity and attenuation spectra in rocks under pressure, *J. Geophys. Res.*, **87**, 10776-10780.
- Young, C.J. and Lay, T., 1987. The core-mantle boundary, *Ann. Rev. Earth Planet. Sci.*, **15**, 25-46.
- Zemansky, M.W., 1957. *Heat and Thermodynamics*, McGraw-Hill, New York.